THREE DIMENSIONAL FREQUENCY DEPENDENT ADDITIVE OPERATOR SPLITTING FDTD METHOD

A thesis submitted to the University of Manchester
for the degree of Master of Philosophy
in the Faculty of Electrical and Electronic Engineering

2015

By
Mario Parreño Centeno
School of Electrical and Electronic Engineering

Contents

List of Figures

Abstract

The Finite-Difference Time-Domain (FDTD) method is a numerical analysis technique used for the simulation of electromagnetic (EM) phenomena. It is one of the most popular computational techniques for modelling the behaviour of electromagnetic waves. As an explicit method, the FDTD scheme is constrained by the Courant-Friedrichs-Lewy (CFL) stability condition, which limits the time step that can be used to obtain stable and accurate simulation results. It can be an important disadvantage for modelling specific scenarios such as large computational EM problems or problems where very fine meshes, compared to the electrical wavelength required. This leads to longer simulation time requiring larger computational requirements. In order to overcome this problem, implicit FDTD methods are an alternative. Numerous researches have been carried out so as to develop schemes to provide the computational stability beyond the limit of the CFL condition. In this Thesis, an Additive Operator Splitting (AOS) FDTD method has been introduced.

Declaration

No portion of the work referred in this thesis has been submitted in support of an application for another degree or qualification of this or any other university or other institute of learning.

Copyright

Dedication

To my parents Marino and Sagrario, my sister Gemma and her husband Xavi, and to all my good friends.

"Without a family, man, alone in the world, trembles with the cold."

Andre Maurois.

Acknowledgements

I have received support and encouragement from a great number of individuals to complete this Thesis. First of all, I would like to mention my supervisor, Dr. Fumie Costen. I will be eternally grateful to her for having inspired me beyond the academic work and for having supported me in crucial circumstances. Dr Tadashi Hemmi provided me with valuable advice about my research. Victoria Berrueco Pastor and Diana Patiño Barriga rendered an essential assistance with my writing. Thanks to Dr. Andrés Camacho García for his unconditional support. And thanks to Universidad Politécnica de Valencia for having awarded me with a grant to come to The University of Manchester as a Visiting Researcher, as that was the time when I decided to pursue my MPhil course.

Chapter 1

Finite Difference Time Domain method

1.1 Introduction

The Finite Difference Time Domain (FDTD) method is a numerical technique used for the simulation of computational electrodynamics. Due to its robustness and simplicity of implementation, this leap-frog-approach has been widely used the past decades. The widespread use of this technique and its popularity have led many contributions since its introduction by Kane S. Yee in 1966 [1]. Although S. Yee is regarded as the father of FDTD, the application of finite differences to the resolution of partial differential equations dates from the works of Courant, Friedrichs, Lewy almost a century ago [2].
FDTD method is a direct solution of Maxwell's time-dependent curl equations, replacing Maxwells equations by a set of finite difference equations.

1.1.1 Finite difference approximation to derivatives

Consider a function $y = f(x)$ which is continuous and differentiable in the closed interval $[a, b]$. Then one can prove the following theorem, due to Lagrange:

If the function $y = f(x)$ is continuous in $[a, b]$ and has a continuous derivative in this interval, then there exists at least one point c between a and b such that:

$$\frac{f(b) - f(a)}{b - a} = f'(c) \tag{1.1}$$

Rewriting (1.1) by setting $a = x$, $b = x + h$ and $c = a + \theta h$ with $\theta \exists [0, 1]$, hence:

$$f(x + h) = f(x) + hf'(x + \theta h) \tag{1.2}$$

According to the Taylor's theorem if the function $f(x)$ is continuous and has continuous derivatives up the mth in the interval $[x, x + h]$, then:

$$f(x + h) = f(x) + hf'(x) + \frac{h^2}{2!}f''(x) + \frac{h^3}{3!}f'''(x) + \cdots + \frac{h^m}{m!}f^{(m)}(x + \theta h) \tag{1.3}$$

where $\theta \exists [0, 1]$.

Assume that the function $f(x)$ has continuous derivatives of any order in the interval $[x, x + h]$. Therefore we can choose m in (1.3) arbitrarily large. Then, if in the limit of $m \to \infty$ we have $f^{(m)}(x + \theta h) \to 0$, the function $f(x)$ can be expanded in a power series:

$$f(x + h) = f(x) + hf'(x) + \frac{h^2}{2!}f''(x) + \frac{h^3}{3!}f'''(x) + \cdots + \frac{h^m}{m!}f^{(m)}(x) \tag{1.4}$$

Also, rewriting (1.1) by setting $a = x - h$, $b = x + h$ and $c = b + \theta h$ with $\theta \exists [0, 1]$, (1.4) is given as:

$$f(x - h) = f(x) - hf'(x) + \frac{h^2}{2!}f''(x) - \frac{h^3}{3!}f'''(x) + \cdots + \frac{h^n}{n!}f^{(n)}(x + \theta h) \tag{1.5}$$

Assuming that the terms containing second and higher powers of h are negligible in comparison with h, (1.4) and (1.5) are approximated to

$$f(x + h) \simeq f(x) + hf'(x) \tag{1.6}$$

and

$$f(x - h) \simeq f(x) - hf'(x). \tag{1.7}$$

Thus, manipulation of (1.6) gives us

$$f'(x) \simeq \frac{1}{h}\{f(x + h) - f(x)\} \tag{1.8}$$

where (1.8) is called the forward difference approximation.

On the other hand, manipulation of (1.7) gives us

$$f'(x) \simeq \frac{1}{h}\{f(x) - f(x-h)\} \tag{1.9}$$

and (1.9) is called the backward difference approximation.

Meanwhile, subtraction of (1.7)) from (1.6)

$$f(x+h) - f(x-h) \simeq 2hf'(x) \tag{1.10}$$

Hence, manipulation of (1.10) gives us

$$f'(x) \simeq \frac{1}{2h}\{f(x+h) - f(x-h)\}. \tag{1.11}$$

Here (1.11) is called the central difference approximation.

Also the addition of (1.4) and (1.5) and neglect of the terms containing fourth and higher powers of h gives the approximation of

$$f(x+h) + f(x-h) \simeq 2f(x) + h^2 f''(x) \tag{1.12}$$

Hence, the second order derivative is given as

$$f''(x) \simeq \frac{1}{h^2}\{f(x+h) - 2f(x) + f(x-h)\}. \tag{1.13}$$

Here (1.13) is called the second order central difference approximation.

These are the approximations used in the finite difference methods.

1.2 Maxwell's equations

Maxwell's curl equations predict the existence of an electric and a magnetic field, whose primary causes are charges and movement of charges, coupled between them so that they self-maintain even in the absence of the charges/currents. Problems of propagation, radiation and scattering of the electromagnetic waves, can be studied obtaining the solutions of these equations. The computational solutions of these equations have important applications in different fields such as defense, communication and medicine.

Maxwell's equations in an isotropic linear medium are [3]:

$$\boldsymbol{D} = \epsilon \boldsymbol{E} \tag{1.14}$$

$$\boldsymbol{B} = \mu \boldsymbol{H} \tag{1.15}$$

$$\boldsymbol{J} = \sigma \boldsymbol{E} \quad \text{Ohm's Law} \tag{1.16}$$

$$\nabla \times \boldsymbol{E} = -\frac{\partial \boldsymbol{B}}{\partial t} \quad \text{Faraday's Law} \tag{1.17}$$

$$\nabla \times \boldsymbol{H} = \boldsymbol{J} + \frac{\partial \boldsymbol{D}}{\partial t} \quad \text{Ampere's Law} \tag{1.18}$$

$$\nabla \cdot \boldsymbol{D} = \rho \quad \text{Gauss' Law for the Electric Field} \tag{1.19}$$

$$\nabla \cdot \boldsymbol{B} = 0 \quad \text{Gauss' Law for the Magnetic Field} \tag{1.20}$$

with:

- $\boldsymbol{E}$ the electric field;
- $\boldsymbol{H}$ the magnetic field;
- $\boldsymbol{D}$ the electric flux density;
- $\boldsymbol{B}$ the magnetic flux density;
- $\boldsymbol{J}$ the conduction current density;
- ϵ the permittivity;
- μ the permeability;
- σ the direct current (DC) conductivity;
- ρ the charge density.

Taking J = 0 (as is the case in a source free medium), (1.17) and (1.18) can be rewritten as six partial differential equations [4], as shown below:

$$\frac{\partial H_x}{\partial t} = \frac{1}{\mu}\left(\frac{\partial E_y}{\partial z} - \frac{\partial E_z}{\partial y}\right) \tag{1.21}$$

$$\frac{\partial H_y}{\partial t} = \frac{1}{\mu}\left(\frac{\partial E_z}{\partial x} - \frac{\partial E_x}{\partial z}\right) \tag{1.22}$$

$$\frac{\partial H_z}{\partial t} = \frac{1}{\mu}\left(\frac{\partial E_x}{\partial y} - \frac{\partial E_y}{\partial x}\right) \tag{1.23}$$

$$\frac{\partial E_x}{\partial t} = \frac{1}{\epsilon}\left(\frac{\partial H_z}{\partial y} - \frac{\partial H_y}{\partial z}\right) \tag{1.24}$$

$$\frac{\partial E_y}{\partial t} = \frac{1}{\epsilon}\left(\frac{\partial H_x}{\partial z} - \frac{\partial H_z}{\partial x}\right) \tag{1.25}$$

$$\frac{\partial E_z}{\partial t} = \frac{1}{\epsilon}\left(\frac{\partial H_y}{\partial x} - \frac{\partial H_x}{\partial y}\right) \tag{1.26}$$

1.3 The Yee algorithm

The Yee algorithm solves for electric and magnetic fields in time and space using the coupled Maxwells curl-equations, rather than solving for only one of the fields using a wave equation. It divides the space in cells, where each of them is called the Yee unit cell, shown in Figure 1.1. The distribution of the points of the magnetic and electric fields is such that the finite set of differential equations (1.21) to (1.26) can be evaluated and the solution will satisfy the boundary conditions.

The Yee's cell arrangement centers $\boldsymbol{E}$ and $\boldsymbol{H}$ components in three-dimensional space so that every $\boldsymbol{E}$ component is surrounded by four circulating $\boldsymbol{H}$ components, and every $\boldsymbol{H}$ component is surrounded by four circulating $\boldsymbol{E}$ components. The signal level at each FDTD grid in the FDTD space at each time step is calculated by using the relation between the neighbouring cells.

Maxwell's continuous mathematical equations (1.21) to (1.26) can be converted into a discrete form (1.27) to (1.32). The FDTD method applies second-order accurate central difference approximations for the space and time derivatives of the electric and magnetic fields directly to the respective differential operators of the curl equations. The values of $\boldsymbol{E}$ and $\boldsymbol{H}$ are calculated at half-time intervals, such that at each half step in time either $\boldsymbol{E}$ is calculated from the previous values of $\boldsymbol{H}$ or vice versa. Discretization is performed with respect to

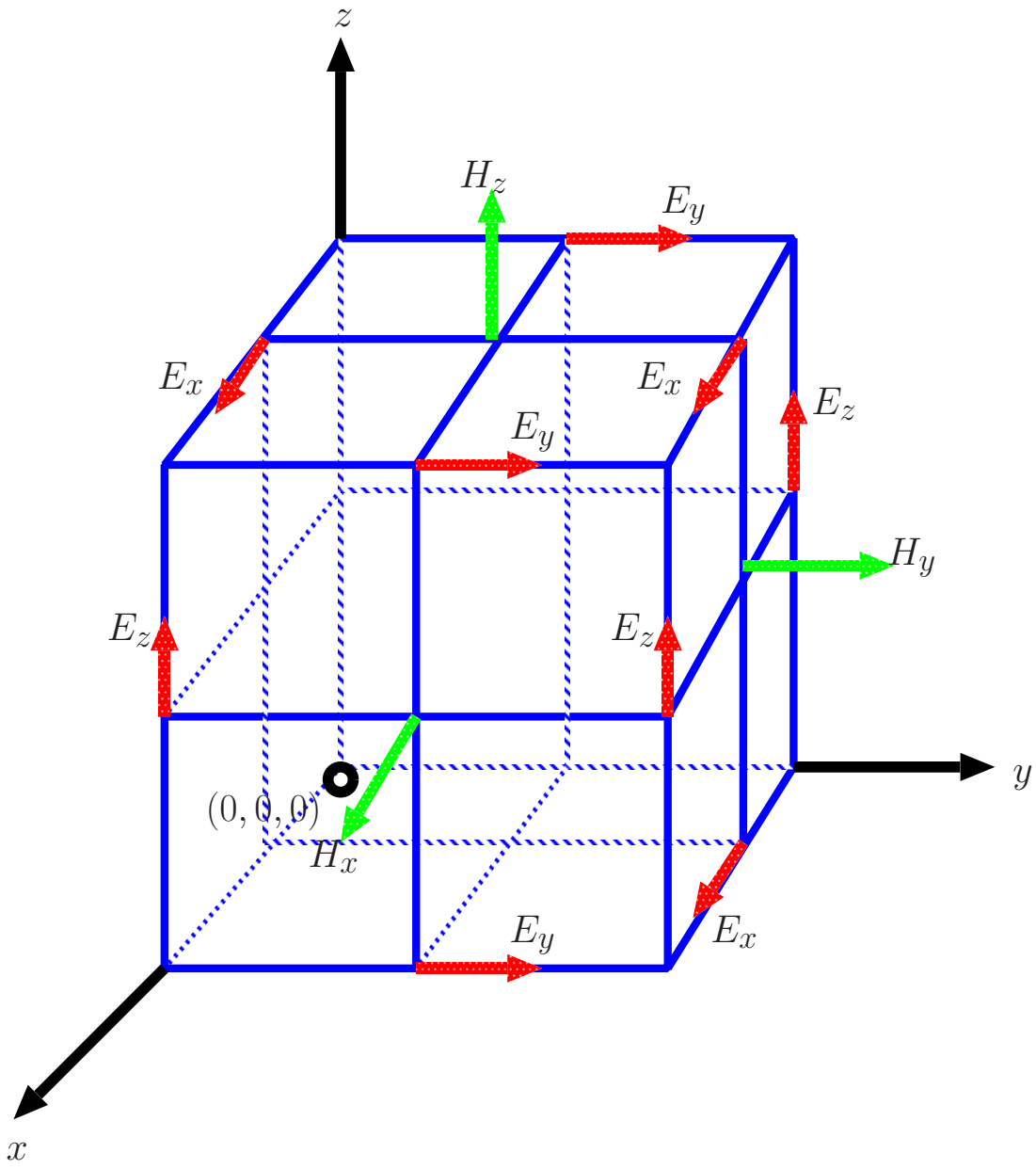

Figure 1.1: Position of the electric and magnetic field vector components about a cubic unit cell of the Yee space lattice.

time Δt and space Δx, Δy and Δz [4]:

$$H_x^{n+\frac{1}{2}}(i,j+\frac{1}{2},k+\frac{1}{2}) = H_x^{n-\frac{1}{2}}(i,j+\frac{1}{2},k+\frac{1}{2}) + \frac{\Delta t}{\mu(i,j+\frac{1}{2},k+\frac{1}{2})\Delta z}\left[E_y^n(i,j+\frac{1}{2},k+1) + E_y^n(i,j+\frac{1}{2},k)\right] + \frac{\delta t}{\mu(i,j+\frac{1}{2},k+\frac{1}{2})\Delta y}\left[(E_z)^n(i,j,k+\frac{1}{2}) + (E_z)^n(i,j+1,k+\frac{1}{2})\right] \tag{1.27}$$

$$H_y^{n+\frac{1}{2}}(i+\frac{1}{2},j,k+\frac{1}{2}) = H_y^{n-\frac{1}{2}}(i+\frac{1}{2},j,k+\frac{1}{2}) + \frac{\Delta t}{\mu(i+\frac{1}{2},j,k+\frac{1}{2})\Delta x}\left[E_z^n(i+1,j,k+\frac{1}{2}) + E_z^n(i+\frac{1}{2},j,k+\frac{1}{2})\right] + \frac{\delta t}{\mu(i+\frac{1}{2},j,k+\frac{1}{2})\Delta z}\left[(E_x)^n(i+\frac{1}{2},j,k) + (E_x)^n(i+\frac{1}{2},j,k+1)\right] \tag{1.28}$$

$$H_z^{n+\frac{1}{2}}(i+\frac{1}{2},j+\frac{1}{2},k) = H_z^{n-\frac{1}{2}}(i+\frac{1}{2},j+\frac{1}{2},k) + \frac{\Delta t}{\mu(i+\frac{1}{2},j+\frac{1}{2},k)\Delta y}\left[E_x^n(i+\frac{1}{2},j+1,k) + E_x^n(i+\frac{1}{2},j,k)\right] + \frac{\delta t}{\mu(i+\frac{1}{2},j+\frac{1}{2},k)\Delta x}\left[(E_y)^n(i,j+\frac{1}{2},k) + (E_y)^n(i+1,j+\frac{1}{2},k)\right] \tag{1.29}$$

$$E_x^{n+1}(i+\frac{1}{2},j,k) = E_x^n(i+\frac{1}{2},j,k) + \frac{\Delta t}{\epsilon(i+\frac{1}{2},j,k)\Delta y}\left[H_z^{n+\frac{1}{2}}(i+\frac{1}{2},j+\frac{1}{2},k) + H_z^{n+\frac{1}{2}}(i+\frac{1}{2},j-\frac{1}{2},k)\right] + \frac{\Delta t}{\epsilon(i+\frac{1}{2},j,k)\Delta z}\left[H_y^{n+\frac{1}{2}}(i+\frac{1}{2},j,k-\frac{1}{2}) + H_z^{n+\frac{1}{2}}(i+\frac{1}{2},j,k+\frac{1}{2})\right] \tag{1.30}$$

$$
\begin{aligned}
E_y^{n+1}(i,j+\frac{1}{2},k) = {} & E_y^n(i,j+\frac{1}{2},k) \\
& + \frac{\Delta t}{\epsilon(i,j+\frac{1}{2},k)\Delta z}\left[H_x^{n+\frac{1}{2}}(i,j+\frac{1}{2},k+\frac{1}{2}) + H_x^{n+\frac{1}{2}}(i,j+\frac{1}{2},k-\frac{1}{2})\right] \\
& + \frac{\Delta t}{\epsilon(i,j+\frac{1}{2},k)\Delta x}\left[H_z^{n+\frac{1}{2}}(i-\frac{1}{2},j+\frac{1}{2},k) + H_z^{n+\frac{1}{2}}(i+\frac{1}{2},j+\frac{1}{2},k)\right]
\end{aligned}
\tag{1.31}
$$

$$
\begin{aligned}
E_z^{n+1}(i,j,k+\frac{1}{2}) = {} & E_z^n(i,j,k+\frac{1}{2}) \\
& + \frac{\Delta t}{\epsilon(i,j,k+\frac{1}{2})\Delta x}\left[H_y^{n+\frac{1}{2}}(i+\frac{1}{2},j,k+\frac{1}{2}) + H_y^{n+\frac{1}{2}}(i-\frac{1}{2},j,k+\frac{1}{2})\right] \\
& + \frac{\Delta t}{\epsilon(i,j,k+\frac{1}{2})\Delta y}\left[H_x^{n+\frac{1}{2}}(i,j-\frac{1}{2},k+\frac{1}{2}) + H_x^{n+\frac{1}{2}}(i,j+\frac{1}{2},k+\frac{1}{2})\right]
\end{aligned}
\tag{1.32}
$$

Yee choose a notation which interleaves $\boldsymbol{E}$ and $\boldsymbol{H}$ components in the space lattice at intervals of $\Delta x/2$, $\Delta y/2$ and $\Delta z/2$ and in time at intervals of $\Delta t/2$. In order to represent this scheme for a computation where the indices of the data structure have to be integers values, the component fields are placed at $E_x(0,0,0)$, $E_y(0,0,0)$, $E_z(0,0,0)$, $H_x(0,0,0)$, $H_y(0,0,0)$ and $H_z(0,0,0)$. For example, Figure 1.2 shows the arrangement for $\boldsymbol{E}$.

Time is also offset by half a time step. Space and time offsetting is shown in equations (1.33) to (1.38) [4]:

$$
\begin{aligned}
H_x^{n+1}(i,j,k) = {} & H_x^n(i,j,k) \\
& + \frac{\Delta t}{\mu(i,j,k)\Delta z}\left[E_y^n(i,j,k) + E_y^n(i,j,k-1)\right] \\
& + \frac{\delta t}{\mu(i,j,k)\Delta y}\left[(E_z)^n(i,j,k) + (E_z)^n(i,j-1,k)\right]
\end{aligned}
\tag{1.33}
$$

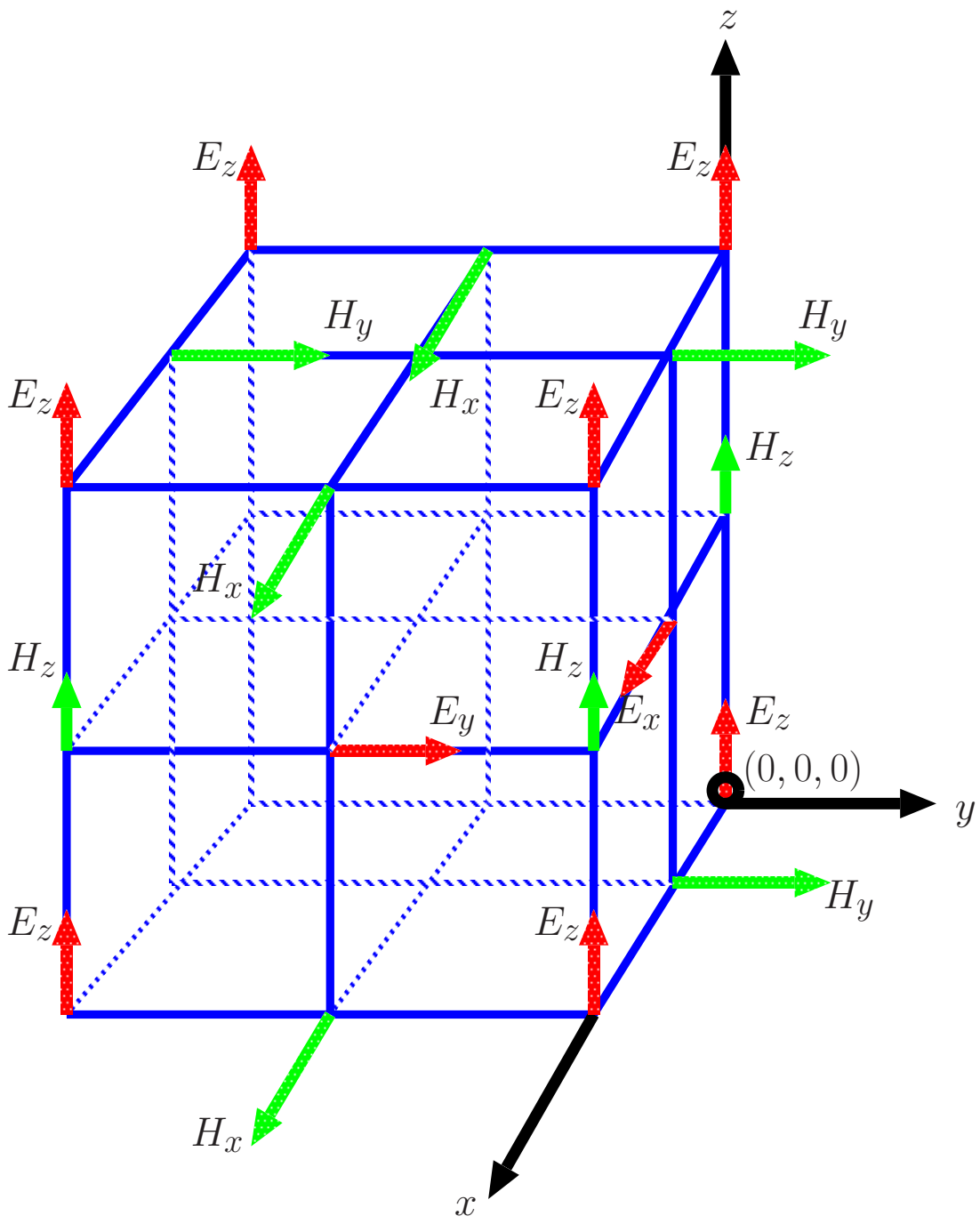

Figure 1.2: Placement of E_z to allow integer coordinates.

$$\begin{aligned} H_y^{n+1}(i,j,k) = H_y^n(i,j,k) \\ + \frac{\Delta t}{\mu(i,j,k)\Delta x}\left[E_z^n(i,j,k) + E_z^n(i-1,j,k)\right] \\ + \frac{\delta t}{\mu(i,j,k)\Delta z}\left[(E_x)^n(i,j,k) + (E_x)^n(i,j,k-1)\right] \end{aligned} \tag{1.34}$$

$$\begin{aligned} H_z^{n+1}(i,j,k) = H_z^n(i,j,k) \\ + \frac{\Delta t}{\mu(i,j,k)\Delta y}\left[E_x^n(i,j,k) + E_x^n(i,j-1,k)\right] \\ + \frac{\delta t}{\mu(i,j,k)\Delta x}\left[E_y^n(i,j,k) + E_y^n(i-1,j,k)\right] \end{aligned} \tag{1.35}$$

$$\begin{aligned} E_x^{n+1}(i,j,k) = E_x^n(i,j,k) \\ + \frac{\Delta t}{\epsilon(i,j,k)\Delta y}\left[H_z^n(i,j+1,k) + H_z^n(i,j,k)\right] \\ + \frac{\Delta t}{\epsilon(i,j,k)\Delta z}\left[H_y^n(i,j,k+1) + H_z^n(i,j,k)\right] \end{aligned} \tag{1.36}$$

$$\begin{aligned} E_y^{n+1}(i,j,k) = E_y^n(i,j,k) \\ + \frac{\Delta t}{\epsilon(i,j,k)\Delta z}\left[H_x^n(i,j,k+1) + H_x^n(i,j,k)\right] \\ + \frac{\Delta t}{\epsilon(i,j,k)\Delta x}\left[H_z^n(i+1,j,k) + H_z^n(i,j,k)\right] \end{aligned} \tag{1.37}$$

$$\begin{aligned} E_z^{n+1}(i,j,k) = E_z^n(i,j,k) \\ + \frac{\Delta t}{\epsilon(i,j,k)\Delta x}\left[H_y^n(i+1,j,k) + H_y^n(i,j,k)\right] \\ + \frac{\Delta t}{\epsilon(i,j,k)\Delta y}\left[H_x^n(i,j+1,k) + H_x^n(i,j,k)\right] \end{aligned} \tag{1.38}$$

1.4 Source excitation

A wide variety of signals have been used as source in FDTD meshes. The basic sources called hard source and soft source are the simplest kinds of source used in the FDTD method to insert a wave source in a simple point of the mesh [5].

While the soft source impresses a current, the hard source impresses an electric field.

In the case of the soft source, the source signal of interest is added in the source point to the previous value of the field, while in the other case of the hard source the value of the amplitude of the source signal is set in the current value of the field. In other words, for example, if the following is a hard source, $E_x(t) = \sin(\omega \cdot t)$ where ω is the angular frequency and t is the time, the following is instead of a soft source, $E_x(t) = E_x(t) + \frac{\partial \sin(\omega \cdot t)}{\partial t}$.

Soft source excitation is stable and accurate in the computation of the FDTD simulation. However, the implementation of a soft source excitation is more complicated than the implementation of a hard source. In the experiments of this thesis a hard source is used for simplicity.

1.5 Setting the Yee's cell size

To discretize the space, the size of the Yee' cell must be established such that an adequate simulation will be obtained. If the simulation is carried on the free-space, Δs is the size of the cell and $\lambda_{min} = \frac{c}{\text{maximum frequency of interest in the source signal}}$, where c is the light speed on the free space. Experience has shown that the spatial step, Δs must be at least ten times smaller than the smallest wavelength of interest for a negligible dispersion error [6]:

$$\Delta s = \frac{\lambda_{min}}{10} \tag{1.39}$$

In the experiments shown in this thesis Δs is set to:

$$\Delta s = \frac{\lambda_{min}}{100} \tag{1.40}$$

1.6 Explicit FDTD constraint: Courant-Friedrichs-Levy stability condition

The Yee-FDTD method is limited by the Courant-Friedrichs-Lewy (CFL) stability condition. The temporal discretization Δt and the spatial discretization of each direction for a three-dimensional scheme Δx, Δy and Δz have to satisfy this constraint. The time-step size Δt must be small enough that it satisfies the

CFL equation (1.41) , otherwise the FDTD algorithm will become numerically unstable:

$$\Delta t \leq \frac{1}{\upsilon}\left(\frac{1}{\Delta x^2}+\frac{1}{\Delta y^2}+\frac{1}{\Delta z^2}\right)^{-1/2} \tag{1.41}$$

where $\upsilon = 1/\sqrt{\epsilon\mu}$ is the wave velocity (ϵ is the electric permittivity and μ the magnetic permeability), Δt is the size of the time-step and Δx, Δy and Δz are the size of the cell in each direction.

As the maximum time-step size is limited by minimum cell size in the computational domain, if an object of analysis has fine scale dimensions compared with wavelength, a small time-step size causes a significant increase in calculation time. Over the years, FDTD applications have been restricted to solving small structures. Obtaining accurate results for large scenarios using an explicit FDTD method requires huge amounts of computational resources such as a significant amount of time of the central-processing-unit and memory.

A physical understanding of the CFL stability constrain is that, assuming that the Yee's cell is a cube, $\Delta x = \Delta y = \Delta z \triangleq \Delta s$ and a wave is travelling at the speed of υ speed, the numerical wave takes $3\Delta t$ to propagate diagonally in the cube; that is, the wave takes three time steps to travel a distance of $\sqrt{3}\Delta s$. If a bigger time step is used for the simulation of the wave with the same propagating speed, υ, the wave will seem to have traveled further than it actually was. As time-marching approach, in the explicit FDTD method, this error will accumulate and eventually grow as time progresses resulting in an unstable system.

Chapter 2

Additive Operator Splitting method

2.1 Introduction

Yee-FDTD approach is an explicit method, it means that the iterative field values are calculated from previously known values. As it was explained in Chapter 1, explicit methods are constrained by the CFL condition. To relax the stability constraint, various time-domain techniques have been developed. Implicit FDTD methods are an alternative to the explicit FDTD method. They provide the computational stability beyond the limit of the CFL stability condition, then the total number of the time steps for the computation can be reduced compared with that for the computation of the explicit FDTD method. They are extremely useful for problems where a very fine mesh is needed over a large geometric area or problems where very fine meshes with respect to an electrical wavelength are required. Simulating electromagnetic propagation in human tissues shows the characteristics of this kind of problem. In this case the spatial cell size used to resolve the fine-scale geometric detail of the human body is orders of magnitude less than the shortest wavelength λ_{min} of the low-frequency source, and the time needed to complete the calculations of the required number of time steps, is related to the cycle time corresponding to λ_{min}.

2.2 Implicit methods

Crank-Nicolson FDTD (CN-FDTF) is an implicit marching-on-in-time (MOT) method . This algorithm manages the discretization of time and space derivatives by second-order central differences, the same as the explicit FDTD method. The difference between both methods is that in the CN-FDTD algorithm the fields affected by the curl operator are averaged in time. The computational results of the CN-FDTD method are unconditionally stable and accurate [7], but until now, this numerical technique has not been widely used in time domain electromagnetics because it requires a huge amount of arithmetic operations for the computation. Crank-Nicolson method is no longer diagonally dominant and iterative solvers require longer solution time at each FDTD iteration as it involves the inversion of huge sparse matrices. In the CN-FDTD method, a system of linear equations is represented as $AN = Q$ where A is a coefficient matrix, N is a vector with the electric field components and Q is the excitation vector. For a 3D problem, solving such an equation is very time- and memory-consuming, even though the associated matrix may be relatively sparse because the size of A is $(3(N_x-1)(N_y-1)(N_z-1)) \times (3(N_x-1)(N_y-1)(N_z-1))$ where N_x, N_y, N_z are the size of the FDTD space in x, y and z directions, respectively [8].

Alternating Direction Implicit FDTD (ADI-FDTD) method is an approximation that derived from the CN-FDTD method. Since its introduction, the ADI FDTD method has been broadly used to solve diffusion problems. This algorithm was introduced in electromagnetic simulation by Takefumi Namiki [9]. This method has been demonstrated to be unconditionally stable [10]. ADI finite difference equations are split into two procedures for a three-dimensional ADI scheme. Each procedure replaces a spatial derivative of the Maxwell's curl equations with an implicit difference approximation. Procedure one is applied for advancement from $n\Delta t$ to $(n+1/2)\Delta t$, while procedure two is used for advancement from $(n+1/2)\Delta t$ to $(n+1)\Delta t$. ADI FDTD method has to solve a tridiagonal matrix system for each equation of each field component at each half-time step. Usually the ADI-FDTD iteration is from six to eight times longer than the conventional FDTD update [11]. Because of its advantage of unconditional stability, the ADI-FDTD method has been extended for many applications and ADI FDTD scheme has brought a resurgence of interest in the unconditionally stable schemes.

Locally One Dimensional FDTD (LOD-FDTD) method is other approximation of the CN-FDTD method. This numerical technique has also been adapted as well for FDTD solutions of Maxwells equations, leading to unconditionally stable approach. The algorithm of the LOD FDTD scheme is simpler than the ADI FDTD algorithm. It leads to a reduction of the computational time [12] [13]. The number of equations to be computed in three-dimensional LOD FDTD method is the same as that with the conventional three-dimensional ADI-FDTD but with reduced arithmetic operations. In the 3D-LOD-FDTD method, the computation of each time step is split into three direction parts, such as the x direction part, the y direction part and the z direction part. Each direction part is computed individually and consecutively [14].

Splitting techniques are commonly employed in solving time-dependent partial differential equations. They are used in order to reduce problems in multiple spatial dimensions to a sequence of problems in one dimension, which are easier to solve. The Additive Operator Splitting (AOS) method is first order in time, semi-implicit and unconditionally stable with respect to its time-step. Efficient numerical schemes for nonlinear diffusion filtering in image processing based on AOS were introduced in [15] and further investigation in [16] shows its accuracy and stability. The most important advantage of the AOS approach is that it can be parallelized on the operator level in a natural way. In the 3D-AOS-FDTD method, the computation of each time step is split into three direction parts, such as the x direction part, the y direction part and the z direction part, shown in Figure 2.1. In the AOS FDTD approach each direction part is computed individually and independently of the others. Other unconditional methods such as ADI and LOD are not suitable for parallel computing, because the computing of the current fractional step (or so called intermediate step) always needs the value of the previous fractional step. In AOS method the computation of the fractional steps are independent from each other, and consequently they can be computed at the same time by parallel processors.

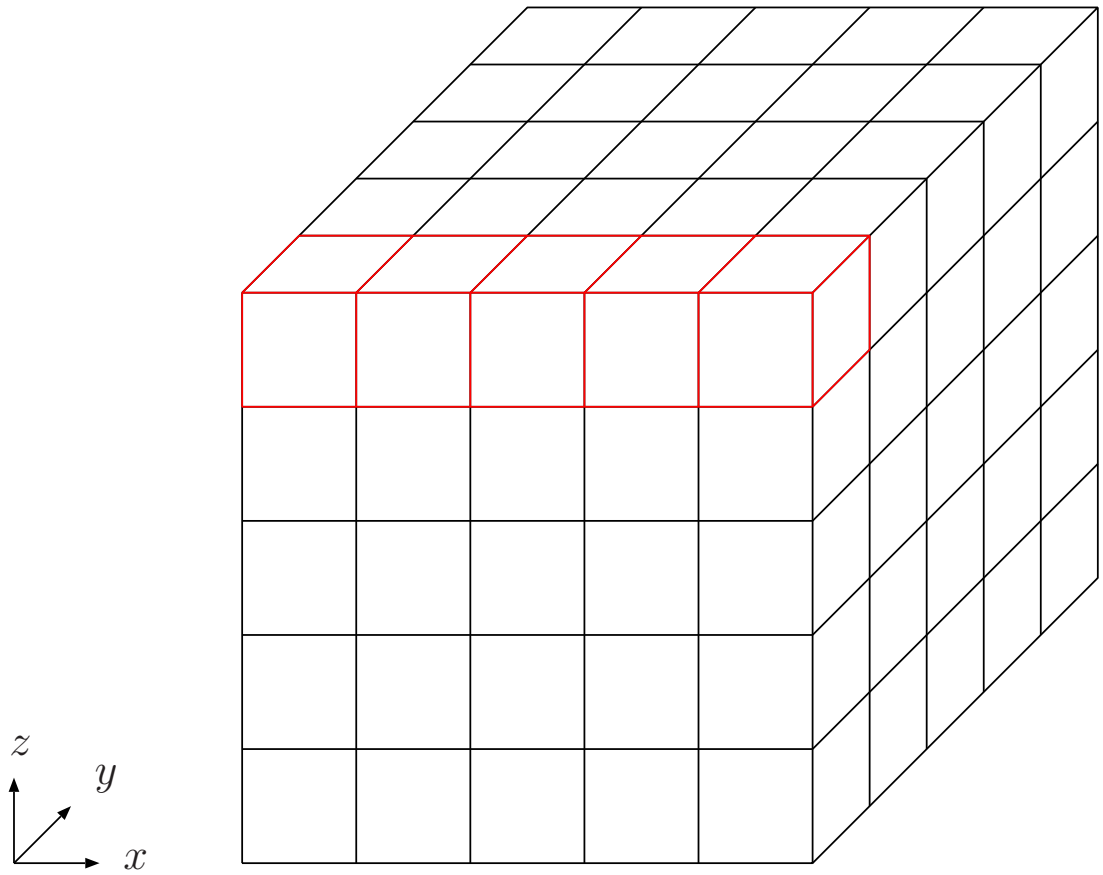

Figure 2.1: The computation of each time step is split into three direction parts, such as the x direction part, the y direction part and the z direction part. Each direction part is computed individually and consecutively.

2.3 Numerical Formulation of the 3D-AOS-FDTD method

Maxwell-Faraday's and Maxwell-Ampere's equations in lossy and frequency independent materials are given as:

$$\nabla \times \boldsymbol{E} = -\mu \frac{\partial \boldsymbol{H}}{\partial t}, \tag{2.1}$$

$$\nabla \times \boldsymbol{H} = \frac{\partial \boldsymbol{D}}{\partial t}, \tag{2.2}$$

$$\frac{\partial \boldsymbol{D}}{\partial t} = \sigma \boldsymbol{E} + \epsilon_0 \epsilon_r \frac{\partial \boldsymbol{E}}{\partial t} \tag{2.3}$$

where σ is the conductivity, μ is the permeability, ϵ_0 is the vacuum permittivity, ϵ_r is the relative permittivity, $\boldsymbol{E}$ is the electric field, $\boldsymbol{D}$ is the electric flux density and $\boldsymbol{H}$ is the magnetic field. (2.2) is Maxwell-Ampere equation without free currents.

Following the same process as given in [14], the temporal discretization and the spatial discretization are processed at the beginning of the numerical formulation. (2.1), (2.2) and (2.3) are re-written in a vectorial form as:

$$\begin{aligned} \nabla \times \boldsymbol{E} &= (\frac{\partial E_z}{\partial y} - \frac{\partial E_y}{\partial z})\boldsymbol{i}_x + (\frac{\partial E_x}{\partial z} - \frac{\partial E_z}{\partial x})\boldsymbol{i}_y + (\frac{\partial E_y}{\partial x} - \frac{\partial E_x}{\partial y})\boldsymbol{i}_z \\ &= -\mu \frac{\partial (H_x \boldsymbol{i}_x + H_y \boldsymbol{i}_y + H_z \boldsymbol{i}_z)}{\partial t}, \end{aligned} \tag{2.4}$$

$$\begin{aligned} \nabla \times \boldsymbol{H} &= (\frac{\partial H_z}{\partial y} - \frac{\partial H_y}{\partial z})\boldsymbol{i}_x + (\frac{\partial H_x}{\partial z} - \frac{\partial H_z}{\partial x})\boldsymbol{i}_y + (\frac{\partial H_y}{\partial x} - \frac{\partial H_x}{\partial y})\boldsymbol{i}_z \\ &= \frac{\partial (D_x \boldsymbol{i}_x + D_y \boldsymbol{i}_y + D_z \boldsymbol{i}_z)}{\partial t}, \end{aligned} \tag{2.5}$$

$$\begin{aligned} \frac{\partial \boldsymbol{D}}{\partial t} &= \frac{\partial (D_x \boldsymbol{i}_x + D_y \boldsymbol{i}_y + D_z \boldsymbol{i}_z)}{\partial t} \\ &= \sigma (E_x \boldsymbol{i}_x + E_y \boldsymbol{i}_y + E_z \boldsymbol{i}_z) + \epsilon_0 \epsilon_r \frac{\partial (E_x \boldsymbol{i}_x + E_y \boldsymbol{i}_y + E_z \boldsymbol{i}_z)}{\partial t}. \end{aligned} \tag{2.6}$$

where $\boldsymbol{i}_x$, $\boldsymbol{i}_y$ and $\boldsymbol{i}_z$ are the unit vectors in x, y and z directions. Then (2.4),

(2.5) and (2.6) are expressed in a scalar manner as:

$$\frac{\partial E_z}{\partial y} - \frac{\partial E_y}{\partial z} = -\mu \frac{\partial H_x}{\partial t}, \tag{2.7}$$

$$\frac{\partial E_x}{\partial z} - \frac{\partial E_z}{\partial x} = -\mu \frac{\partial H_y}{\partial t}, \tag{2.8}$$

$$\frac{\partial E_y}{\partial x} - \frac{\partial E_x}{\partial y} = -\mu \frac{\partial H_z}{\partial t}, \tag{2.9}$$

$$\frac{\partial H_z}{\partial y} - \frac{\partial H_y}{\partial z} = \frac{\partial D_x}{\partial t}, \tag{2.10}$$

$$\frac{\partial H_x}{\partial z} - \frac{\partial H_z}{\partial x} = \frac{\partial D_y}{\partial t}, \tag{2.11}$$

$$\frac{\partial H_y}{\partial x} - \frac{\partial H_x}{\partial y} = \frac{\partial D_z}{\partial t}, \tag{2.12}$$

$$\frac{\partial D_x}{\partial t} = \sigma E_x + \epsilon_0 \epsilon_r \frac{\partial E_x}{\partial t}, \tag{2.13}$$

$$\frac{\partial D_y}{\partial t} = \sigma E_y + \epsilon_0 \epsilon_r \frac{\partial E_y}{\partial t}, \tag{2.14}$$

$$\frac{\partial D_z}{\partial t} = \sigma E_z + \epsilon_0 \epsilon_r \frac{\partial E_z}{\partial t}. \tag{2.15}$$

Hear, the time and space derivatives are discretized by central differences and the fields affected by the curl operators are averaged in time, (2.7) $\sim$ (2.12) are discretized as:

$$\frac{1}{2}\left\{\frac{E_z^{n+1}(i,j+1,k)-E_z^{n+1}(i,j,k)}{\Delta y}-\frac{E_y^{n+1}(i,j,k+1)-E_y^{n+1}(i,j,k)}{\Delta z}\right. \quad +(2.16)$$
$$\left.\frac{E_z^{n}(i,j+1,k)-E_z^{n}(i,j,k)}{\Delta y}-\frac{E_y^{n}(i,j,k+1)-E_y^{n}(i,j,k)}{\Delta z}\right\} =$$
$$-\mu\frac{H_x^{n+1}(i,j,k)-H_x^{n}(i,j,k)}{\Delta t},$$
$$\frac{1}{2}\left\{\frac{E_x^{n+1}(i,j,k+1)-E_x^{n+1}(i,j,k)}{\Delta z}-\frac{E_z^{n+1}(i+1,j,k)-E_z^{n+1}(i,j,k)}{\Delta x}\right. \quad +(2.17)$$
$$\left.\frac{E_x^{n}(i,j,k+1)-E_x^{n}(i,j,k)}{\Delta z}-\frac{E_z^{n}(i+1,j,k)-E_z^{n}(i,j,k)}{\Delta x}\right\} =$$
$$-\mu\frac{H_y^{n+1}(i,j,k)-H_y^{n}(i,j,k)}{\Delta t},$$
$$\frac{1}{2}\left\{\frac{E_y^{n+1}(i+1,j,k)-E_y^{n+1}(i,j,k)}{\Delta x}-\frac{E_x^{n+1}(i,j+1,k)-E_x^{n+1}(i,j,k)}{\Delta y}\right\} \quad +(2.18)$$
$$\frac{E_y^{n}(i+1,j,k)-E_y^{n}(i,j,k)}{\Delta x}-\frac{E_x^{n}(i,j+1,k)-E_x^{n}(i,j,k)}{\Delta y} =$$
$$-\mu\frac{H_z^{n+1}(i,j,k)-H_z^{n}(i,j,k)}{\Delta t},$$

$$\frac{1}{2}\left\{\frac{H_z^{n+1}(i,j,k)-H_z^{n+1}(i,j-1,k)}{\Delta y}-\frac{H_y^{n+1}(i,j,k)-H_y^{n+1}(i,j,k-1)}{\Delta z}\right. \quad +(2.19)$$
$$\left.\frac{H_z^{n}(i,j,k)-H_z^{n}(i,j-1,k)}{\Delta y}-\frac{H_y^{n}(i,j,k)-H_y^{n}(i,j,k-1)}{\Delta z}\right\} =$$
$$\frac{D_x^{n+1}(i,j,k)-D_x^{n}(i,j,k)}{\Delta t},$$
$$\frac{1}{2}\left\{\frac{H_x^{n+1}(i,j,k)-H_x^{n+1}(i,j,k-1)}{\Delta z}-\frac{H_z^{n+1}(i,j,k)-H_z^{n+1}(i-1,j,k)}{\Delta x}\right. \quad +(2.20)$$
$$\left.\frac{H_x^{n}(i,j,k)-H_x^{n}(i,j,k-1)}{\Delta z}-\frac{H_z^{n}(i,j,k)-H_z^{n}(i-1,j,k)}{\Delta x}\right\} =$$
$$\frac{D_y^{n+1}(i,j,k)-D_y^{n}(i,j,k)}{\Delta t},$$
$$\frac{1}{2}\left\{\frac{H_y^{n+1}(i,j,k)-H_y^{n+1}(i-1,j,k)}{\Delta x}-\frac{H_x^{n+1}(i,j,k)-H_x^{n+1}(i,j-1,k)}{\Delta y}\right. \quad +(2.21)$$
$$\left.\frac{H_y^{n}(i,j,k)-H_y^{n}(i-1,j,k)}{\Delta x}-\frac{H_x^{n}(i,j,k)-H_x^{n}(i,j-1,k)}{\Delta y}\right\} =$$
$$\frac{D_z^{n+1}(i,j,k)-D_z^{n}(i,j,k)}{\Delta t}.$$

Also (2.13), (2.14) and (2.15) are discretized and the last conductivity and $\boldsymbol{E}$ term is averaged in time, then:

$$\frac{D_x^{n+1}(i,j,k) - D_x^n(i,j,k)}{\Delta t} = \sigma \frac{E_x^{n+1}(i,j,k) + E_x^n(i,j,k)}{2} + \epsilon_0 \epsilon_r \frac{E_x^{n+1}(i,j,k) - E_x^n(i,j,k)}{\Delta t}, \quad (2.22)$$

$$\frac{D_y^{n+1}(i,j,k) - D_y^n(i,j,k)}{\Delta t} = \sigma \frac{E_y^{n+1}(i,j,k) + E_y^n(i,j,k)}{2} + \epsilon_0 \epsilon_r \frac{E_y^{n+1}(i,j,k) - E_y^n(i,j,k)}{\Delta t}, \quad (2.23)$$

$$\frac{D_z^{n+1}(i,j,k) - D_z^n(i,j,k)}{\Delta t} = \sigma \frac{E_z^{n+1}(i,j,k) + E_z^n(i,j,k)}{2} + \epsilon_0 \epsilon_r \frac{E_z^{n+1}(i,j,k) - E_z^n(i,j,k)}{\Delta t}. \quad (2.24)$$

Then (2.16) $\sim$ (2.24) were split into the three direction parts. For example, (2.16) is split into the y direction part and the z direction part.
The y direction part is

$$\frac{E_z^{n+\frac{2}{3}}(i,j+1,k) - E_z^{n+\frac{2}{3}}(i,j,k)}{\Delta y} + \frac{E_z^{n+\frac{1}{3}}(i,j+1,k) - E_z^{n+\frac{1}{3}}(i,j,k)}{\Delta y} = -\mu \frac{H_x^{n+\frac{2}{3}}(i,j,k) - H_x^{n+\frac{1}{3}}(i,j,k)}{\Delta t} \quad (2.25)$$

$$\therefore H_x^{n+\frac{2}{3}}(i,j,k) = H_x^{n+\frac{1}{3}}(i,j,k) - \frac{\Delta t}{\mu \Delta y}\left[E_z^{n+\frac{2}{3}}(i,j+1,k) - E_z^{n+\frac{2}{3}}(i,j,k) + E_z^{n+\frac{1}{3}}(i,j+1,k) - E_z^{n+\frac{1}{3}}(i,j,k)\right]$$

and the z direction part is

$$-\frac{E_y^{n+1}(i,j,k+1) - E_y^{n+1}(i,j,k)}{\Delta z} - \frac{E_y^{n+\frac{2}{3}}(i,j,k+1) - E_y^{n+\frac{2}{3}}(i,j,k)}{\Delta z} = -\mu \frac{H_x^{n+1}(i,j,k) - H_x^{n+\frac{2}{3}}(i,j,k)}{\Delta t} \quad (2.26)$$

$$\therefore H_x^{n+1}(i,j,k) = H_x^{n+\frac{2}{3}}(i,j,k) + \frac{\Delta t}{\mu \Delta z}\left[E_y^{n+1}(i,j,k+1) - E_y^{n+1}(i,j,k) + E_y^{n+\frac{2}{3}}(i,j,k+1) - E_y^{n+\frac{2}{3}}(i,j,k)\right].$$

(2.17) $\sim$ (2.24) were also split into two directions.

Finally the elimination of $\boldsymbol{E}$ and $\boldsymbol{H}$ components of the following time step in the simultaneous equation of $\boldsymbol{D}$ was proceeded.
For example, $H_z^{n+\frac{2}{3}}$ and $E_x^{n+\frac{2}{3}}$ were eliminated from the y direction part of (2.19)

for the simultaneous equation of $D_x^{n+\frac{2}{3}}$. This simultaneous equation gives $D_x^{n+\frac{2}{3}}$ and then $H_z^{n+\frac{2}{3}}$ and $E_x^{n+\frac{2}{3}}$ were obtained by using $D_x^{n+\frac{2}{3}}$.

2.4 Implementation of the 3D-AOS-FDTD method

Each field value in the 3D-AOS-FDTD method has three components, such as E_x, E_y, E_z, H_x, H_y, H_z, D_x, D_y and D_z, and each component is calculated for two direction parts. The numerical formulation in Section 2.3 shows how the equation of each component is split into two direction parts in the 3D-AOS-FDTD method, so that the computation of each component has two steps in one FDTD time iteration. For example, the computation of D_x in the 3D-AOS-FDTD method has the y direction part and the z direction part, the computation of D_y has the x direction part and the z direction part and the computation of D_z has the x direction part and the y direction part. In contrast, the computation of each component in the explicit 3D-FDTD method has only one step in one FDTD time iteration, so that the amount of arithmetic operations in the 3D-AOS-FDTD method is at least twice as large as that in the explicit 3D-FDTD method.

On the other hand, because in the 3D-AOS FDTD method each part of each component is calculated independently, each component must be averaged. That means, the result from both parts of each component in the 3D-AOS-FDTD method are added and divided by two. The average of all the components take place after both direction parts of all the components have been calculated. The result of the average of each component will be the input value for both parts of the component in the next time step. Furthermore, because the independence between the calculations between the parts of the same component, those calculus can be parallelized. The 3D-AOS FDTD algorithm is shown in Figure 2.2. These extra calculations are not made in the explicit FDTD method, which means more computation time in the 3D-AOS-FDTD algorithm.

As an implicit method, in the 3D-AOS-FDTD scheme the computational parts having simultaneous linear equations, such as the computations of D_x, D_y and D_z, require a tridiagonal solver. For implementing the 3D-AOS-FDTD method the LAPACK tridiagonal solver is used [17]. Computations of a tridiagonal solver generally demands large amount of arithmetic operations, so that the computational parts having simultaneous linear equations have large number of the arithmetic operations in the 3D-AOS-FDTD method.

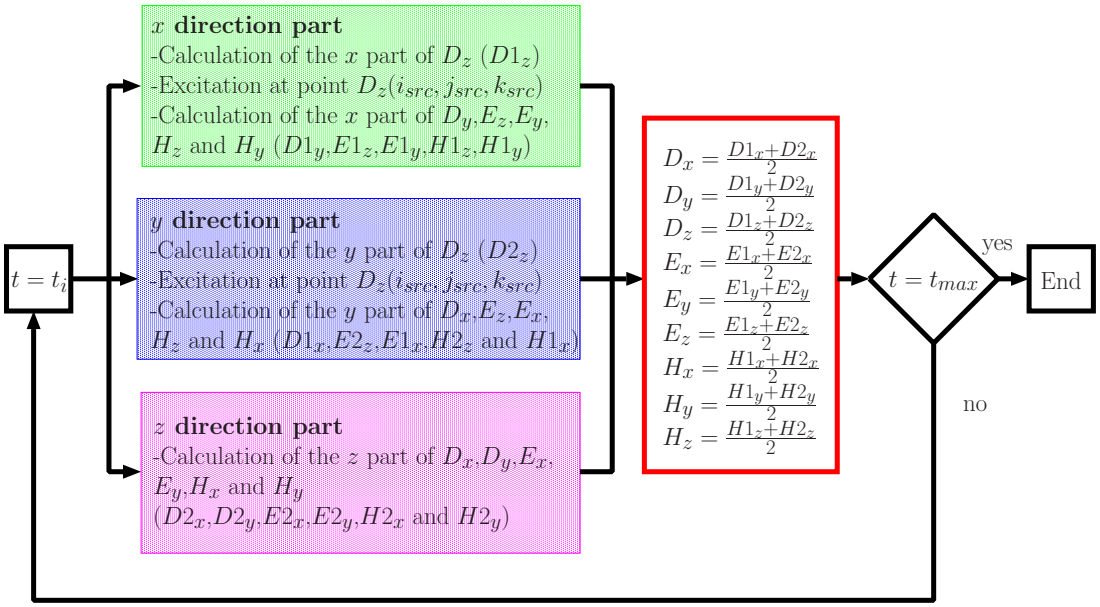

Figure 2.2: AOS FDTD algorithm. The average of the parts of a component is the input of both parts in the next time step.

Chapter 3

Frequency Dependent AOS method

3.1 Introduction

Dispersion is in first order a material property due to the fact that electromagnetic waves with different frequencies propagate at different velocities. Several techniques have been introduced recently to incorporate frequency dispersion into FDTD models. The existing frequency-dependent FDTD methods can roughly be categorized into three types:

1. methods that efficiently implement a discrete convolution of the dispersion relation $\boldsymbol{D}(r,t) = \epsilon(t) * \boldsymbol{E}(r,t)$
2. methods that discretize a differential equation relating $\boldsymbol{D}(r,t)$ to $\boldsymbol{E}(r,t)$
3. Z-transform methods

where r is the location vector and $*$ is the discrete convolution.

The three more common models of frequency dependent (FD) materials are the Debye model [18], the Lorentz model [19], and the Drude model [20]. Debye model is the most widely used for modeling the frequency characteristics of human tissues. When expressed in terms of Debye parameters, dispersive human tissue dielectric properties can be efficiently incorporated into FDTD codes. The one-pole Debye model requires less computational overhead than other models such as the Cole Cole model [21].

In this chapter, we present a new AOS FDTD formulation for frequency dependent materials, a 3D-FD-AOS-FDTD scheme.

3.2 Numerical Formulation of the 3D-FD-AOS-FDTD method

The numerical formulation of the 3D-AOS-FDTD method presented in Section 2.3 is frequency independent. The media parameters utilized for the numerical formulation, the conductivity σ, the permeability μ and the vacuum permittivity ϵ_0, are specified as constants across frequencies, which is a serious limitation. For many practical applications which involve materials of interest, these parameters vary with frequency, for example studying the phenomenon of nonuniform distribution of time-varying currents in conductor known as the skin effect or signal reflections in lossy media for microwave imaging with UltraWideBand (UWB) systems. These UWB systems typically have frequency dependent lossy media parameters [22]. To model dispersive media, adaptation of AOS-FDTD formulation to such dispersive environments is required.

The one-pole Debye model for FD media is easily introduced in the numerical formulation of the 3D-AOS-FDTD method. The steps of the numerical formulation are the same as in 3D-AOS-FDTD scheme. First the differential equations are discretized in time and space, after the equations are split into the three directions parts and finally the simultaneous equations of $\boldsymbol{D}$ are formed by the elimination of $\boldsymbol{E}$ and $\boldsymbol{H}$ from each direction part of $\boldsymbol{D}$.

3.2.1 Discretization

(2.1) is re-written in a vectorial manner as

$$\begin{aligned} \nabla \times \boldsymbol{E} &= (\frac{\partial E_z}{\partial y} - \frac{\partial E_y}{\partial z})\boldsymbol{i}_x + (\frac{\partial E_x}{\partial z} - \frac{\partial E_z}{\partial x})\boldsymbol{i}_y + (\frac{\partial E_y}{\partial x} - \frac{\partial E_x}{\partial y})\boldsymbol{i}_z \\ &= -\mu \frac{\partial (H_x \boldsymbol{i}_x + H_y \boldsymbol{i}_y + H_z \boldsymbol{i}_z)}{\partial t}. \end{aligned} \tag{3.1}$$

where $\boldsymbol{i}_x$, $\boldsymbol{i}_y$ and $\boldsymbol{i}_z$ are the unit vectors in x, y and z directions respectively.

(3.1) is expressed in a scalar manner as

$$\frac{\partial E_z}{\partial y} - \frac{\partial E_y}{\partial z} = -\mu \frac{\partial H_x}{\partial t}, \tag{3.2}$$

$$\frac{\partial E_x}{\partial z} - \frac{\partial E_z}{\partial x} = -\mu \frac{\partial H_y}{\partial t}, \tag{3.3}$$

$$\frac{\partial E_y}{\partial x} - \frac{\partial E_x}{\partial y} = -\mu \frac{\partial H_z}{\partial t}. \tag{3.4}$$

As (3.2), (3.3) and (3.4) do not have any frequency dependent part, (3.2), (3.3) and (3.4) are the same as (2.7), (2.8) and (2.9) respectively.

When the time and space derivatives are discretized by central differences while the fields affected by the curl operators are averaged in time, (3.2), (3.3) and (3.4) are discretized as (2.16), (2.17) and (2.18) respectively.

(2.2) is also re-written in a vectorial manner as

$$\begin{aligned} \nabla \times \boldsymbol{H} &= (\frac{\partial H_z}{\partial y} - \frac{\partial H_y}{\partial z})\boldsymbol{i}_x + (\frac{\partial H_x}{\partial z} - \frac{\partial H_z}{\partial x})\boldsymbol{i}_y + (\frac{\partial H_y}{\partial x} - \frac{\partial H_x}{\partial y})\boldsymbol{i}_z \\ &= \frac{\partial (D_x \boldsymbol{i}_x + D_y \boldsymbol{i}_y + D_z \boldsymbol{i}_z)}{\partial t}. \end{aligned} \tag{3.5}$$

(3.5) is expressed in a scalar manner as

$$\frac{\partial H_z}{\partial y} - \frac{\partial H_y}{\partial z} = \frac{\partial D_x}{\partial t}, \tag{3.6}$$

$$\frac{\partial H_x}{\partial z} - \frac{\partial H_z}{\partial x} = \frac{\partial D_y}{\partial t}, \tag{3.7}$$

$$\frac{\partial H_y}{\partial x} - \frac{\partial H_x}{\partial y} = \frac{\partial D_z}{\partial t}. \tag{3.8}$$

As (3.6), (3.7) and (3.8) do not have any frequency dependent part, (3.6), (3.7) and (3.8) are the same as (2.10), (2.11) and (2.12) respectively. Then (3.6), (3.7) and (3.8) are discretized as (2.19), (2.20) and (2.21) respectively.

3D-FD-AOS-FDTD is based on Faradays law, Amperes law,and the relationship between $\boldsymbol{D}$ and the electric field $\boldsymbol{E}$. When the one-pole Debye model for FD media is utilized, the relative permittivity μ is expressed as:

$$\epsilon_r = \epsilon_\infty + \frac{\epsilon_\mathrm{S} - \epsilon_\infty}{1 + \jmath\omega\tau_\mathrm{D}} \tag{3.9}$$

where ϵ_r is the complex relative permittivity, ϵ_∞ is the optical permittivity, $\epsilon_{\rm S}$ is the static permittivity, ω is the angular frequency and $\tau_{\rm D}$ is the characteristic relaxation time. (2.3) and (3.9) yield

$$\begin{aligned} \boldsymbol{D} &= (\epsilon_0\epsilon_\infty + \frac{\epsilon_0\epsilon_{\rm S} - \epsilon_0\epsilon_\infty}{1+\jmath\omega\tau_{\rm D}} - \jmath\frac{\sigma}{\omega})\boldsymbol{E} \\ &= (\epsilon_0\epsilon_\infty + \frac{\epsilon_0\epsilon_{\rm S} - \epsilon_0\epsilon_\infty}{1+\jmath\omega\tau_{\rm D}} + \frac{\sigma}{\jmath\omega})\boldsymbol{E} \\ &= \frac{(\jmath\omega)^2\epsilon_0\epsilon_\infty\tau_{\rm D} + \jmath\omega(\epsilon_0\epsilon_{\rm S} + \sigma\tau_{\rm D}) + \sigma}{\jmath\omega(1+\jmath\omega\tau_{\rm D})}\boldsymbol{E}. \end{aligned} \tag{3.10}$$

(3.10) is simplified to

$$(\jmath\omega)^2\tau_{\rm D}\boldsymbol{D} + (\jmath\omega)\boldsymbol{D} = (\jmath\omega)^2\epsilon_0\epsilon_\infty\tau_{\rm D}\boldsymbol{E} + \jmath\omega(\epsilon_0\epsilon_{\rm S} + \sigma\tau_{\rm D})\boldsymbol{E} + \sigma\boldsymbol{E}. \tag{3.11}$$

Assuming $\exp(\jmath\omega t)$ dependence and interpreting the $\jmath\omega$ terms in frequency domain as time derivatives in time domain, (3.11) can be re-written as a differential equation in time domain,

$$\frac{\partial^2(\tau_{\rm D}\boldsymbol{D})}{\partial t^2} + \frac{\partial\boldsymbol{D}}{\partial t} = \frac{\partial^2(\epsilon_0\epsilon_\infty\tau_{\rm D}\boldsymbol{E})}{\partial t^2} + \frac{\partial(\epsilon_0\epsilon_{\rm S} + \sigma\tau_{\rm D})\boldsymbol{E}}{\partial t} + \sigma\boldsymbol{E}. \tag{3.12}$$

Then (3.12) is re-written in a scalar manner,

$$\frac{\partial^2(\tau_{\rm D}D_x)}{\partial t^2} + \frac{\partial D_x}{\partial t} = \frac{\partial^2(\epsilon_0\epsilon_\infty\tau_{\rm D}E_x)}{\partial t^2} + \frac{\partial(\epsilon_0\epsilon_{\rm S} + \sigma\tau_{\rm D})E_x}{\partial t} + \sigma E_x, \tag{3.13}$$

$$\frac{\partial^2(\tau_{\rm D}D_y)}{\partial t^2} + \frac{\partial D_y}{\partial t} = \frac{\partial^2(\epsilon_0\epsilon_\infty\tau_{\rm D}E_y)}{\partial t^2} + \frac{\partial(\epsilon_0\epsilon_{\rm S} + \sigma\tau_{\rm D})E_y}{\partial t} + \sigma E_y, \tag{3.14}$$

$$\frac{\partial^2(\tau_{\rm D}D_z)}{\partial t^2} + \frac{\partial D_z}{\partial t} = \frac{\partial^2(\epsilon_0\epsilon_\infty\tau_{\rm D}E_z)}{\partial t^2} + \frac{\partial(\epsilon_0\epsilon_{\rm S} + \sigma\tau_{\rm D})E_z}{\partial t} + \sigma E_z. \tag{3.15}$$

When (3.13), (3.14) and (3.15) are discretized and the last conductivity and $\boldsymbol{E}$

term is averaged over time, we get:

$$\tau_{\mathrm{D}(i,j,k)}\frac{D_x^{n+1}(i,j,k)-2D_x^n(i,j,k)+D_x^{n-1}(i,j,k)}{(\Delta t)^2}+\frac{D_x^{n+1}(i,j,k)-D_x^n(i,j,k)}{\Delta t}= \tag{3.16}$$
$$a_{1(i,j,k)}\frac{E_x^{n+1}(i,j,k)-2E_x^n(i,j,k)+E_x^{n-1}(i,j,k)}{(\Delta t)^2}+a_{2(i,j,k)}\frac{E_x^{n+1}(i,j,k)-E_x^n(i,j,k)}{\Delta t}+$$
$$\sigma_{(i,j,k)}\frac{E_x^{n+1}(i,j,k)+E_x^n(i,j,k)}{2},$$
$$\tau_{\mathrm{D}(i,j,k)}\frac{D_y^{n+1}(i,j,k)-2D_y^n(i,j,k)+D_y^{n-1}(i,j,k)}{(\Delta t)^2}+\frac{D_y^{n+1}(i,j,k)-D_y^n(i,j,k)}{\Delta t}= \tag{3.17}$$
$$a_{1(i,j,k)}\frac{E_y^{n+1}(i,j,k)-2E_y^n(i,j,k)+E_y^{n-1}(i,j,k)}{(\Delta t)^2}+a_{2(i,j,k)}\frac{E_y^{n+1}(i,j,k)-E_y^n(i,j,k)}{\Delta t}+$$
$$\sigma_{(i,j,k)}\frac{E_y^{n+1}(i,j,k)+E_y^n(i,j,k)}{2},$$
$$\tau_{\mathrm{D}(i,j,k)}\frac{D_z^{n+1}(i,j,k)-2D_z^n(i,j,k)+D_z^{n-1}(i,j,k)}{(\Delta t)^2}+\frac{D_z^{n+1}(i,j,k)-D_z^n(i,j,k)}{\Delta t}= \tag{3.18}$$
$$a_{1(i,j,k)}\frac{E_z^{n+1}(i,j,k)-2E_z^n(i,j,k)+E_z^{n-1}(i,j,k)}{(\Delta t)^2}+a_{2(i,j,k)}\frac{E_z^{n+1}(i,j,k)-E_z^n(i,j,k)}{\Delta t}+$$
$$\sigma_{(i,j,k)}\frac{E_z^{n+1}(i,j,k)+E_z^n(i,j,k)}{2}$$

where $a_{1(i,j,k)}=\epsilon_0\epsilon_{\infty(i,j,k)}\tau_{\mathrm{D}(i,j,k)}$ and $a_{2(i,j,k)}=(\epsilon_0\epsilon_{\mathrm{S}(i,j,k)}+\sigma_{(i,j,k)}\tau_{\mathrm{D}(i,j,k)})$.

The equations of all nine components, such as E_x, E_y, E_z, H_x, H_y, H_z, D_x, D_y and D_z, are discretized in space and time.

3.2.2 Splitting

The next step is the splitting of the equations into the three directions. (2.16) is split into the y direction part and the z direction part.
The y direction part is

$$\frac{E_z^{n+\frac{2}{3}}(i,j+1,k)-E_z^{n+\frac{2}{3}}(i,j,k)}{\Delta y}+\frac{E_z^{n+\frac{1}{3}}(i,j+1,k)-E_z^{n+\frac{1}{3}}(i,j,k)}{\Delta y}= \tag{3.19}$$
$$-\mu\frac{H_x^{n+\frac{2}{3}}(i,j,k)-H_x^{n+\frac{1}{3}}(i,j,k)}{\Delta t}$$
$$\therefore H_x^{n+\frac{2}{3}}(i,j,k)=H_x^{n+\frac{1}{3}}(i,j,k)-$$
$$\frac{\Delta t}{\mu\Delta y}\left[E_z^{n+\frac{2}{3}}(i,j+1,k)-E_z^{n+\frac{2}{3}}(i,j,k)+E_z^{n+\frac{1}{3}}(i,j+1,k)-E_z^{n+\frac{1}{3}}(i,j,k)\right].$$

and the z direction part is

$$-\frac{E_y^{n+1}(i,j,k+1)-E_y^{n+1}(i,j,k)}{\Delta z}-\frac{E_y^{n+\frac{2}{3}}(i,j,k+1)-E_y^{n+\frac{2}{3}}(i,j,k)}{\Delta z}= \quad (3.20)$$
$$-\mu\frac{H_x^{n+1}(i,j,k)-H_x^{n+\frac{2}{3}}(i,j,k)}{\Delta t}$$
$$\therefore H_x^{n+1}(i,j,k)=H_x^{n+\frac{2}{3}}(i,j,k)+$$
$$\frac{\Delta t}{\mu\Delta z}\left[E_y^{n+1}(i,j,k+1)-E_y^{n+1}(i,j,k)+E_y^{n+\frac{2}{3}}(i,j,k+1)-E_y^{n+\frac{2}{3}}(i,j,k)\right].$$

(2.17) is split into the x direction part and the z direction part.
The x direction part is

$$-\frac{E_z^{n+\frac{1}{3}}(i+1,j,k)-E_z^{n+\frac{1}{3}}(i,j,k)}{\Delta x}-\frac{E_z^{n}(i+1,j,k)-E_z^{n}(i,j,k)}{\Delta x}= \quad (3.21)$$
$$-\mu\frac{H_y^{n+\frac{1}{3}}(i,j,k)-H_y^{n}(i,j,k)}{\frac{1}{2}\Delta t}$$
$$\therefore H_y^{n+\frac{1}{3}}(i,j,k)=H_y^{n}(i,j,k)+$$
$$\frac{\frac{1}{2}\Delta t}{\mu\Delta z}\left[E_z^{n+\frac{1}{3}}(i+1,j,k)-E_z^{n+\frac{1}{3}}(i,j,k)+E_z^{n}(i+1,j,k)-E_z^{n}(i,j,k)\right]$$

and the z direction part is

$$\frac{E_x^{n+1}(i,j,k+1)-E_x^{n+1}(i,j,k)}{\Delta z}+\frac{E_x^{n+\frac{2}{3}}(i,j,k+1)-E_x^{n+\frac{2}{3}}(i,j,k)}{\Delta z}= \quad (3.22)$$
$$-\mu\frac{H_y^{n+1}(i,j,k)-H_y^{n+\frac{2}{3}}(i,j,k)}{\Delta t}$$
$$\therefore H_y^{n+1}(i,j,k)=H_y^{n+\frac{2}{3}}(i,j,k)-$$
$$\frac{\Delta t}{\mu\Delta z}\left[E_x^{n+1}(i,j,k+1)-E_x^{n+1}(i,j,k)+E_x^{n+\frac{2}{3}}(i,j,k+1)-E_x^{n+\frac{2}{3}}(i,j,k)\right].$$

(2.18) is split into the x direction part and the y direction part.

The x direction part is

$$\frac{E_y^{n+\frac{1}{3}}(i+1,j,k)-E_y^{n+\frac{1}{3}}(i,j,k)}{\Delta x}+\frac{E_y^{n}(i+1,j,k)-E_y^{n}(i,j,k)}{\Delta x}= \tag{3.23}$$
$$-\mu\frac{H_z^{n+\frac{1}{3}}(i,j,k)-H_z^{n}(i,j,k)}{\Delta t}$$
$$\therefore H_z^{n+\frac{1}{3}}(i,j,k)=H_z^{n}(i,j,k)-$$
$$\frac{\Delta t}{\mu\Delta x}\left[E_y^{n+\frac{1}{3}}(i+1,j,k)-E_y^{n+\frac{1}{3}}(i,j,k)+E_y^{n}(i+1,j,k)-E_y^{n}(i,j,k)\right]$$

and the y direction part is

$$-\frac{E_x^{n+\frac{2}{3}}(i,j+1,k)-E_x^{n+\frac{2}{3}}(i,j,k)}{\Delta y}-\frac{E_x^{n+\frac{1}{3}}(i,j+1,k)-E_x^{n+\frac{1}{3}}(i,j,k)}{\Delta y}= \tag{3.24}$$
$$-\mu\frac{H_z^{n+\frac{2}{3}}(i,j,k)-H_z^{n+\frac{1}{3}}(i,j,k)}{\Delta t}$$
$$\therefore H_z^{n+\frac{2}{3}}(i,j,k)=H_z^{n+\frac{1}{3}}(i,j,k)+$$
$$\frac{\Delta t}{\mu\Delta y}\left[E_x^{n+\frac{2}{3}}(i,j+1,k)-E_x^{n+\frac{2}{3}}(i,j,k)+E_x^{n+\frac{1}{3}}(i,j+1,k)-E_x^{n+\frac{1}{3}}(i,j,k)\right].$$

(2.19) is split into the y direction part and the z direction part.
The y direction part is

$$\frac{H_z^{n+\frac{2}{3}}(i,j,k)-H_z^{n+\frac{2}{3}}(i,j-1,k)}{\Delta y}+\frac{H_z^{n+\frac{1}{3}}(i,j,k)-H_z^{n+\frac{1}{3}}(i,j-1,k)}{\Delta y}= \tag{3.25}$$
$$\frac{D_x^{n+\frac{2}{3}}(i,j,k)-D_x^{n+\frac{1}{3}}(i,j,k)}{\Delta t}$$
$$\therefore D_x^{n+\frac{2}{3}}(i,j,k)=D_x^{n+\frac{1}{3}}(i,j,k)+$$
$$\frac{\Delta t}{\Delta y}\left[H_z^{n+\frac{2}{3}}(i,j,k)-H_z^{n+\frac{2}{3}}(i,j-1,k)+H_z^{n+\frac{1}{3}}(i,j,k)-H_z^{n+\frac{1}{3}}(i,j-1,k)\right]$$

and the z direction part is

$$-\frac{H_y^{n+1}(i,j,k)-H_y^{n+1}(i,j,k-1)}{\Delta z}-\frac{H_y^{n+\frac{2}{3}}(i,j,k)-H_y^{n+\frac{2}{3}}(i,j,k-1)}{\Delta z}= \tag{3.26}$$
$$\frac{D_x^{n+1}(i,j,k)-D_x^{n+\frac{2}{3}}(i,j,k)}{\Delta t}$$
$$\therefore D_x^{n+1}(i,j,k)=D_x^{n+\frac{2}{3}}(i,j,k)-$$
$$\frac{\Delta t}{\Delta z}\left[H_y^{n+1}(i,j,k)-H_y^{n+1}(i,j,k-1)+H_y^{n+\frac{2}{3}}(i,j,k)-H_y^{n+\frac{2}{3}}(i,j,k-1)\right].$$

(2.20) is split into the x direction part and the z direction part. The x direction part is

$$-\frac{H_z^{n+\frac{1}{3}}(i,j,k)-H_z^{n+\frac{1}{3}}(i-1,j,k)}{\Delta x}-\frac{H_z^{n}(i,j,k)-H_z^{n}(i-1,j,k)}{\Delta x}= \tag{3.27}$$

$$\frac{D_y^{n+\frac{1}{3}}(i,j,k)-D_y^{n}(i,j,k)}{\Delta t}$$

$$\therefore D_y^{n+\frac{1}{3}}(i,j,k)=D_y^{n}(i,j,k)-$$

$$\frac{\Delta t}{\Delta z}\left[H_z^{n+\frac{1}{3}}(i,j,k)-H_z^{n+\frac{1}{3}}(i-1,j,k)+H_z^{n}(i,j,k)-H_z^{n}(i-1,j,k)\right]$$

and the z direction part is

$$\frac{H_x^{n+1}(i,j,k)-H_x^{n+1}(i,j,k-1)}{\Delta z}+\frac{H_x^{n+\frac{2}{3}}(i,j,k)-H_x^{n+\frac{2}{3}}(i,j,k-1)}{\Delta z}= \tag{3.28}$$

$$\frac{D_y^{n+1}(i,j,k)-D_y^{n+\frac{2}{3}}(i,j,k)}{\Delta t}$$

$$\therefore D_y^{n+1}(i,j,k)=D_y^{n+\frac{2}{3}}(i,j,k)+$$

$$\frac{\Delta t}{\Delta z}\left[H_x^{n+1}(i,j,k)-H_x^{n+1}(i,j,k-1)+H_x^{n+\frac{2}{3}}(i,j,k)-H_x^{n+\frac{2}{3}}(i,j,k-1)\right].$$

(2.21) is split into the x direction part and the y direction part. The x direction part is

$$\frac{H_y^{n+\frac{1}{3}}(i,j,k)-H_y^{n+\frac{1}{3}}(i-1,j,k)}{\Delta x}+\frac{H_y^{n}(i,j,k)-H_y^{n}(i-1,j,k)}{\Delta x}= \tag{3.29}$$

$$\frac{D_z^{n+\frac{1}{3}}(i,j,k)-D_z^{n}(i,j,k)}{\Delta t}$$

$$\therefore D_z^{n+\frac{1}{3}}(i,j,k)=D_z^{n}(i,j,k)+$$

$$\frac{\Delta t}{\Delta x}\left[H_y^{n+\frac{1}{3}}(i,j,k)-H_y^{n+\frac{1}{3}}(i-1,j,k)+H_y^{n}(i,j,k)-H_y^{n}(i-1,j,k)\right]$$

and the y direction part is

$$-\frac{H_x^{n+\frac{2}{3}}(i,j,k)-H_x^{n+\frac{2}{3}}(i,j-1,k)}{\Delta y}-\frac{H_x^{n+\frac{1}{3}}(i,j,k)-H_x^{n+\frac{1}{3}}(i,j-1,k)}{\Delta y}= \quad (3.30)$$

$$\frac{D_z^{n+\frac{2}{3}}(i,j,k)-D_z^{n+\frac{1}{3}}(i,j,k)}{\Delta t}$$

$$\therefore D_z^{n+\frac{2}{3}}(i,j,k)=D_z^{n+\frac{1}{3}}(i,j,k)-$$

$$\frac{\Delta t}{\Delta y}\left[H_x^{n+\frac{2}{3}}(i,j,k)-H_x^{n+\frac{2}{3}}(i,j-1,k)+H_x^{n+\frac{1}{3}}(i,j,k)-H_x^{n+\frac{1}{3}}(i,j-1,k)\right].$$

(3.16) is modified to be used in the y direction part in (3.24) and the z direction part in (3.22).
The y direction part is

$$\tau_{\mathrm{D}(i,j,k)}\frac{D_x^{n+\frac{2}{3}}(i,j,k)-2D_x^{n+\frac{1}{3}}(i,j,k)+D_x^{n}(i,j,k)}{\Delta t^2}+\frac{D_x^{n+\frac{2}{3}}(i,j,k)-D_x^{n+\frac{1}{3}}(i,j,k)}{\Delta t}= \quad (3.31)$$

$$a_{1(i,j,k)}\frac{E_x^{n+\frac{2}{3}}(i,j,k)-2E_x^{n+\frac{1}{3}}(i,j,k)+E_x^{n}(i,j,k)}{(\Delta t^2}+a_{2(i,j,k)}\frac{E_x^{n+\frac{2}{3}}(i,j,k)-E_x^{n+\frac{1}{3}}(i,j,k)}{\Delta t}$$

$$+\sigma_{(i,j,k)}\frac{E_x^{n+\frac{2}{3}}(i,j,k)+E_x^{n+\frac{1}{3}}(i,j,k)}{2}$$

$$\therefore E_x^{n+\frac{2}{3}}(i,j,k)=c_{1(i,j,k)}D_x^{n+\frac{2}{3}}(i,j,k)-c_{2(i,j,k)}D_x^{n+\frac{1}{3}}(i,j,k)+c_{3(i,j,k)}D_x^{n}(i,j,k)+$$

$$c_{4(i,j,k)}E_x^{n+\frac{1}{3}}(i,j,k)-c_{5(i,j,k)}E_x^{n}(i,j,k),$$

where

$$c_{1(i,j,k)}=\frac{\tau_{\mathrm{D}(i,j,k)}+\Delta t}{\epsilon_0\epsilon_{\infty(i,j,k)}\tau_{\mathrm{D}(i,j,k)}+\Delta t(\epsilon_0\epsilon_{\mathrm{S}(i,j,k)}+\sigma_{(i,j,k)}\tau_{\mathrm{D}(i,j,k)})+\frac{\Delta t^2\sigma_{(i,j,k)}}{2}},$$

$$c_{2(i,j,k)}=\frac{2\tau_{\mathrm{D}(i,j,k)}+\Delta t}{\epsilon_0\epsilon_{\infty(i,j,k)}\tau_{\mathrm{D}(i,j,k)}+\Delta t(\epsilon_0\epsilon_{\mathrm{S}(i,j,k)}+\sigma_{(i,j,k)}\tau_{\mathrm{D}(i,j,k)})+\frac{\Delta t^2\sigma_{(i,j,k)}}{2}},$$

$$c_{3(i,j,k)}=\frac{\tau_{\mathrm{D}(i,j,k)}}{\epsilon_0\epsilon_{\infty(i,j,k)}\tau_{\mathrm{D}(i,j,k)}+\frac{1}{2}\Delta t(\epsilon_0\epsilon_{\mathrm{S}(i,j,k)}+\sigma_{(i,j,k)}\tau_{\mathrm{D}(i,j,k)})+\frac{\Delta t^2\sigma_{(i,j,k)}}{2}},$$

$$c_{4(i,j,k)}=\frac{2\epsilon_0\epsilon_{\infty(i,j,k)}\tau_{\mathrm{D}(i,j,k)}+\Delta t(\epsilon_0\epsilon_{\mathrm{S}(i,j,k)}+\sigma_{(i,j,k)}\tau_{\mathrm{D}(i,j,k)})-\frac{\Delta t^2\sigma_{(i,j,k)}}{2}}{\epsilon_0\epsilon_{\infty(i,j,k)}\tau_{\mathrm{D}(i,j,k)}+\Delta t(\epsilon_0\epsilon_{\mathrm{S}(i,j,k)}+\sigma_{(i,j,k)}\tau_{\mathrm{D}(i,j,k)})+\frac{\Delta t^2\sigma_{(i,j,k)}}{2}},$$

$$c_{5(i,j,k)}=\frac{\epsilon_0\epsilon_{\infty(i,j,k)}\tau_{\mathrm{D}(i,j,k)}}{\epsilon_0\epsilon_{\infty(i,j,k)}\tau_{\mathrm{D}(i,j,k)}+\Delta t(\epsilon_0\epsilon_{\mathrm{S}(i,j,k)}+\sigma_{(i,j,k)}\tau_{\mathrm{D}(i,j,k)})+\frac{\Delta t^2\sigma_{(i,j,k)}}{2}}.$$

and the z direction part is

$$\tau_{\mathrm{D}(i,j,k)}\frac{D_x^{n+1}(i,j,k)-2D_x^{n+\frac{2}{3}}(i,j,k)+D_x^{n+\frac{1}{3}}(i,j,k)}{\Delta t^2}+\frac{D_x^{n+1}(i,j,k)-D_x^{n+\frac{2}{3}}(i,j,k)}{\Delta t}= \tag{3.32}$$
$$a_{1(i,j,k)}\frac{E_x^{n+1}(i,j,k)-2E_x^{n+\frac{2}{3}}(i,j,k)+E_x^{n+\frac{1}{3}}(i,j,k)}{\Delta t^2}+a_{2(i,j,k)}\frac{E_x^{n+1}(i,j,k)-E_x^{n+\frac{2}{3}}(i,j,k)}{\Delta t}+$$
$$\sigma_{(i,j,k)}\frac{E_x^{n+1}(i,j,k)+E_x^{n+\frac{2}{3}}(i,j,k)}{2}$$
$$\therefore E_x^{n+1}(i,j,k)=c_{1(i,j,k)}D_x^{n+1}(i,j,k)-c_{2(i,j,k)}D_x^{n+\frac{2}{3}}(i,j,k)+c_{3(i,j,k)}D_x^{n+\frac{1}{3}}(i,j,k)+$$
$$c_{4(i,j,k)}E_x^{n+\frac{2}{3}}(i,j,k)-c_{5(i,j,k)}E_x^{n+\frac{1}{3}}(i,j,k).$$

(3.17) is modified to be used in the x direction part in (3.23) and the z direction part in (3.20).
The x direction part is

$$\tau_{\mathrm{D}(i,j,k)}\frac{D_y^{n+\frac{1}{3}}(i,j,k)-2D_y^{n}(i,j,k)+D_y^{n-\frac{1}{3}}(i,j,k)}{\Delta t^2}+\frac{D_y^{n+\frac{1}{3}}(i,j,k)-D_y^{n}(i,j,k)}{\Delta t}= \tag{3.33}$$
$$a_{1(i,j,k)}\frac{E_y^{n+\frac{1}{3}}(i,j,k)-2E_y^{n}(i,j,k)+E_y^{n-\frac{1}{3}}(i,j,k)}{\Delta t^2}+a_{2(i,j,k)}\frac{E_y^{n+\frac{1}{3}}(i,j,k)-E_y^{n}(i,j,k)}{\Delta t}+$$
$$\sigma_{(i,j,k)}\frac{E_y^{n+\frac{1}{3}}(i,j,k)+E_y^{n}(i,j,k)}{2}$$
$$\therefore E_y^{n+\frac{1}{3}}(i,j,k)=c_{1(i,j,k)}D_y^{n+\frac{1}{3}}(i,j,k)-c_{2(i,j,k)}D_y^{n}(i,j,k)+c_{3(i,j,k)}D_y^{n-\frac{1}{3}}(i,j,k)+$$
$$c_{4(i,j,k)}E_y^{n}(i,j,k)-c_{5(i,j,k)}E_y^{n-\frac{1}{3}}(i,j,k)$$

and the z direction part is

$$\tau_{\mathrm{D}(i,j,k)}\frac{D_y^{n+1}(i,j,k)-2D_y^{n+\frac{2}{3}}(i,j,k)+D_y^{n+\frac{1}{3}}(i,j,k)}{\Delta t^2}+\frac{D_y^{n+1}(i,j,k)-D_y^{n+\frac{2}{3}}(i,j,k)}{\Delta t}= \tag{3.34}$$
$$a_{1(i,j,k)}\frac{E_y^{n+1}(i,j,k)-2E_y^{n+\frac{2}{3}}(i,j,k)+E_y^{n+\frac{1}{3}}(i,j,k)}{\Delta t^2}+a_{2(i,j,k)}\frac{E_y^{n+1}(i,j,k)-E_y^{n+\frac{2}{3}}(i,j,k)}{\Delta t}$$
$$+\sigma_{(i,j,k)}\frac{E_y^{n+1}(i,j,k)+E_y^{n+\frac{2}{3}}(i,j,k)}{2}$$
$$\therefore E_y^{n+1}(i,j,k)=c_{1(i,j,k)}D_y^{n+1}(i,j,k)-c_{2(i,j,k)}D_y^{n+\frac{2}{3}}(i,j,k)+c_{3(i,j,k)}D_y^{n+\frac{1}{3}}(i,j,k)+$$
$$c_{4(i,j,k)}E_y^{n+\frac{2}{3}}(i,j,k)-c_{5(i,j,k)}E_y^{n+\frac{1}{3}}(i,j,k)$$

(3.18) is modified to be used in the x direction part in (3.21) and the y direction part in (3.19).

The x direction part

$$\tau_{\mathrm{D}(i,j,k)} \frac{D_z^{n+\frac{1}{3}}(i,j,k) - 2D_z^n(i,j,k) + D_z^{n-\frac{1}{3}}(i,j,k)}{\Delta t^2} + \frac{D_z^{n+\frac{1}{3}}(i,j,k) - D_z^n(i,j,k)}{\Delta t} = \tag{3.35}$$
$$a_{1(i,j,k)} \frac{E_z^{n+\frac{1}{3}}(i,j,k) - 2E_z^n(i,j,k) + E_z^{n-\frac{1}{3}}(i,j,k)}{\Delta t^2} + a_{2(i,j,k)} \frac{E_z^{n+\frac{1}{3}}(i,j,k) - E_z^n(i,j,k)}{\Delta t} +$$
$$\sigma_{(i,j,k)} \frac{E_z^{n+\frac{1}{3}}(i,j,k) + E_z^n(i,j,k)}{2}$$
$$\therefore E_z^{n+\frac{1}{3}}(i,j,k) = c_{1(i,j,k)} D_z^{n+\frac{1}{3}}(i,j,k) - c_{2(i,j,k)} D_z^n(i,j,k) + c_{3(i,j,k)} D_z^{n-\frac{1}{3}}(i,j,k) +$$
$$c_{4(i,j,k)} E_z^n(i,j,k) - c_{5(i,j,k)} E_z^{n-\frac{1}{3}}(i,j,k)$$

and the y direction part

$$\tau_{\mathrm{D}(i,j,k)} \frac{D_z^{n+\frac{2}{3}}(i,j,k) - 2D_z^{n+\frac{1}{3}}(i,j,k) + D_z^n(i,j,k)}{\Delta t^2} + \frac{D_z^{n+\frac{2}{3}}(i,j,k) - D_z^{n+\frac{1}{3}}(i,j,k)}{\Delta t} = \tag{3.36}$$
$$a_{1(i,j,k)} \frac{E_z^{n+\frac{2}{3}}(i,j,k) - 2E_z^{n+\frac{1}{3}}(i,j,k) + E_z^n(i,j,k)}{\Delta t^2} + a_{2(i,j,k)} \frac{E_z^{n+\frac{2}{3}}(i,j,k) - E_z^{n+\frac{1}{3}}(i,j,k)}{\Delta t}$$
$$+\sigma_{(i,j,k)} \frac{E_z^{n+\frac{2}{3}}(i,j,k) + E_z^{n+\frac{1}{3}}(i,j,k)}{2}$$
$$\therefore E_z^{n+\frac{2}{3}}(i,j,k) = c_{1(i,j,k)} D_z^{n+\frac{2}{3}}(i,j,k) - c_{2(i,j,k)} D_z^{n+\frac{1}{3}}(i,j,k) + c_{3(i,j,k)} D_z^n(i,j,k) +$$
$$c_{4(i,j,k)} E_z^{n+\frac{1}{3}}(i,j,k) - c_{5(i,j,k)} E_z^n(i,j,k)$$

The computation of $\boldsymbol{D}$, $\boldsymbol{E}$ and $\boldsymbol{H}$ are split into the x direction part, the y direction part and the z direction part. The x direction part, the y direction part and the z direction part are computed in one FDTD time step successively.

3.2.3 Elimination

(3.19) $\sim$ (3.36) are the implicit form, so that the elimination of H and E components of the further time step was enabled for the simultaneous equation of D.

For example, (3.27) is used to form the simultaneous equation of $D_y^{n+\frac{1}{3}}(i,j,k)$ for the x direction part. $H_z^{n+\frac{1}{3}}$ in (3.27) is eliminated by using (3.23) and $E_y^{n+\frac{1}{3}}$ in (3.23) is eliminated by using (3.33). $H_z^{n+\frac{1}{3}}$ and $E_y^{n+\frac{1}{3}}$ were obtained by using $D_x^{n+\frac{1}{3}}$, which is given by the the simultaneous equation of $D_y^{n+\frac{1}{3}}(i,j,k)$.

Also (3.29) is used to form the simultaneous equation of $D_z^{n+\frac{1}{3}}(i,j,k)$ for the x direction part. (3.25) is used to form the simultaneous equation of $D_x^{n+\frac{2}{3}}(i,j,k)$ and (3.30) is used to form the simultaneous equation of $D_z^{n+\frac{2}{3}}(i,j,k)$ for the y direction part. (3.26) is used to form the simultaneous equation of $D_x^{n+1}(i,j,k)$

and (3.28) is used to form the simultaneous equation of $D_y^{n+1}(i,j,k)$ for the z direction part.

3.2.3.1 X direction

(3.33) is put into (3.23) to remove $E_y^{n+\frac{1}{3}}(i+1,j,k)$ and $E_y^{n+\frac{1}{3}}(i,j,k)$. This yields

$$\begin{aligned} H_z^{n+\frac{1}{3}}(i,j,k) = \\ -d_1c_{1(i+1,j,k)}D_y^{n+\frac{1}{3}}(i+1,j,k) + d_1c_{2(i+1,j,k)}D_y^{n}(i+1,j,k) - \\ d_1c_{3(i+1,j,k)}D_y^{n-\frac{1}{3}}(i+1,j,k) - \\ (d_1c_{4(i+1,j,k)}+d_1)E_y^{n}(i+1,j,k) + d_1c_5E_y^{n-\frac{1}{3}}(i+1,j,k) + \\ d_1c_{1(i,j,k)}D_y^{n+\frac{1}{3}}(i,j,k) - d_1c_{2(i,j,k)}D_y^{n}(i,j,k) + \\ d_1c_{3(i,j,k)}D_y^{n-\frac{1}{3}}(i,j,k) + \\ (d_1c_{4(i,j,k)}+d_1)E_y^{n}(i,j,k) - d_1c_{5(i,j,k)}E_y^{n-\frac{1}{3}}(i,j,k) + H_z^{n}(i,j,k) \end{aligned} \tag{3.37}$$

where $d_1 = \frac{\Delta t}{\mu \Delta x}$.

(3.37) is put into (3.27) to remove $H_z^{n+\frac{1}{3}}(i,j,k)$ and $H_z^{n+\frac{1}{3}}(i-1,j,k)$. This yields

$$\begin{aligned} d_1c_{1(i+1,j,k)}D_y^{n+\frac{1}{3}}(i+1,j,k) - (2d_1c_{1(i,j,k)} + \frac{\Delta x}{\Delta t})D_y^{n+\frac{1}{3}}(i,j,k) + \\ d_1c_{1(i-1,j,k)}D_y^{n+\frac{1}{3}}(i-1,j,k) = \\ d_1c_{2(i+1,j,k)}D_y^{n}(i+1,j,k) - (2d_1c_{2(i,j,k)} + \frac{\Delta x}{\Delta t})D_y^{n}(i,j,k) + \\ d_1c_{2(i-1,j,k)}D_y^{n}(i-1,j,k) - \\ d_1c_{3(i+1,j,k)}D_y^{n-\frac{1}{3}}(i+1,j,k) + 2d_1c_{3(i,j,k)}D_y^{n-\frac{1}{3}}(i,j,k) - \\ d_1c_{3(i-1,j,k)}D_y^{n-\frac{1}{3}}(i-1,j,k) - \\ (d_1c_{4(i+1,j,k)}+d_1)E_y^{n}(i+1,j,k) + 2(d_1c_{4(i,j,k)}+d_1)E_y^{n}(i,j,k) - \\ (d_1c_{4(i-1,j,k)}+d_1)E_y^{n}(i-1,j,k) + \\ d_1c_{5(i+1,j,k)}E_y^{n-\frac{1}{3}}(i+1,j,k) - 2d_1c_{5(i,j,k)}E_y^{n-\frac{1}{3}}(i,j,k) + \\ d_1c_{5(i-1,j,k)}E_y^{n-\frac{1}{3}}(i-1,j,k) + \\ 2H_z^{n}(i,j,k) - 2H_z^{n}(i-1,j,k) \end{aligned} \tag{3.38}$$

(3.38) is the simultaneous equations. Thus, $D_y^{n+\frac{1}{3}}(i,j,k)$ is obtained through solving (3.38). $D_y^{n+\frac{1}{3}}(i,j,k)$ solved in (3.38) and (3.33) produce $E_y^{n+\frac{1}{3}}(i,j,k)$ and this $E_y^{n+\frac{1}{3}}(i,j,k)$ and (3.23) produce $H_z^{n+\frac{1}{3}}(i,j,k)$.

(3.35) is put into (3.21) to remove $E_z^{n+\frac{1}{3}}(i+1,j,k)$ and $E_z^{n+\frac{1}{3}}(i,j,k)$. This yields

$$\begin{aligned} H_y^{n+\frac{1}{3}}(i,j,k) = \quad (3.39)\\ d_1c_{1(i+1,j,k)}D_z^{n+\frac{1}{3}}(i+1,j,k) - d_1c_{2(i+1,j,k)}D_z^{n}(i+1,j,k) +\\ d_1c_{3(i+1,j,k)}D_z^{n-\frac{1}{3}}(i+1,j,k) +\\ (d_1c_{4(i+1,j,k)} + d_1)E_z^{n}(i+1,j,k) - d_1c_{5(i+1,j,k)}E_z^{n-\frac{1}{3}}(i+1,j,k) -\\ d_1c_{1(i,j,k)}D_z^{n+\frac{1}{3}}(i,j,k) + d_1c_{2(i,j,k)}D_z^{n}(i,j,k) -\\ d_1c_{3(i,j,k)}D_z^{n-\frac{1}{3}}(i,j,k) -\\ (d_1c_{4(i,j,k)} + d_1)E_z^{n}(i,j,k) + d_1c_{5(i,j,k)}E_z^{n-\frac{1}{3}}(i,j,k) + H_y^{n}(i,j,k) \end{aligned}$$

(3.39) is put into (3.29) to remove $H_y^{n+\frac{1}{3}}(i,j,k)$ and $H_y^{n+\frac{1}{3}}(i-1,j,k)$. This yields

$$\begin{aligned} d_1c_{1(i+1,j,k)}D_z^{n+\frac{1}{3}}(i+1,j,k) - (2d_1c_{2(i,j,k)} + \frac{\Delta x}{\Delta t})D_z^{n+\frac{1}{3}}(i,j,k) + \quad (3.40)\\ d_1c_{1(i-1,j,k)}D_z^{n+\frac{1}{3}}(i-1,j,k) =\\ d_1c_{2(i+1,j,k)}D_z^{n}(i+1,j,k) - (2d_1c_{2(i,j,k)} + \frac{\Delta x}{\Delta t})D_z^{n}(i,j,k) +\\ d_1c_{2(i-1,j,k)}D_z^{n}(i-1,j,k) -\\ d_1c_{3(i+1,j,k)}D_z^{n-\frac{1}{3}}(i+1,j,k) + 2d_1c_{3(i,j,k)}D_z^{n-\frac{1}{3}}(i,j,k) -\\ d_1c_{3(i-1,j,k)}D_z^{n-\frac{1}{3}}(i-1,j,k) -\\ (d_1c_{4(i+1,j,k)} + d_1)E_z^{n}(i+1,j,k) + 2(d_1c_{4(i,j,k)} + d_1)E_z^{n}(i,j,k) -\\ (d_1c_{4(i-1,j,k)} + d_1)E_z^{n}(i-1,j,k) +\\ d_1c_{5(i+1,j,k)}E_z^{n-\frac{1}{3}}(i+1,j,k) - 2d_1c_{5(i,j,k)}E_z^{n-\frac{1}{3}}(i,j,k) +\\ d_1c_{5(i-1,j,k)}E_z^{n-\frac{1}{3}}(i-1,j,k) -\\ 2H_y^{n}(i,j,k) + 2H_y^{n}(i-1,j,k) \end{aligned}$$

(3.40) is the simultaneous equations. Thus, $D_z^{n+\frac{1}{3}}(i,j,k)$ is obtained through

solving (3.40). $D_z^{n+\frac{1}{3}}(i,j,k)$ solved in (3.40) and (3.35) produce $E_z^{n+\frac{1}{3}}(i,j,k)$ and this $E_z^{n+\frac{1}{3}}(i,j,k)$ and (3.21) produce $H_y^{n+\frac{1}{3}}(i,j,k)$.

3.2.3.2 Y direction

(3.36) is put into (3.19) to remove $E_z^{n+\frac{2}{3}}(i+1,j,k)$ and $E_z^{n+\frac{2}{3}}(i,j,k)$. This yields

$$\begin{aligned} H_x^{n+\frac{2}{3}}(i,j,k) = \\ -d_2c_{1(i,j+1,k)}D_z^{n+\frac{2}{3}}(i,j+1,k) + d_2c_{2(i,j+1,k)}D_z^{n+\frac{1}{3}}(i,j+1,k) - \\ d_2c_{3(i,j+1,k)}D_z^{n}(i,j+1,k) - \\ (d_2c_{4(i,j+1,k)}+d_2)E_z^{n+\frac{1}{3}}(i,j+1,k) + d_2c_{5(i,j+1,k)}E_z^{n}(i,j+1,k) + \\ d_2c_{1(i,j,k)}D_z^{n+\frac{2}{3}}(i,j,k) - d_2c_{2(i,j,k)}D_z^{n+\frac{1}{3}}(i,j,k) + \\ d_2c_{3(i,j,k)}D_z^{n}(i,j,k) + \\ (d_2c_{4(i,j,k)}+d_2)E_z^{n+\frac{1}{3}}(i,j,k) - d_2c_{5(i,j,k)}E_z^{n}(i,j,k) + H_x^{n+\frac{1}{3}}(i,j,k). \end{aligned} \tag{3.41}$$

where $d_2 = \frac{\Delta t}{\mu \Delta y}$.

(3.41) is put into (3.30) to remove $H_x^{n+\frac{2}{3}}(i,j,k)$ and $H_x^{n+\frac{2}{3}}(i,j-1,k)$. This yields

$$\begin{aligned} d_2c_{1(i,j+1,k)}D_z^{n+\frac{2}{3}}(i,j+1,k) - (2d_2c_{2(i,j,k)} + \frac{\Delta y}{\Delta t})D_z^{n+\frac{2}{3}}(i,j,k) + \\ d_2c_{1(i,j-1,k)}D_z^{n+\frac{2}{3}}(i,j-1,k) = \\ d_2c_{2(i,j+1,k)}D_z^{n+\frac{1}{3}}(i,j+1,k) - (2d_2c_{2(i,j,k)} + \frac{\Delta y}{\Delta t})D_z^{n+\frac{1}{3}}(i,j,k) + \\ d_2c_{2(i,j-1,k)}D_z^{n+\frac{1}{3}}(i,j-1,k) - \\ d_2c_{3(i,j+1,k)}D_z^{n}(i,j+1,k) + 2d_2c_{3(i,j,k)}D_z^{n}(i,j,k) - \\ d_2c_{3(i,j-1,k)}D_z^{n}(i,j-1,k) - \\ (d_2c_{4(i,j+1,k)}+d_2)E_z^{n+\frac{1}{3}}(i,j+1,k) + 2(d_2c_{4(i,j,k)}+d_2)E_z^{n+\frac{1}{3}}(i,j,k) - \\ (d_2c_{4(i,j-1,k)}+d_2)E_z^{n+\frac{1}{3}}(i,j-1,k) + \\ d_2c_{5(i,j+1,k)}E_z^{n}(i,j+1,k) - 2d_2c_{5(i,j,k)}E_z^{n}(i,j,k) + \\ d_2c_{5(i,j-1,k)}E_z^{n}(i,j-1,k) + \\ 2H_x^{n+\frac{1}{3}}(i,j,k) - 2H_x^{n+\frac{1}{3}}(i,j-1,k). \end{aligned} \tag{3.42}$$

(3.42) is the simultaneous equations. Thus, $D_z^{n+\frac{2}{3}}(i,j,k)$ is obtained through solving (3.42). $D_z^{n+\frac{2}{3}}(i,j,k)$ solved in (3.42) and (3.36) produce $E_z^{n+\frac{2}{3}}(i,j,k)$ and this $E_z^{n+\frac{2}{3}}(i,j,k)$ and (3.19) produce $H_x^{n+\frac{2}{3}}(i,j,k)$.

(3.31) is put into (3.24) to remove $E_x^{n+\frac{2}{3}}(i,j+1,k)$ and $E_x^{n+\frac{2}{3}}(i,j,k)$. This yields

$$\begin{aligned} H_z^{n+\frac{2}{3}}(i,j,k) = \quad (3.43)\\ d_1c_{1(i,j+1,k)}D_x^{n+\frac{2}{3}}(i,j+1,k) - d_1c_{2(i,j+1,k)}D_x^{n+\frac{1}{3}}(i,j+1,k) + \\ d_1c_{3(i,j+1,k)}D_x^{n}(i,j+1,k) + \\ (d_1c_{4(i,j+1,k)}+d_1)E_x^{n+\frac{1}{3}}(i,j+1,k) - d_1c_{5(i,j+1,k)}E_x^{n}(i,j+1,k) - \\ d_1c_{1(i,j,k)}D_x^{n+\frac{2}{3}}(i,j,k) + d_1c_{2(i,j,k)}D_x^{n+\frac{1}{3}}(i,j,k) - \\ d_1c_{3(i,j,k)}D_x^{n}(i,j,k) - \\ (d_1c_{4(i,j,k)}+d_1)E_x^{n+\frac{1}{3}}(i,j,k) + d_1c_{5(i,j,k)}E_x^{n}(i,j,k) + H_z^{n+\frac{1}{3}}(i,j,k). \end{aligned}$$

(3.43) is put into (3.25) to remove $H_z^{n+\frac{2}{3}}(i,j,k)$ and $H_z^{n+\frac{2}{3}}(i,j-1,k)$. This yields

$$\begin{aligned} d_1c_{1(i,j+1,k)}D_x^{n+\frac{2}{3}}(i,j+1,k) - (2d_1c_{2(i,j,k)} + \frac{\Delta y}{\Delta t})D_x^{n+\frac{2}{3}}(i,j,k) + \quad (3.44)\\ d_1c_{1(i,j-1,k)}D_x^{n+\frac{2}{3}}(i,j-1,k) = \\ d_1c_{2(i,j+1,k)}D_x^{n+\frac{1}{3}}(i,j+1,k) - (2d_1c_{2(i,j,k)} + \frac{\Delta y}{\Delta t})D_x^{n+\frac{1}{3}}(i,j,k) + \\ d_1c_{2(i,j-1,k)}D_x^{n+\frac{1}{3}}(i,j-1,k) - \\ d_1c_{3(i,j+1,k)}D_x^{n}(i,j+1,k) + 2d_1c_{3(i,j,k)}D_x^{n}(i,j,k) - \\ d_1c_{3(i,j-1,k)}D_x^{n}(i,j-1,k) - \\ (d_1c_{4(i,j+1,k)}+d_1)E_x^{n+\frac{1}{3}}(i,j+1,k) + 2(d_1c_{4(i,j,k)}+d_1)E_x^{n+\frac{1}{3}}(i,j,k) - \\ (d_1c_{4(i,j-1,k)}+d_1)E_x^{n+\frac{1}{3}}(i,j-1,k) + \\ d_1c_{5(i,j+1,k)}E_x^{n}(i,j+1,k) - 2d_1c_{5(i,j,k)}E_x^{n}(i,j,k) + \\ d_1c_{5(i,j-1,k)}E_x^{n}(i,j-1,k) - \\ 2H_z^{n+\frac{1}{3}}(i,j,k) + 2H_z^{n+\frac{1}{3}}(i,j-1,k) \end{aligned}$$

(3.44) is the simultaneous equations. Thus, $D_x^{n+\frac{2}{3}}(i,j,k)$ is obtained through solving (3.44). $D_x^{n+\frac{2}{3}}(i,j,k)$ solved in (3.44) and (3.31) produce $E_x^{n+\frac{2}{3}}(i,j,k)$ and this $E_x^{n+\frac{2}{3}}(i,j,k)$ and (3.24) produce $H_z^{n+\frac{2}{3}}(i,j,k)$.

3.2.3.3 Z direction

(3.32) is put into (3.22) to remove $E_x^{n+1}(i,j,k+1)$ and $E_x^{n+1}(i,j,k)$. This yields

$$\begin{aligned} H_y^{n+1}(i,j,k) = \qquad (3.45)\\ -d_3c_{1(i,j,k+1)}D_x^{n+1}(i,j,k+1) + d_3c_{2(i,j,k+1)}D_x^{n+\frac{2}{3}}(i,j,k+1) -\\ d_3c_{3(i,j,k+1)}D_x^{n+\frac{1}{3}}(i,j,k+1) -\\ (d_3c_{4(i,j,k+1)} + d_3)E_x^{n+\frac{2}{3}}(i,j,k+1) + d_3c_{5(i,j,k+1)}E_x^{n+\frac{1}{3}}(i,j,k+1) +\\ d_3c_{1(i,j,k)}D_x^{n+1}(i,j,k) - d_3c_{2(i,j,k)}D_x^{n+\frac{2}{3}}(i,j,k) +\\ d_3c_{3(i,j,k)}D_x^{n+\frac{1}{3}}(i,j,k) +\\ (d_3c_{4(i,j,k)} + d_3)E_x^{n+\frac{2}{3}}(i,j,k) - d_3c_{5(i,j,k)}E_x^{n+\frac{1}{3}}(i,j,k) + H_y^{n+\frac{2}{3}}(i,j,k). \end{aligned}$$

where $d_3 = \frac{\Delta t}{\mu \Delta z}$.

(3.45) is put into (3.26) to remove $H_y^{n+1}(i,j,k)$ and $H_y^{n+1}(i,j,k-1)$. This yields

$$\begin{aligned} d_3c_{1(i,j,k+1)}D_x^{n+1}(i,j,k+1) - (2d_3c_{2(i,j,k)} + \frac{\Delta x}{\Delta t})D_x^{n+1}(i,j,k) + \qquad (3.46)\\ d_3c_{1(i,j,k-1)}D_x^{n+1}(i,j,k-1) =\\ d_3c_{2(i,j,k+1)}D_x^{n+\frac{2}{3}}(i,j,k+1) - (2d_3c_{2(i,j,k)} + \frac{\Delta x}{\Delta t})D_x^{n+\frac{2}{3}}(i,j,k) +\\ d_3c_{2(i,j,k-1)}D_x^{n+\frac{2}{3}}(i,j,k-1) -\\ d_3c_{3(i,j,k+1)}D_x^{n+\frac{1}{3}}(i,j,k+1) + 2d_3c_{3(i,j,k)}D_x^{n+\frac{1}{3}}(i,j,k) -\\ d_3c_{3(i,j,k-1)}D_x^{n+\frac{1}{3}}(i,j,k-1) -\\ (d_3c_{4(i,j,k+1)} + d_3)E_x^{n+\frac{2}{3}}(i,j,k+1) + 2(d_3c_{4(i,j,k)} + d_3)E_x^{n+\frac{2}{3}}(i,j,k) -\\ (d_3c_{4(i,j,k-1)} + d_3)E_x^{n+\frac{2}{3}}(i,j,k-1) +\\ d_3c_{5(i,j,k+1)}E_x^{n+\frac{1}{3}}(i,j,k+1) - 2d_3c_{5(i,j,k)}E_x^{n+\frac{1}{3}}(i,j,k) +\\ d_3c_{5(i,j,k-1)}E_x^{n+\frac{1}{3}}(i,j,k-1) +\\ 2H_y^{n+\frac{2}{3}}(i,j,k) - 2H_y^{n+\frac{2}{3}}(i,j,k-1). \end{aligned}$$

(3.46) is the simultaneous equations. Thus, $D_x^{n+1}(i,j,k)$ is obtained through solving (3.46). $D_x^{n+1}(i,j,k)$ solved in (3.46) and (3.32) produce $E_x^{n+1}(i,j,k)$ and this $E_x^{n+1}(i,j,k)$ and (3.22) produce $H_y^{n+1}(i,j,k)$.

(3.34) is put into (3.21) to remove $E_y^{n+1}(i,j,k+1)$ and $E_y^{n+1}(i,j,k)$ This yields

$$\begin{aligned} H_x^{n+1}(i,j,k) = \qquad (3.47)\\ d_3c_{1(i,j,k+1)}D_y^{n+1}(i,j,k+1) - d_3c_{2(i,j,k+1)}D_y^{n+\frac{2}{3}}(i,j,k+1) + \\ d_3c_{3(i,j,k+1)}D_y^{n+\frac{1}{3}}(i,j,k+1) + \\ (d_3c_{4(i,j,k+1)} + d_3)E_y^{n+\frac{2}{3}}(i,j,k+1) - d_3c_{5(i,j,k+1)}E_y^{n+\frac{1}{3}}(i,j,k+1) - \\ d_3c_{1(i,j,k)}D_y^{n+1}(i,j,k) + d_3c_{2(i,j,k)}D_y^{n+\frac{2}{3}}(i,j,k) - \\ d_3c_{3(i,j,k)}D_y^{n+\frac{1}{3}}(i,j,k) - \\ (d_3c_{4(i,j,k)} + d_3)E_y^{n+\frac{2}{3}}(i,j,k) + d_3c_{5(i,j,k)}E_y^{n+\frac{1}{3}}(i,j,k) + H_x^{n+\frac{2}{3}}(i,j,k) \end{aligned}$$

(3.47) is put into (3.28) to remove $H_x^{n+1}(i,j,k)$ and $H_x^{n+1}(i,j,k-1)$. This yields

$$\begin{aligned} d_3c_{1(i,j,k+1)}D_y^{n+1}(i,j,k+1) - (2d_3c_{2(i,j,k)} + \frac{\Delta z}{\Delta t})D_y^{n+1}(i,j,k) + \qquad (3.48)\\ d_3c_{1(i,j,k-1)}D_y^{n+1}(i,j,k-1) = \\ d_3c_{2(i,j,k+1)}D_y^{n+\frac{2}{3}}(i,j,k+1) - (2d_3c_{2(i,j,k)} + \frac{\Delta z}{\Delta t})D_y^{n+\frac{2}{3}}(i,j,k) + \\ d_3c_{2(i,j,k-1)}D_y^{n+\frac{2}{3}}(i,j,k-1) - \\ d_3c_{3(i,j,k+1)}D_y^{n+\frac{1}{3}}(i,j,k+1) + 2d_3c_{3(i,j,k)}D_y^{n+\frac{1}{3}}(i,j,k) - \\ d_3c_{3(i,j,k-1)}D_y^{n+\frac{1}{3}}(i,j,k-1) - \\ (d_3c_{4(i,j,k+1)} + d_3)E_y^{n+\frac{2}{3}}(i,j,k+1) + 2(d_3c_{4(i,j,k)} + d_3)E_y^{n+\frac{2}{3}}(i,j,k) - \\ (d_3c_{4(i,j,k-1)} + d_3)E_y^{n+\frac{2}{3}}(i,j,k-1) + \\ d_3c_{5(i,j,k+1)}E_y^{n+\frac{1}{3}}(i,j,k+1) - 2d_3c_{5(i,j,k)}E_y^{n+\frac{1}{3}}(i,j,k) + \\ d_3c_{5(i,j,k-1)}E_y^{n+\frac{1}{3}}(i,j,k-1) - \\ 2H_x^{n+\frac{2}{3}}(i,j,k) + 2H_x^{n+\frac{2}{3}}(i,j,k-1). \end{aligned}$$

(3.48) is put into the simultaneous equations. Thus, $D_y^{n+1}(i,j,k)$ is obtained through solving (3.48). $D_y^{n+1}(i,j,k)$ solved in (3.48) and (3.34) produce $E_y^{n+1}(i,j,k)$ and this $E_y^{n+1}(i,j,k)$ and (3.20) produce $H_x^{n+1}(i,j,k)$.

This numerical formulation of the three direction parts are implemented into the 3D-FD-AOS-FDTD method.

Chapter 4

Excitation Scheme

4.1 Introduction

The excitation method chosen in the development of a FDTD scheme has a significant impact on the results of the simulation [5]. We excited the FDTD space by a z-directed electric flux density (D_z). Because in the 3D-FD-AOS-FDTD method each component is split into two independent direction parts, the computation of each component has two steps in one FDTD time iteration. The D_z component is split into the x direction part and into the y direction part at each FDTD time step. In the 3D-FD-AOS-FDTD scheme, two source excitation updates are given at the same time step of Δt, each of them taking place in each direction part of the D_z component. Both source excitation updates are given after updating the values of the x direction part and the y direction part of the D_z component at current time step Δt.

As it was stated in section 1.4, a hard source has been used for simplicity in this thesis. To radiate an electromagnetic wave from a single point $(i_{src}\Delta x, j_{src}\Delta y, k_{src}\Delta z)$ of the FDTD grid in Cartesian coordinates with Δx, Δy, Δz the spatial step sizes in x, y, z directions, respectively, the hard source method simply consists of impressing a field component at each time step of $n\Delta t$ as follows:

$$D_z(i_{src}, j_{src}, k_{src}) = J_z(t_n) \tag{4.1}$$

where Δt is the temporal step size and $J_z(t_n)$ is a given function of time. Thus, we set the value of $J_z(t_n)$ at current time step Δt to the coordinates of the source location in both parts of the D_z component. The coordinates of the

source location are optional parameters of the FDTD computation such as the dimension of the FDTD space and the number of iterations.

The excitation waveform $J_z(t_n)$ can be the same in both directions parts of the D_z component at the same time step Δt or they can be different, which leads to a different behaviour of the algorithm. We are going to study the behaviour of the 3D-FD-AOS-FDTD scheme when the excitation waveform used in each direction part of the D_z component are the same excitation waveform at the same time step t and when they are different. In addition, we are going to ilustrate the propagation of different excitation waveforms. Observation of the explicit FDTD method will be shown as a reference. Both algorithms have been run under the same set of input parameters:

- FDTD space: $128\Delta x \times 128\Delta y \times 128\Delta z$
- Number of time steps: 500
- $\Delta s = 10^{-3}$ m
- $\Delta t = 1.9245008 \cdot 10^{-12}$ seconds
- Location of the source: $(64\Delta x, 64\Delta y, 64\Delta z)$

4.2 The Gaussian pulse as an excitation waveform

First of all, we are going to display the observation in the 3D-FD-AOS-FDTD scheme when the excitation waveform is an unmodulated Gaussian pulse, one of the most widely-used signals employed as a source in FDTD meshes. The waveform of the unmodulated Gaussian pulse used to excite the 3D-FD-AOS-FDTD scheme is shown in Figure 4.1. The same value of the excitation waveform $J_z(t_n)$ is used at each excitation update in each direction part of the D_z component at the same time step Δt .

Observation of the D_z component at point $(94, 64, 64)$ in the 3D-FD-AOS-FDTD scheme when the excitation waveform is the unmodulated Gaussian pulse, is shown in Figure 4.2. Observation of the same component at the same point in the explicit FDTD scheme is shown as a reference. The explicit scheme has been excited with the same excitation waveform used in the 3D-FD-AOS-FDTD

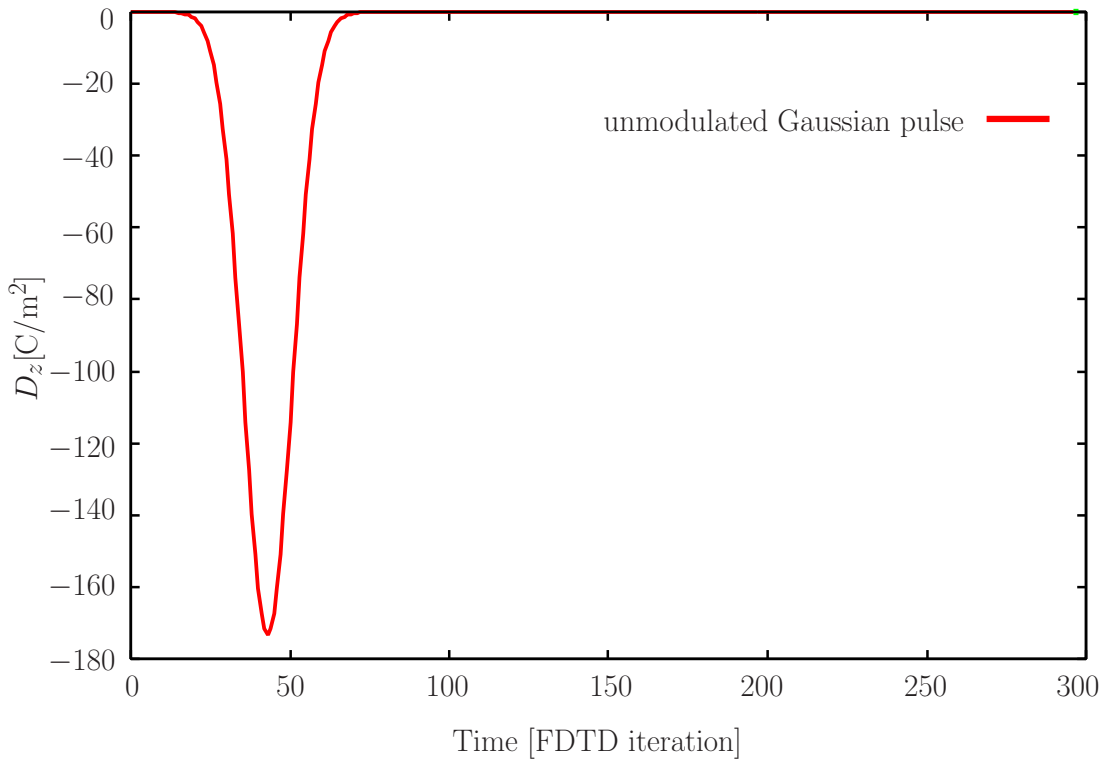

Figure 4.1: Waveform of the unmodulated Gaussian pulse used to excite the 3D-FD-AOS-FDTD scheme and the explicit FDTD scheme.

scheme. The observation of the D_z component at point $(94, 64, 64)$ in the 3D-FD-AOS-FDTD scheme diverges.

Observation of the D_z component in the plane $z = 64\Delta z$ when the excitation waveform is an unmodulated Gaussian pulse in the 3D-FD-AOS-FDTD scheme is shown in Figure 4.3. The waveform remains in the middle of the algorithm as a big hole, in other words, the waveform does not propagate through the cells of the mesh. Observation of the D_z component in the plane $z = 64\Delta z$ when the excitation waveform is an unmodulated Gaussian pulse in the explicit FDTD scheme is shown as a reference. In the explicit FDTD scheme when the exciation waveform is an unmodulated Gaussian pulse, the waveform propagates through the cells of the mesh.

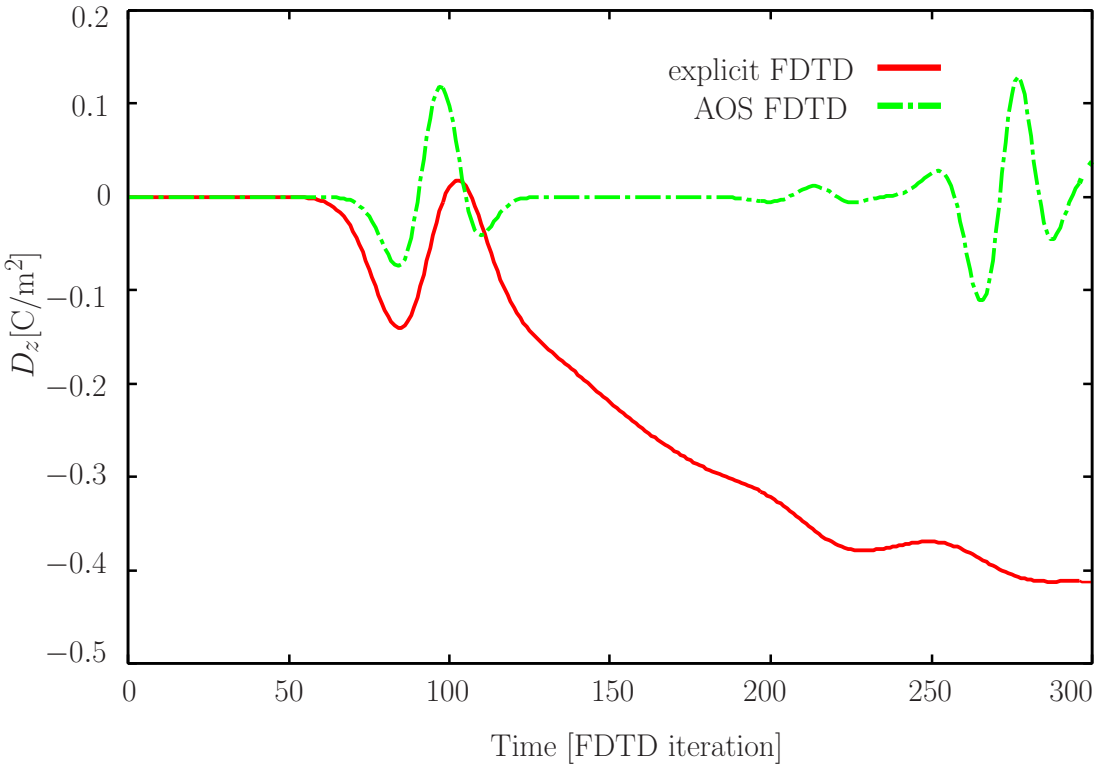

Figure 4.2: Observation of the D_z component at point $(94, 64, 64)$ in the 3D-FD-AOS-FDTD scheme when the excitation waveform is an unmodulated Gaussian pulse.

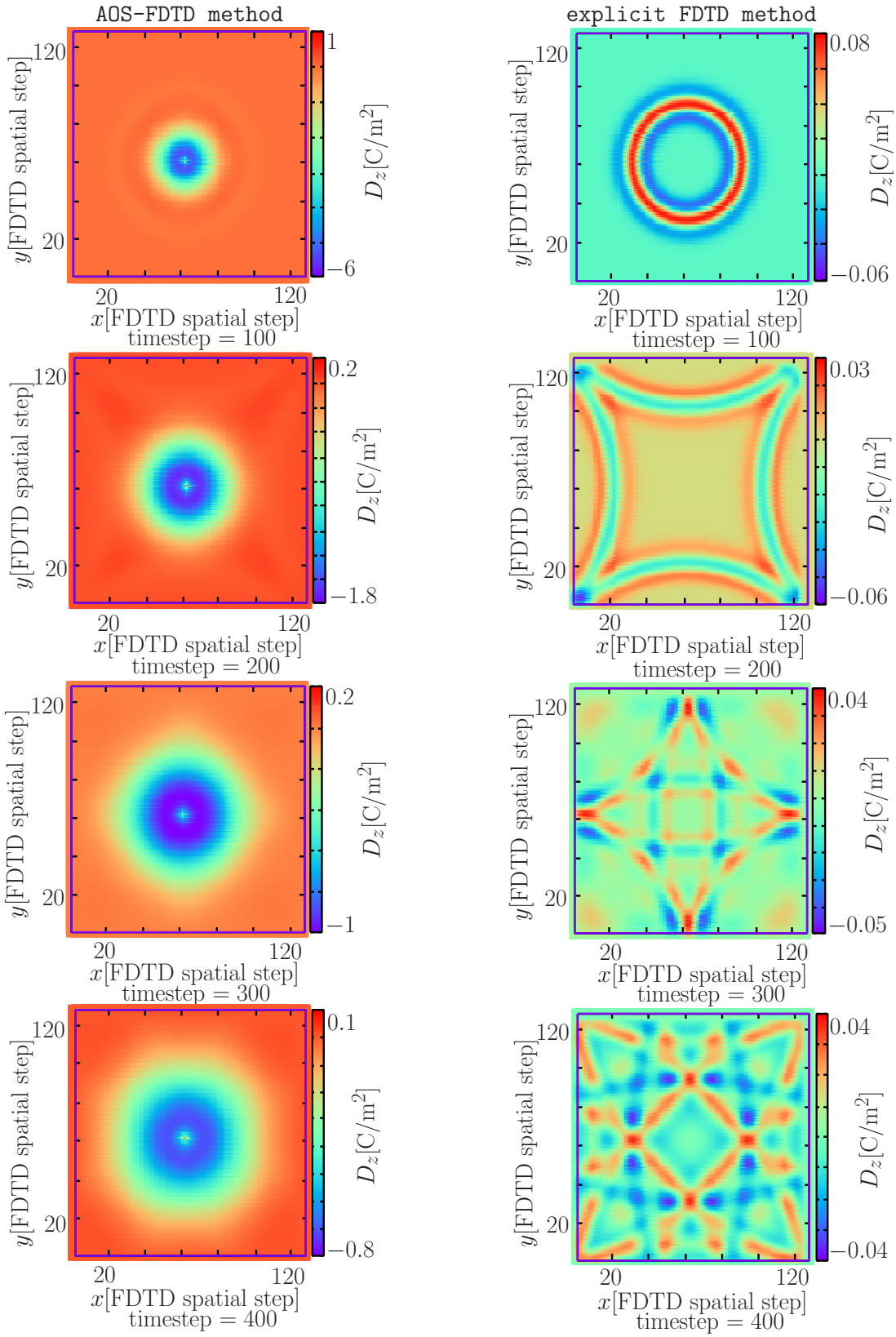

Figure 4.3: Observation of the D_z component in the plane $z = 64\Delta z$ in the 3D-FD-AOS-FDTD scheme when the excitation waveform is an unmodulated Gaussian pulse.

4.3 Modulated Gaussian pulse as excitation waveform

Now we are going to show the observation of the 3D-FD-FDTD-AOS scheme when the excitation waveform is a modulated Gaussian pulse. The waveform of the modulated Gaussian pulse used to excite the 3D-FD-AOS-FDTD is shown in Figure 4.4.

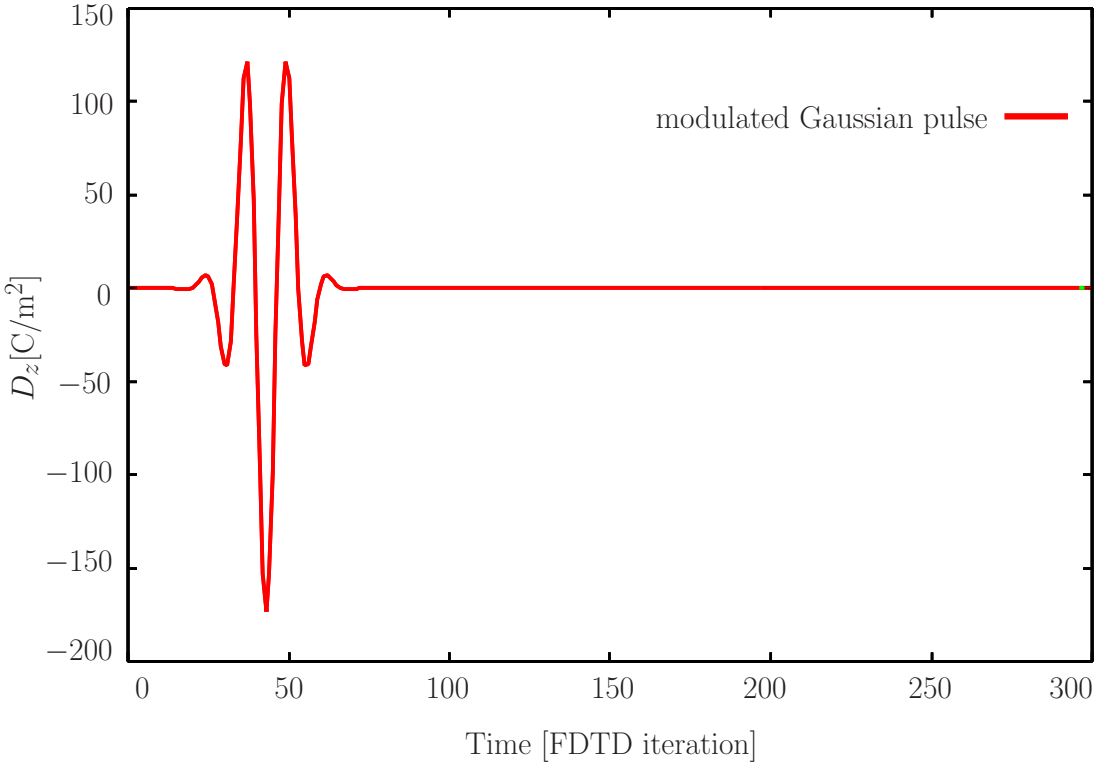

Figure 4.4: Waveform of the modulated Gaussian pulse used to excite the 3D-FD-AOS-FDTD scheme.

Observation of the D_z component at points $(94, 64, 64)$ and $(74, 64, 64)$ in the 3D-FD-AOS-FDTD scheme when the excitation waveform is the modulated Gaussian pulse, is shown in Figure 4.5 and Figure 4.6 respectively. Observation of the same component at same points in the explicit FDTD scheme when the excitation waveform is an unmodulated Gaussian pulse is shown as a reference. Note that the amplitude of the observation signal of the D_z component in the 3D-FD-AOS-FDTD scheme decreases with the propagation distance. Observation of the 3D-FD-AOS-FDTD scheme at point $(94, 64, 64)$ has been divided by a factor of 15 and at point $(74, 64, 64)$ by a factor of 60. Observation of the D_z component

at points $(94, 64, 64)$ and $(74, 64, 64)$ in the 3D-FD-AOS-FDTD scheme when the excitation waveform is the modulated Gaussian pulse matches relatively well with the observation of the same component at same points in the explicit FDTD scheme when the excitation waveform is an unmodulated Gaussian pulse.

Figure 4.7 shows the observation of the D_z component in the plane $z = 64\Delta z$ in the 3D-FD-AOS-FDTD scheme when the excitation waveform is a modulated Gaussian pulse, which is quite different to the observation of the same component at the same plane in the explicit FDTD scheme when the excitation waveform is an unmodulated Gaussian pulse. Observation of the D_z component in the plane $z = 64\Delta z$ in the 3D-FD-AOS-FDTD scheme when the excitation waveform is a modulated Gaussian pulse, is not symmetric as the observation of the same component at the same plane in the explicit FDTD scheme when the excitation waveform is an unmodulated Gaussian pulse.

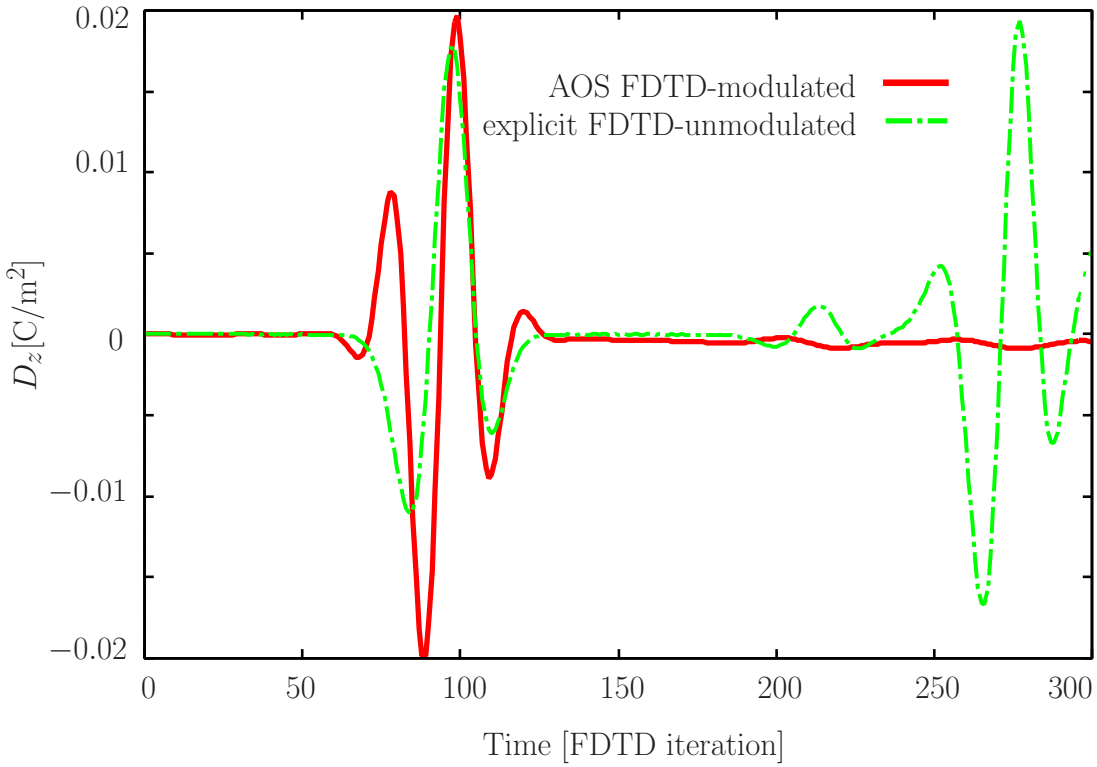

Figure 4.5: Observation of the D_z component at point $(94, 64, 64)$ in the 3D-FD-AOS-FDTD scheme when the excitation waveform is a modulated Gaussian pulse.

Figure 4.8 and Figure 4.9 show the observation of the D_z component at points $(94, 64, 64)$ and $(74, 64, 64)$ respectively, when the excitation waveform is a

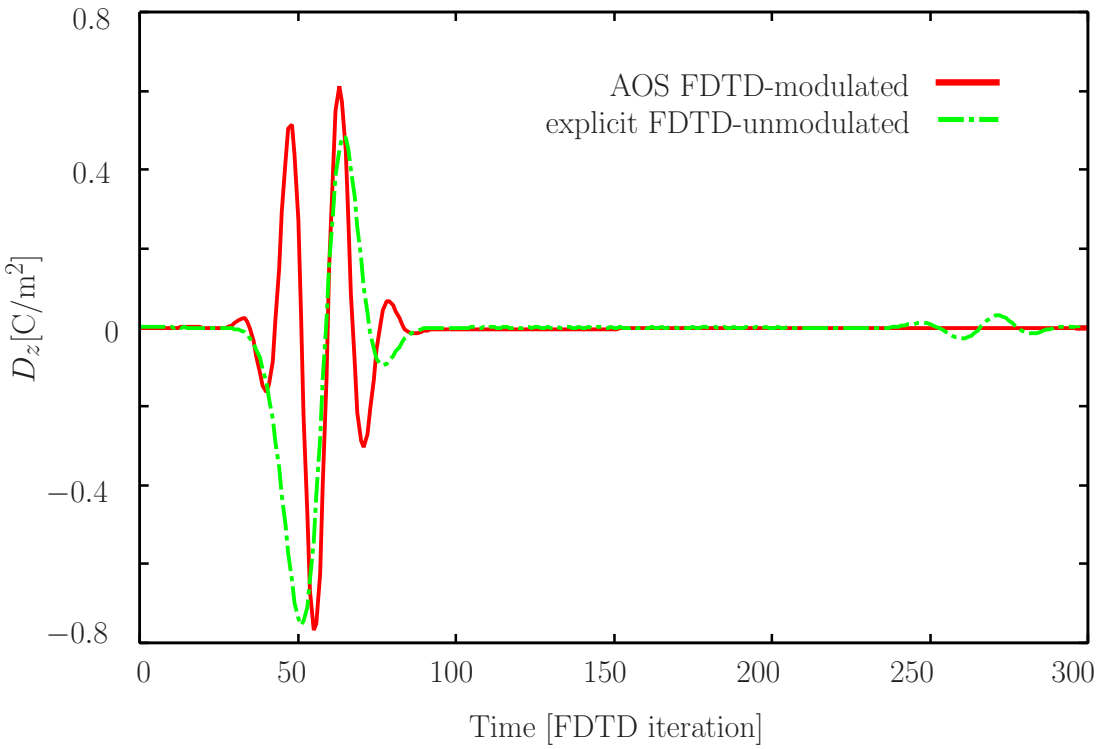

Figure 4.6: Observation of the D_z component at point $(74, 64, 64)$ in the 3D-FD-AOS-FDTD scheme when the excitation waveform is a modulated Gaussian pulse.

modulated Gaussian pulse in the 3D-FD-AOS-FDTD scheme and in the explicit FDTD scheme. Note that the amplitude of the observation signal of the 3D-FD-AOS-FDTD scheme is reduced with the propagation distance. Observation in the 3D-FD-AOS-FDTD scheme at point $(74, 64, 64)$ has been divided by a factor of 10. Observation of the D_z component at point $(74, 64, 64)$ in the 3D-FD-AOS-FDTD scheme when the excitation waveform is the modulated Gaussian pulse matches relatively well with the observation of the same component at the same point in the explicit FDTD scheme when the excitation waveform is a modulated Gaussian pulse. Observation at point $(94, 64, 64)$ in the 3D-FD-AOS-FDTD scheme is quite different to the observation at the same point in the explicit scheme.

In Figure 4.10 we can perceive that the observation of the D_z component in the plane $z = 64\Delta z$ in the 3D-FD-AOS-FDTD scheme when the excitation waveform is a modulated Gaussian pulse is also quite different to the observation of the same component at the same plane in the explicit FDTD scheme when the excitation waveform is a modulated Gaussian pulse. Observation of the D_z component in the plane $z = 64\Delta z$ in the 3D-FD-AOS-FDTD scheme when the excitation waveform is a modulated Gaussian pulse, is not symmetric as it is in the observation of the same component at the same plane in the explicit FDTD scheme when the excitation waveform is a modulated Gaussian pulse.

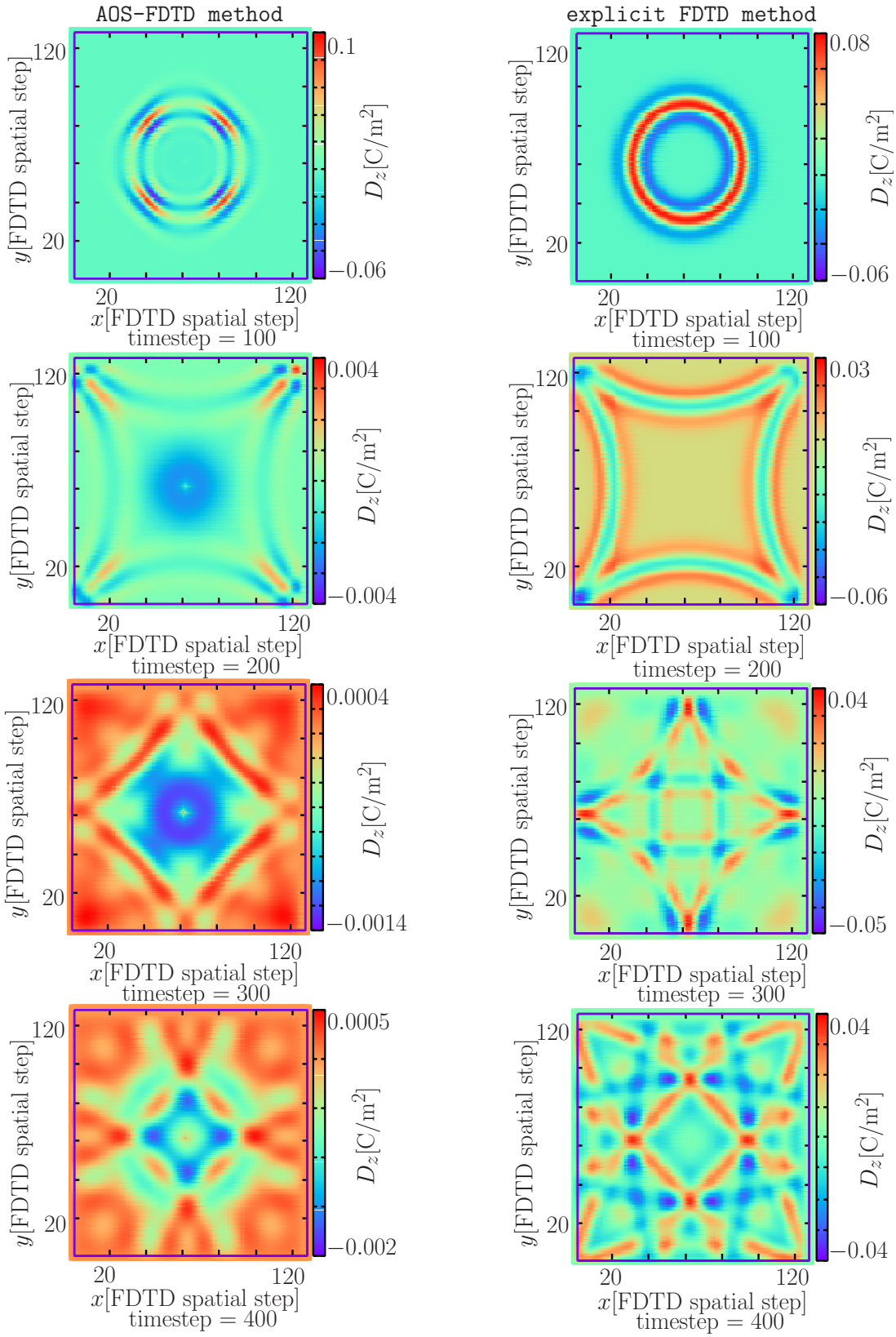

Figure 4.7: Observation of the D_z component in the plane $64\Delta z$ in the 3D-FD-AOS-FDTD scheme when the excitation waveform is a modulated Gaussian pulse.

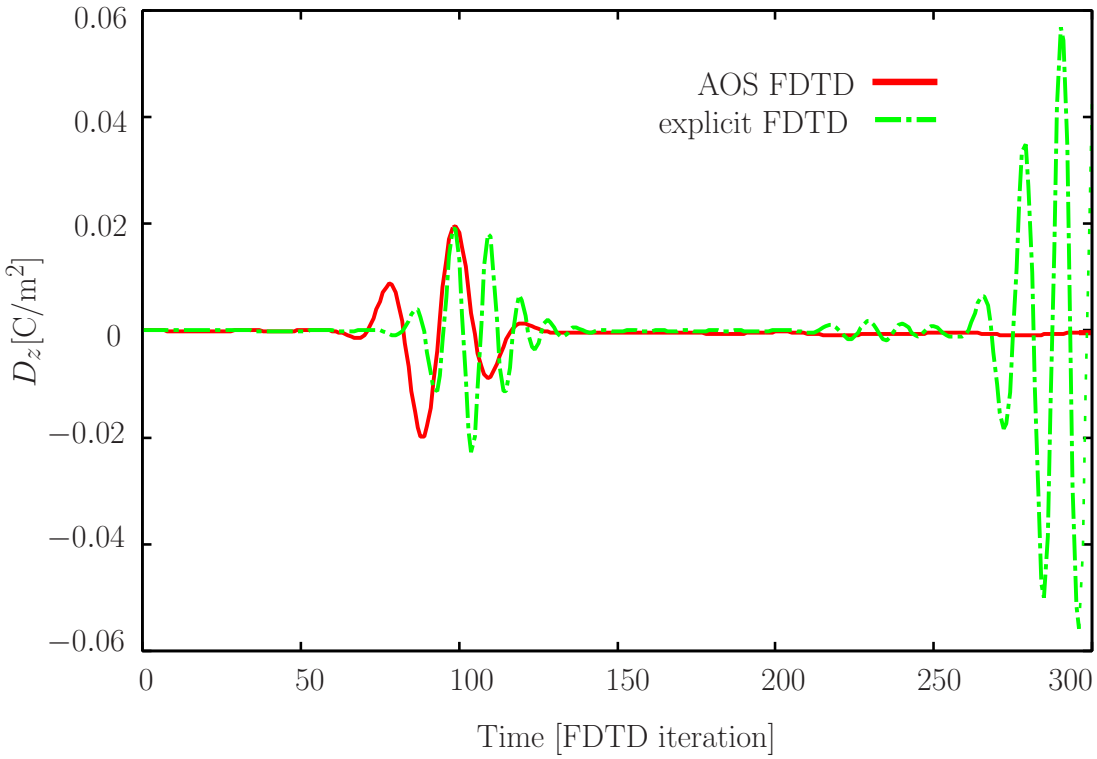

Figure 4.8: Observation of the D_z component at point $(94, 64, 64)$ when the excitation waveform is the modulated Gaussian pulse in the 3D-FD-AOS-FDTD scheme.

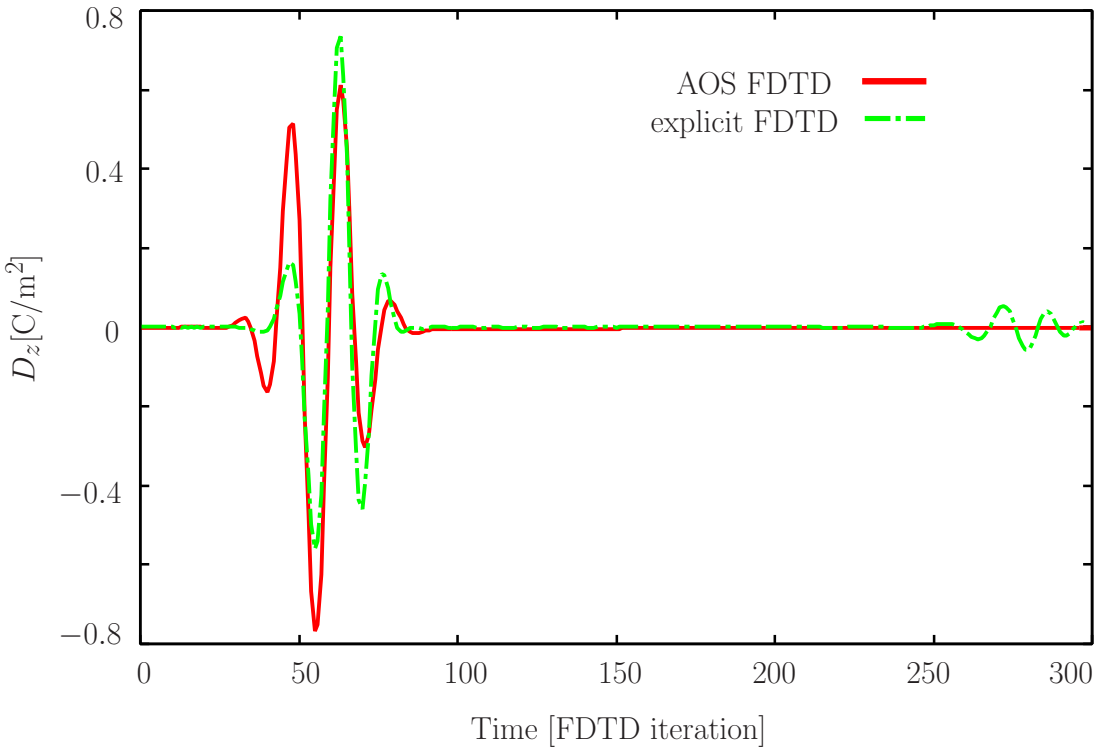

Figure 4.9: Observation of the D_z component at point $(74, 64, 64)$ when the excitation waveform is the modulated Gaussian pulse in the 3D-FD-AOS-FDTD scheme.

4.4 The excitation waveform built from past and future values of an unmodulated Gaussian pulse.

We are now moving on to consider an excitation waveform which has been built taking into consideration past and future values of the value of an unmodulated Gaussian pulse at the current time-step t. In other words, if $J_z(t_n)$ is the function of an unmodulated Gaussian pulse, the excitation waveform considering past and future values of an unmodulated Gaussian pulse at the current time step Δt will have the form $J_z(t_n + \Delta t) - ((J_z(t_n + 2\Delta t) - J_z(t_n))/2)$. The excitation waveform that has been built considering past and future values of the value of an unmodulated Gaussian pulse at the current time-step t is shown in Figure 4.11.

When the excitation waveform in the 3D-FD-AOS-FDTD approach is the signal built having considered past and future values of the value of an unmodulated Gaussian pulse at the current time-step t, the observation does not diverge. Observation of the D_z component at points $(94, 64, 64)$ and $(74, 64, 64)$ is shown in Figure 4.12 and Figure 4.13, respectively. Observation is quite similar to the observation of the 3D-FD-AOS-FDTD when the excitation waveform is a modulated waveform, but we will see later that when the excitation waveform is built considering past and future values of the value of an unmodulated Gaussian pulse, we are able to change the propagation of the waveform changing the parameters of the excitation waveform.

Observation of the D_z component in the plane $z = 64\Delta z$ in the 3D-FD-AOS-FDTD scheme when the excitation waveform is the signal built considering past and future values of the value of an unmodulated Gaussian pulse at the current time-step t is shown in Figure 4.14. Observation of the same component in the same plane in the explicit FDTD scheme when the excitation waveform is an unmodulated Gaussian pulse is shown as a reference. When the excitation waveform in the 3D-FD-AOS-FDTD scheme is built considering past and future values of the value of an unmodulated Gaussian pulse at the current time-step t, observation of the D_z component in the plane $z = 64\Delta z$ propagates through the cells of the mesh.

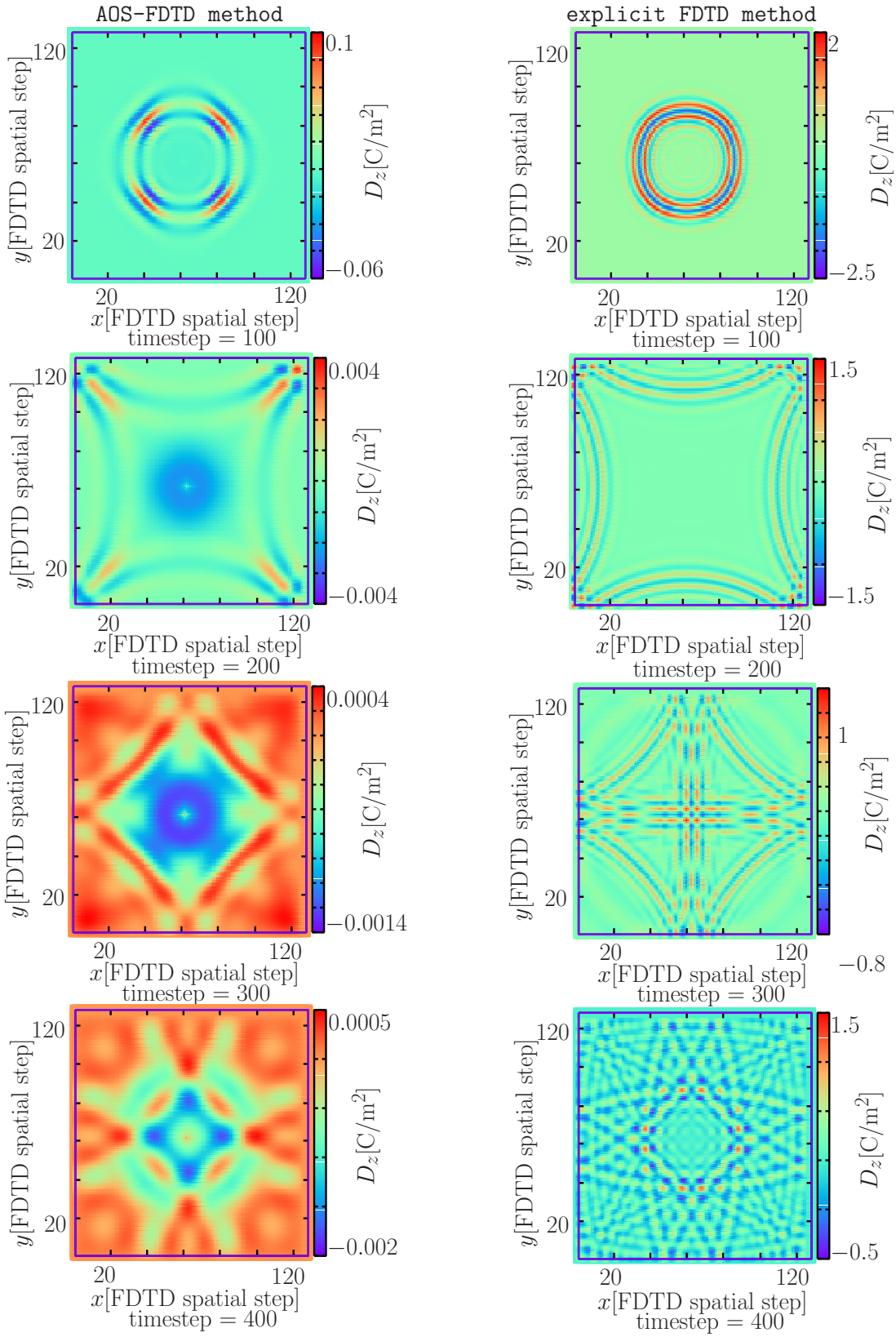

Figure 4.10: Observation of the D_z component in the plane $64\Delta z$ in the 3D-FD-AOS-FDTD scheme when the excitation waveform is a modulated Gaussian pulse.

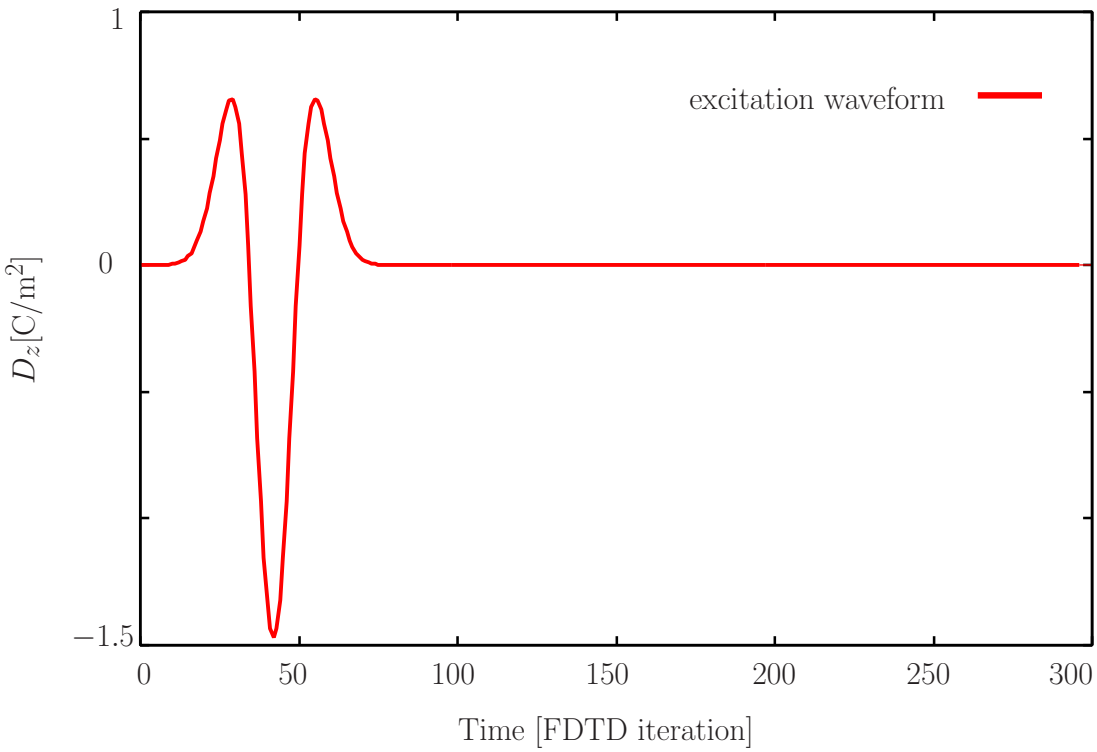

Figure 4.11: Excitation waveform built considering past and future values of a Gaussian pulse at the current time-step t.

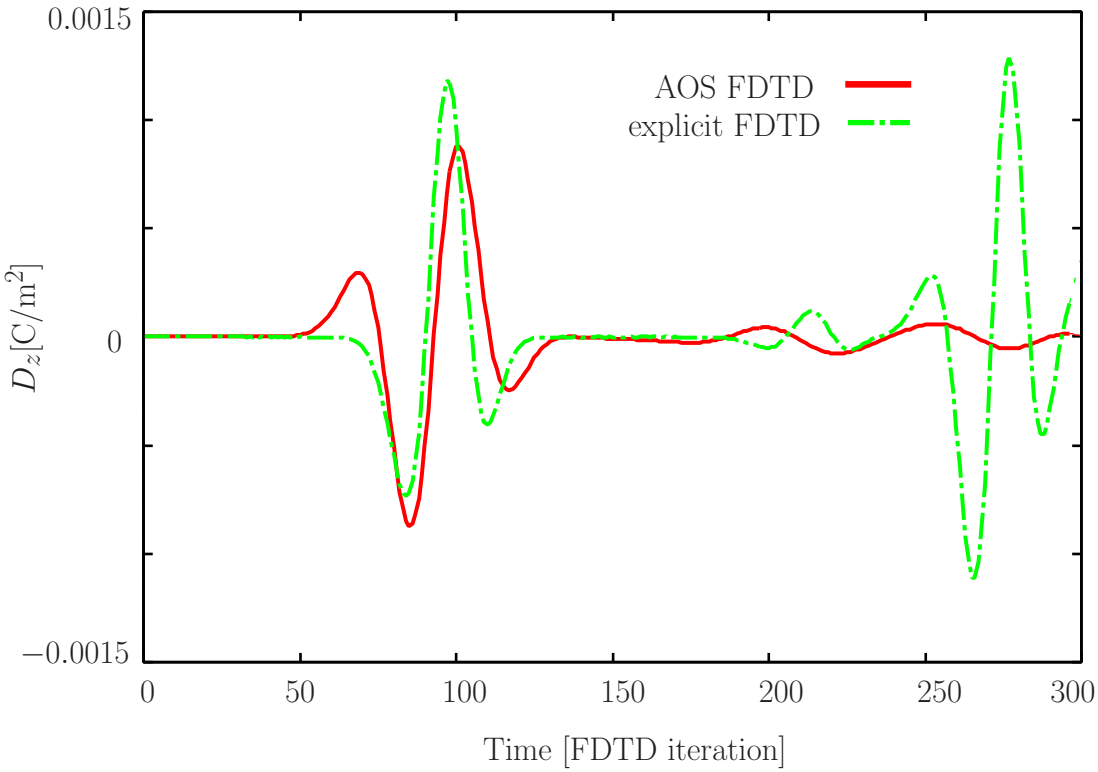

Figure 4.12: Observation of the D_z component at point $(94, 64, 64)$ in the 3D-FD-AOS-FDTD scheme when the excitation waveform is the pulse built with past and future values of the value of a Gaussian pulse at the current time-step t.

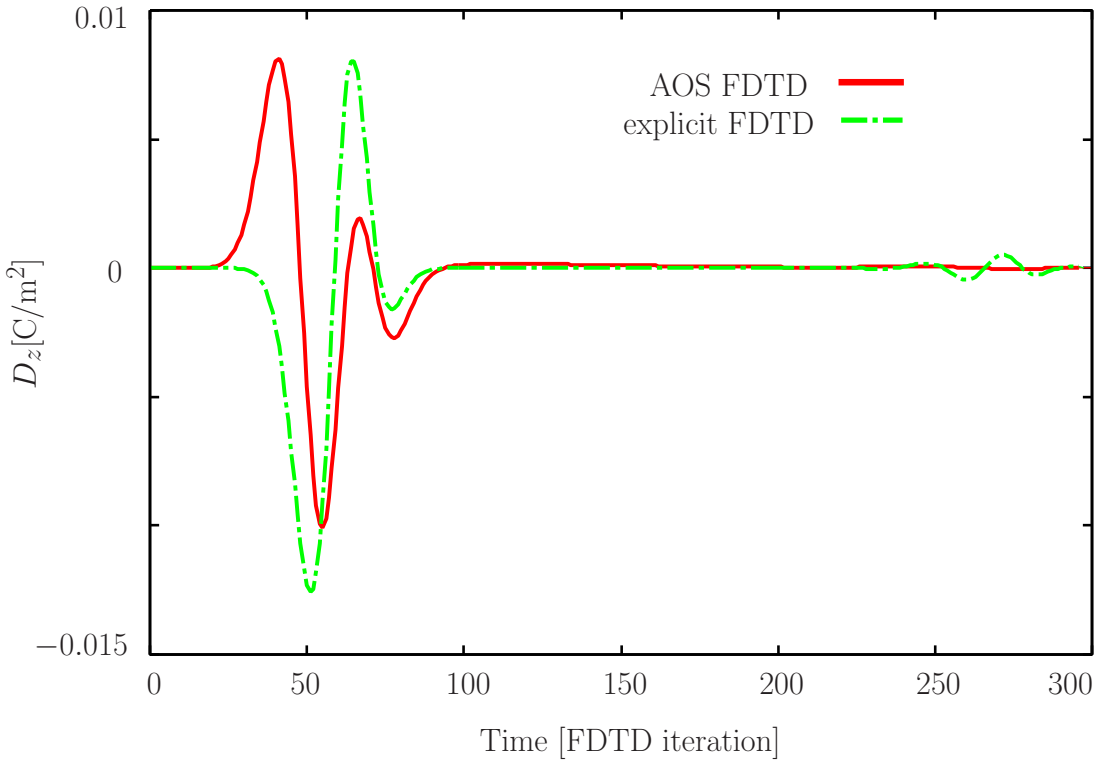

Figure 4.13: Observation of the D_z component at point $(74, 64, 64)$ in the 3D-FD-AOS-FDTD scheme when the excitation waveform is the pulse built with past and future values of the value of a Gaussian pulse at the current time-step t.

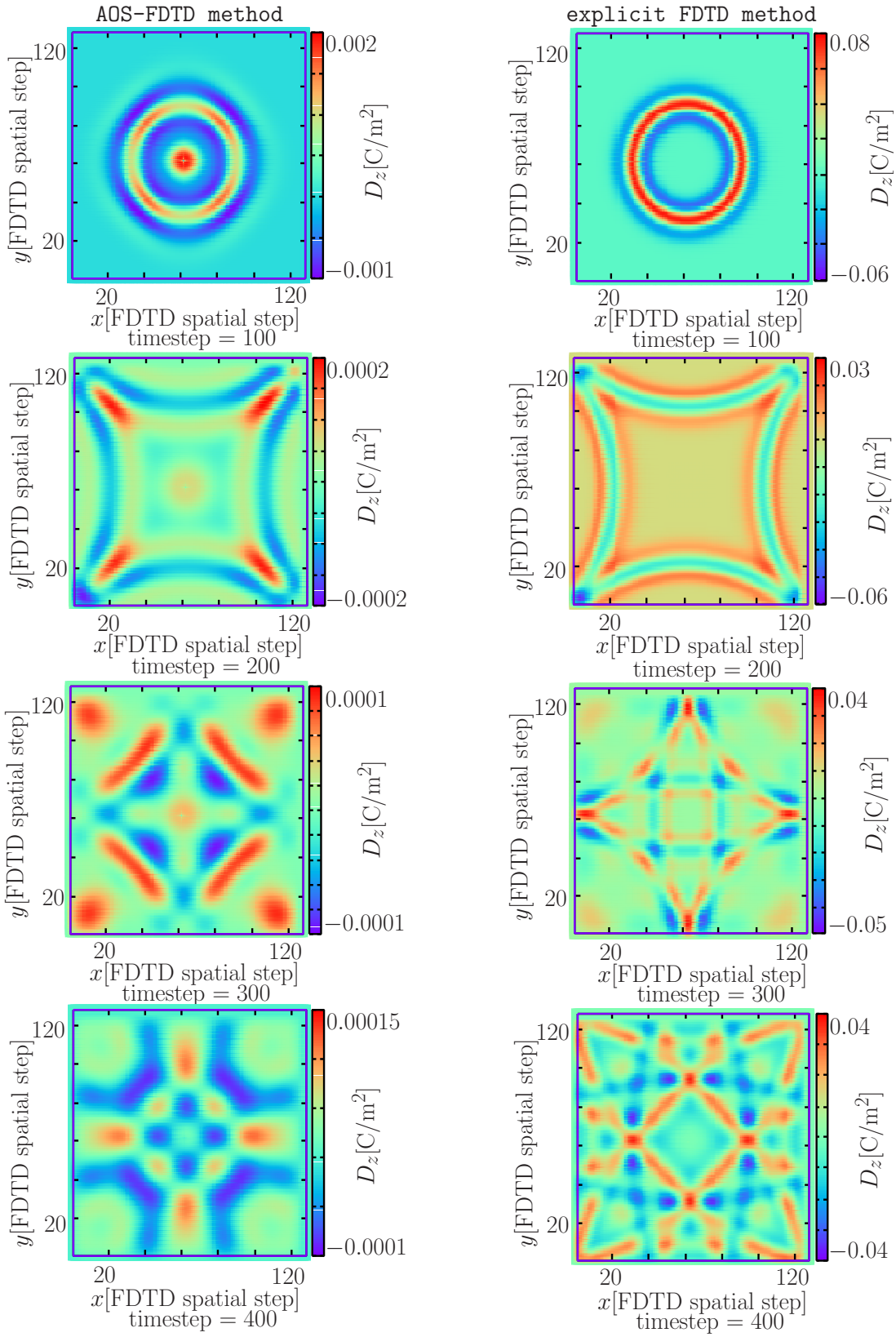

Figure 4.14: Observation of the D_z component in the plane $z = 64\Delta z$ in the 3D-FD-AOS-FDTD scheme when the excitation waveform is built with past and future values of the value of a Gaussian pulse at current time-step t.

4.5 Different excitation waveform in every update of the D_z component at the same time step.

As it was stated in Section 4.1, in the 3D-AOS-FDTD scheme, two source excitation updates are given at the same time step t, each of them taking place in each direction part of the D_z component. Up until now, the same excitation waveform has been used in both parts of the D_z component at the same time step Δt. We are now going to use (4.2) to excite the x direction part of the D_z component and (4.3) to excite the y direction part of the D_z component.

$$D_z(i_{src}, j_{src}, k_{src}) = J_z(t_n + \Delta t) - ((J_z(t_n + 2\Delta t) - J_z(t_n)/2)) \tag{4.2}$$

$$D_z(i_{src}, j_{src}, k_{src}) = ((J_z(t_n + 2\Delta t) - J_z(t_n)/2)) - J_z(t_n + \Delta t) \tag{4.3}$$

The excitation waveforms used in each part in the 3D-FD-AOS-FDTD scheme are displayed in Figure 4.15.

Figure 4.16 and Figure 4.17 show respectively the observation of the D_z component at points $(94, 64, 64)$ and $(74, 64, 64)$ in the 3D-FD-AOS-FDTD scheme when the excitation waveforms used in each direction part of the D_z component are those shown in Figure 4.15. Observation of the same component at the same points in the explicit FDTD scheme when the exciation waveform is an unmodulated Gaussian pulse are shown as a reference. Note that observation signal of the 3D-FD-AOS-FDTD scheme has been multiplied by a factor of 10 in Figure 4.16 and Figure 4.17. Observation in the 3D-FD-AOS-FDTD scheme when the excitation waveforms used in each direction part of the D_z component are shown in Figure 4.15. Observation the 3D-FD-AOS-FDTD scheme matches relatively well with the observation of the same component at the same points in the explicit FDTD scheme when the exciation waveform is an unmodulated Gaussian pulse.

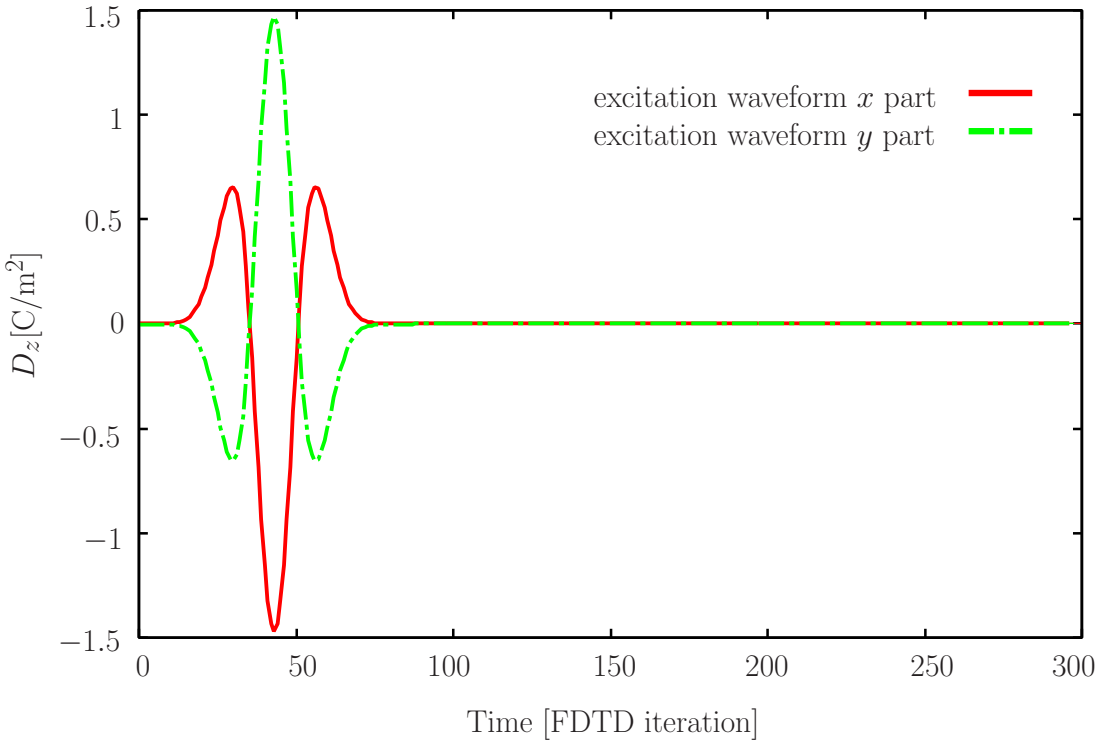

Figure 4.15: Excitation waveforms in the x direction part and in the y direction part in the 3D-FD-AOS-FDTD scheme.

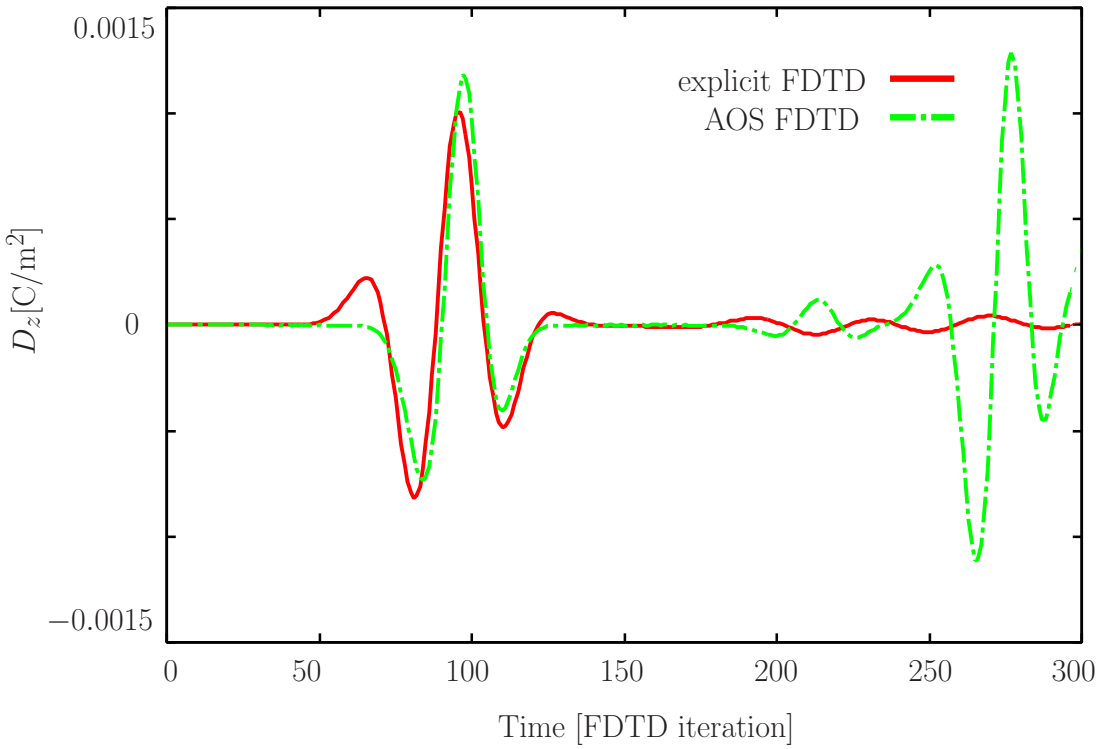

Figure 4.16: Observation of the D_z component at point $(94, 64, 64)$ in the 3D-FD-AOS-FDTD scheme when the excitation waveforms used in each direction part of the D_z component are those shown in Figure 4.15.

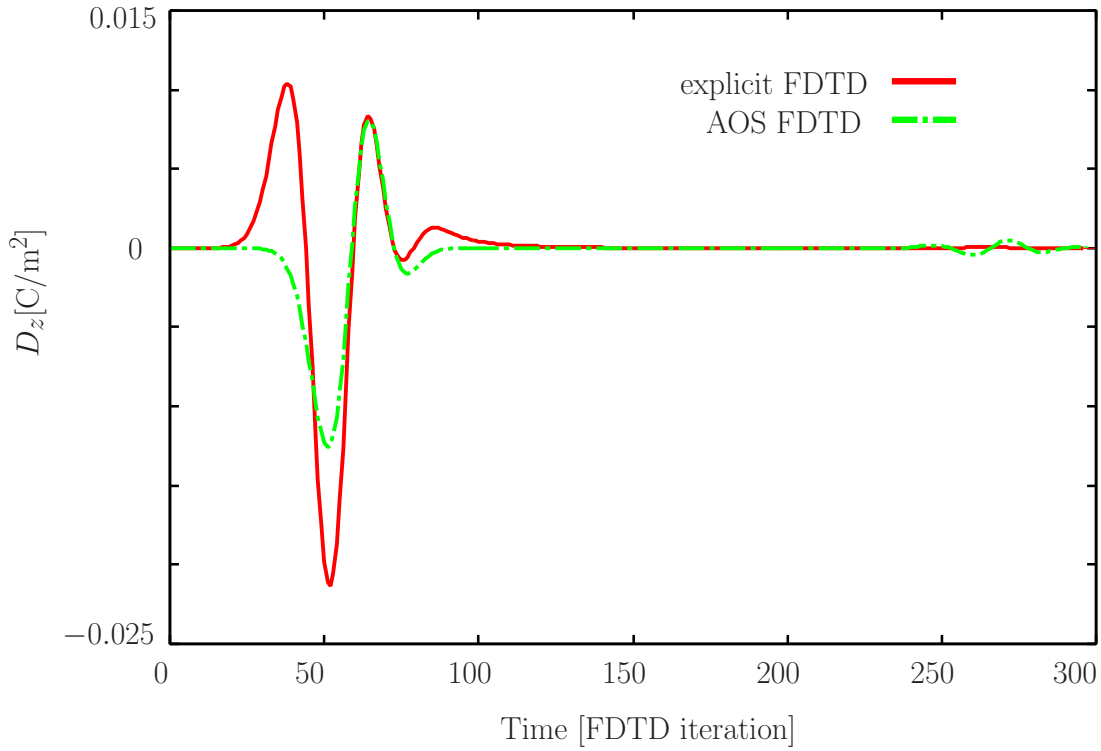

Figure 4.17: Observation of the D_z component at point $(74, 64, 64)$ in the 3D-FD-AOS-FDTD scheme when the excitation waveforms used in each direction part of the D_z component are those shown in Figure 4.15.

Figure 4.18 shows the observation of the D_z component in the plane $z = 64\Delta z$ in the 3D-FD-FDTD-AOS scheme when the excitation waveform used in each direction part of the D_z component are those shown in Figure 4.15. Observation of the D_z component in the plane $z = 64\Delta z$ in the explicit FDTD scheme when the excitation waveform used in each direction part of the D_z component is the same unmodulated Gaussian pulse is shown as a reference. Observation of the D_z component in the plane $z = 64\Delta z$ in the 3D-FD-FDTD-AOS scheme propagates through the cell of the mesh. Observation of the D_z component in the plane $z = 64\Delta z$ in the 3D-FD-FDTD-AOS scheme when the excitation waveform used in each direction part of the D_z component are the excitation waveforms shown in Figure 4.15 is quite different to the observation of the D_z component in the plane $z = 64\Delta z$ in the explicit FDTD scheme when the excitation waveform used in each direction part of the D_z component are the same unmodulated Gaussian pulse.

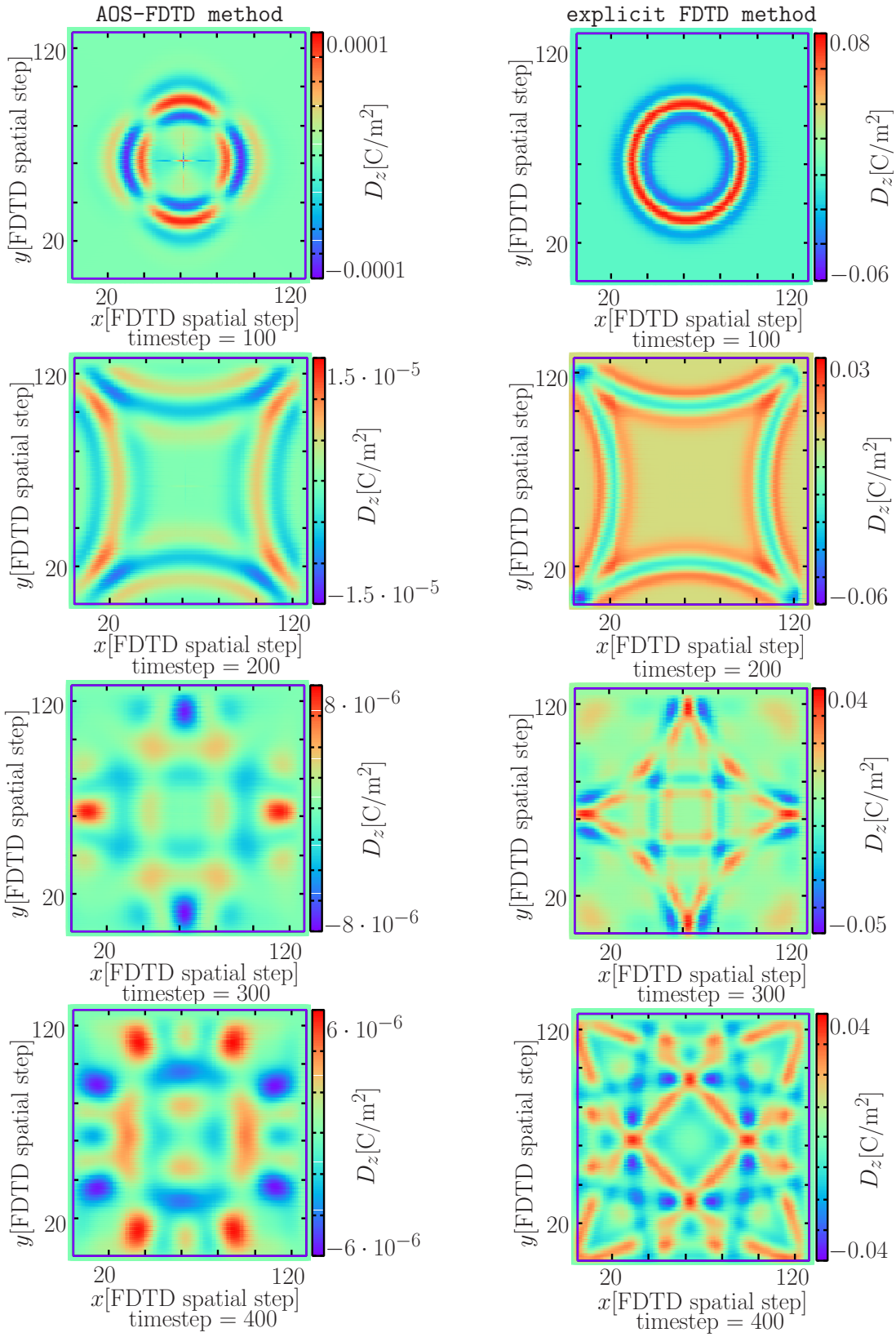

Figure 4.18: Observation of the plane $z = 64\Delta z$ of the D_z component in the 3D-FD-AOS-FDTD scheme when the excitation waveform in the x direction part and in the y direction of the algorithm are those shown in the Figure 4.15.

4.6 Setting the parameters of the excitation waveform built from past and future values of an unmodulated Gaussian pulse.

In the 3D-FD-AOS-FDTD scheme, the alteration of the equation parameters of the excitation waveform built with past and future values of the value of an unmodulated Gaussian pulse leads to different propagation of the waveform. In the previous Section 4.5 above, the equations of the excitation waveform used to excite each direction part of the D_z component are as follow:

$$D_z(i_{src}, j_{src}, k_{src}) = J_z(t_n + \Delta t) - ((J_z(t_n + 2\Delta t) - J_z(t_n)/2)) \tag{4.4}$$

The equation used to excite the x direction part of the D_z component.

$$D_z(i_{src}, j_{src}, k_{src}) = ((J_z(t_n + 2\Delta t) - J_z(t_n)/2)) - J_z(t_n + \Delta t) \tag{4.5}$$

The equation used to excite the y direction part of the D_z component.

If we keep the same equation for the x direction part and we add Δt to every term dependant of t in the equation of the y direction part, it results as follows:

$$D_z(i_{src}, j_{src}, k_{src}) = ((J_z(t_n + 3\Delta t) - J_z(t_n + \Delta t)/2)) - J_z(t_n + 2\Delta t) \tag{4.6}$$

The equation used to excite the y direction part of the D_z component.

Figure 4.19 shows the waveform of the equations (4.4) and (4.6). (4.5) is shown as a reference, to compare how the excitation waveform used to excite the x direction part of the D_z component is delayed Δt in time with respect to the excitation waveform used to excite the y direction part.

Observation of the D_z component in the plane $z = 64\Delta z$ in the 3D-FD-AOS-FDTD scheme when the excitation waveform used to excite the x direction part of the D_z component is (4.4) and the equation used to excite the y direction part of the D_z component is (4.6), is shown in Figure 4.20. When we add Δt to every term dependant of t in the equation used to excite the y direction part of the D_z component, the wave propagates parallelly to the y-axis.

On the other hand, If we keep the same equation for the y direction part and we add Δt to every term dependant on t in the equation of the x direction part,

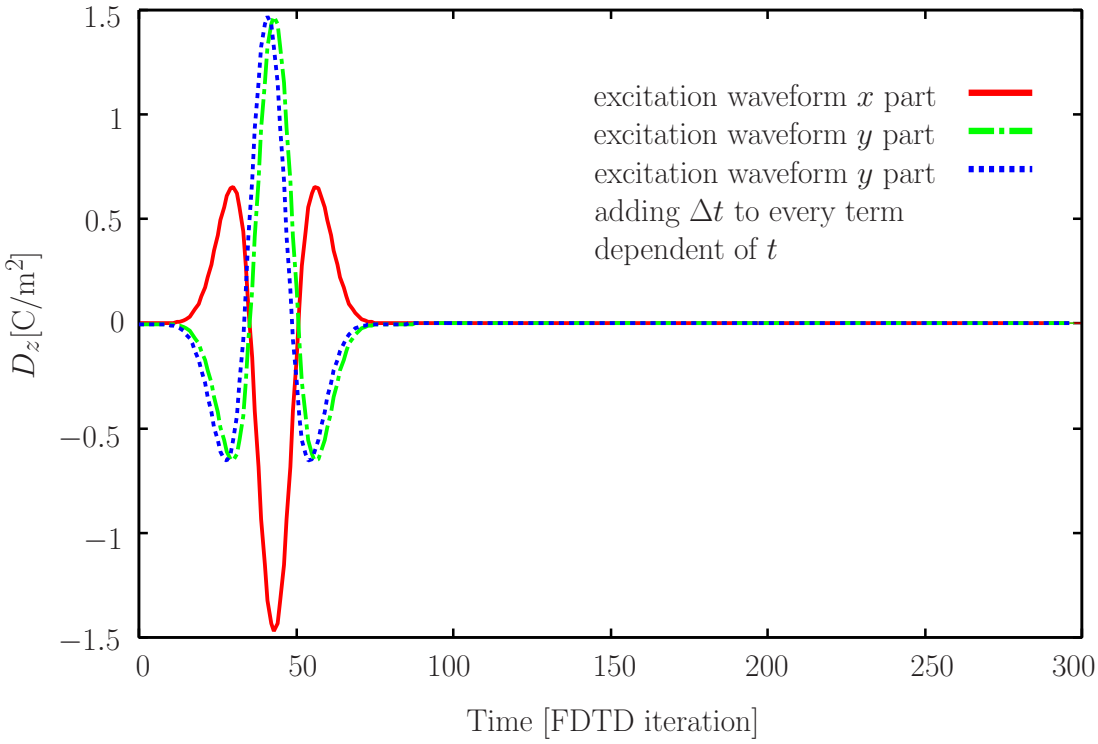

Figure 4.19: Excitation waveform of the x and y direction part in the 3D-FD-AOS-FDTD scheme.

it result as follows:

$$D_z(i_{src}, j_{src}, k_{src}) = J_z(t_n + 2\Delta t) - ((J_z(t_n + 3\Delta t) - J_z(t_n + \Delta t)/2)) \qquad (4.7)$$

The equation use to excite the x direction part of the D_z component.

Figure 4.21 shows the waveform of the equations (4.7) and (4.5). (4.4) is shown as a reference, to compare how the excitation waveform use to excite the y direction part of the D_z component is delayed Δt in time with respect to the excitation waveform use to excite the x direction part.

Observation of the D_z component in the plane $z = 64\Delta z$ in the 3D-FD-AOS-FDTD scheme when the excitation waveform used to excite the x direction part of the D_z component is (4.7) and the equation to excite the y direction part of the D_z component is (4.5) is shown in Figure 4.22. When we add Δt to every term dependant on t in the equation use to excite the x direction part of the D_z component, the wave propagates parallelly to the x-axis.

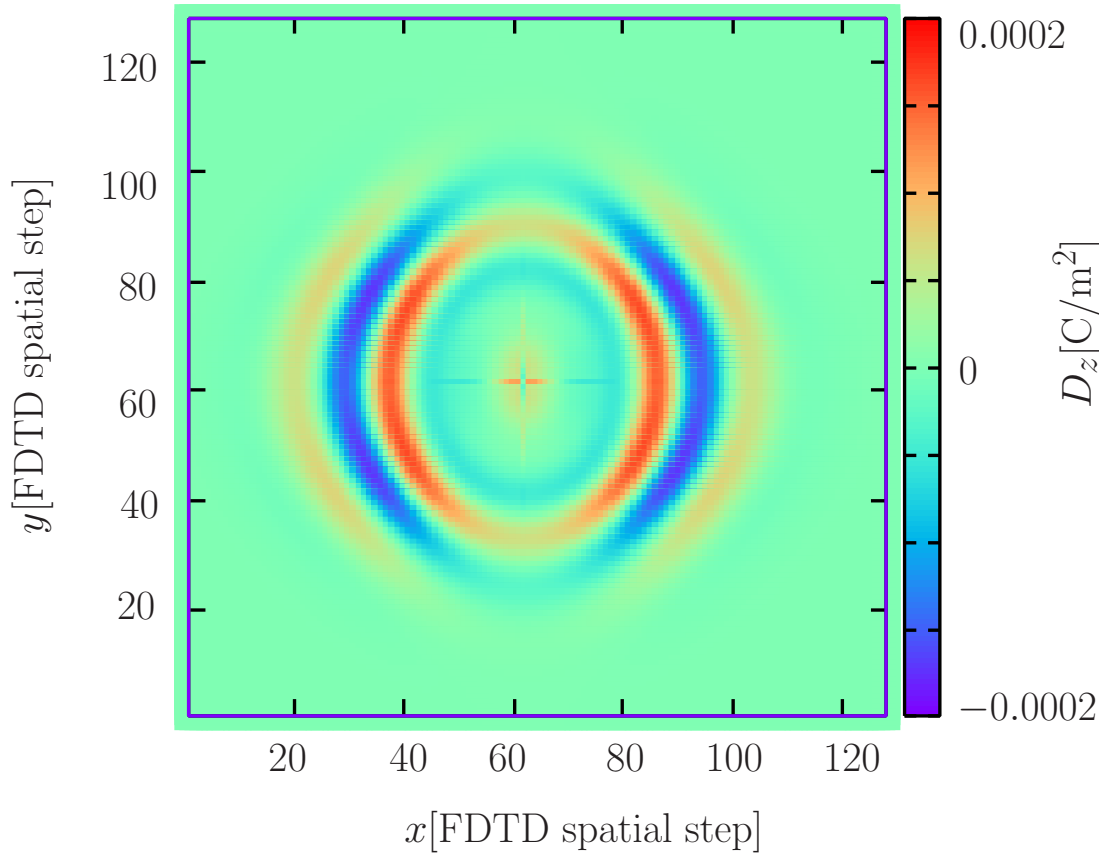

Figure 4.20: Observation of the D_z component in the plane $z = 64\Delta z$ in the 3D-FD-AOS-FDTD scheme at time step $\Delta t = 100$ when the excitation waveform used in the x direction part is is (4.4) and in the y direction part is (4.6).

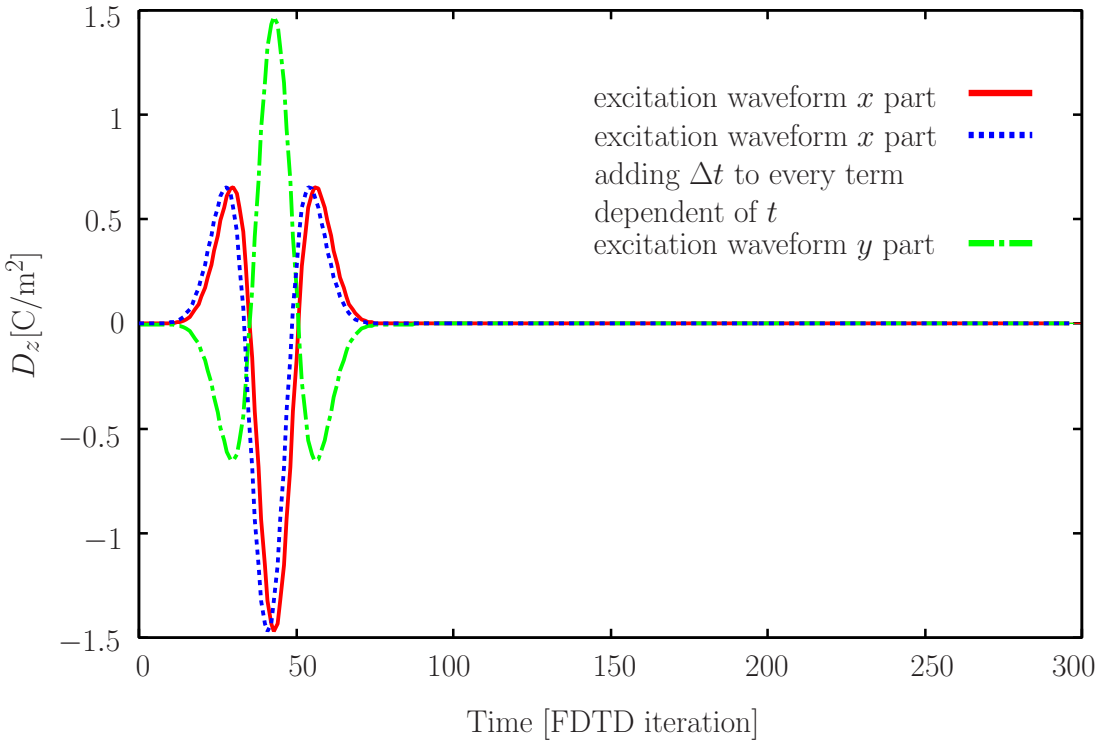

Figure 4.21: Excitation waveform of the x and y direction part in the 3D-FD-AOS-FDTD scheme.

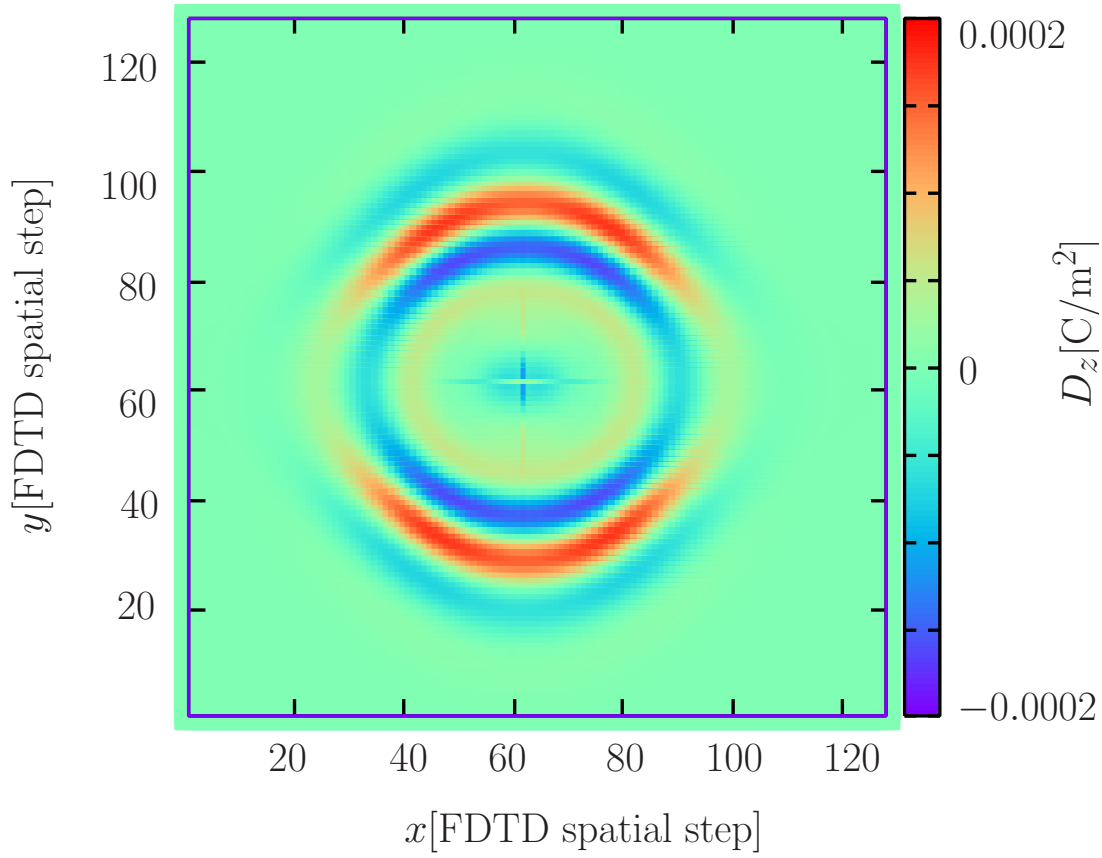

Figure 4.22: Observation of the D_z component in the plane $z = 64\Delta z$ in the 3D-FD-AOS-FDTD scheme at time step $\Delta t = 100$ when the excitation waveform used in the x direction part is is (4.7) and in the y direction part is (4.5).

In the 3D-AOS-FDTD method, combining equations (4.4) and (4.7) to build the excitation waveform used to excite the x direction part of the D_z component and combining equations (4.6) and (4.5) to build the excitation waveform used to excite the y direction part of the D_z component, and setting other values to indicate what future and past times are considered, we obtain the excitation waveform equations:

$$\begin{aligned} D_z(i,j,k) = (J_z(t+4\Delta) - ((J_z(t+7\Delta) - J_z(t+\Delta))/2))) \\ - ((J_z(t+5\Delta) - J_z(t+\Delta)/2) - J_z(t+3\Delta)) \end{aligned} \tag{4.8}$$

The equation use to excite the x direction part of the D_z component.

$$\begin{aligned} D_z(i,j,k) = (((J_z(t+8\Delta) - J_z(t+2\Delta)/2) - J_z(t+5\Delta)) \\ - (J_z(t+2\Delta) - ((J_z(t+4\Delta) - J_z(t)/2)) \end{aligned} \tag{4.9}$$

The equation used to excite the y direction part of the D_z component.

Figure 4.23 shows the excitation waveforms of the equations (4.8) and (4.9). Equations (4.4) and (4.5) are shown as a reference.

Observation of the output signal of the D_z component at points $(94, 64, 64)$ and $(74, 64, 64)$ are shown in Figure 4.24 and Figure 4.25 respectively. Observation in the 3D FD explicit FDTD scheme of the same component at the same points when the excitation waveform is a unmodulated Gaussian pulse is shown as a reference. Observation of the D_z component in the 3D-FD-AOS-FDTD scheme coincides relatively well with the observation of the D_z component in the explicit FDTD scheme.

Observation of the D_z component of the plane $z = 64\Delta z$ in the 3D-FD-AOS-FDTD scheme when the excitation waveforms used to excite the x direction part of the D_z component is (4.8) and the excitation waveform used to excite the y direction part of the D_z component is (4.9), are shown in Figure 4.26. Observation of the component D_z in the explicit FDTD scheme of the plane $64\Delta z$ when the excitation waveform is an unmodulated Gaussian pulse is shown as a reference. Observation of the D_z component in the 3D-FD-AOS-FDTD scheme in the plane $64\Delta z$ when the excitation waveforms are (4.8) and (4.9), is quite similar to the observation of the component D_z in the explicit FDTD scheme of the plane $64\Delta z$ when the excitation waveform is an unmodulated Gaussian pulse.

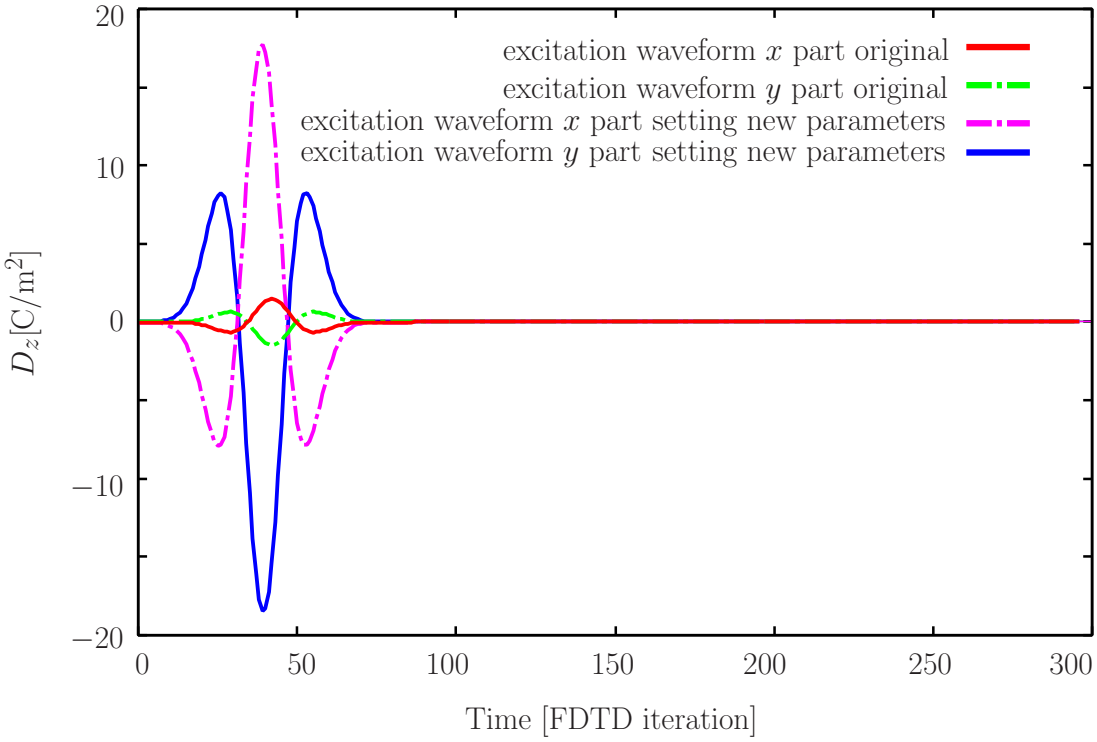

Figure 4.23: Excitation waveform (4.8) used in the x direction part and excitation wave form (4.9) used in the y direction part in the 3D-FD-AOS-FDTD scheme.

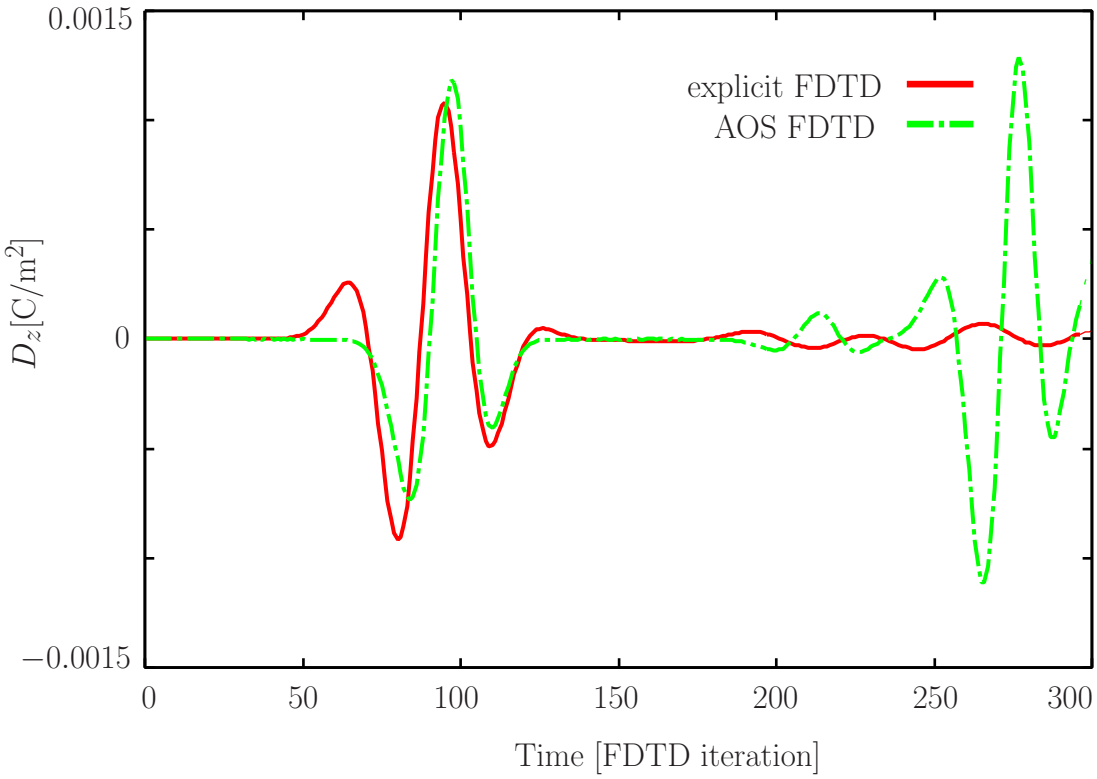

Figure 4.24: Observation of the D_z component at point $(94, 64, 64)$ in the 3D-FD-AOS-FDTD scheme when the excitation waveform used to excite the x direction part of the D_z component is (4.8) and the excitation waveform used to excite the y direction part of the D_z component is (4.9).

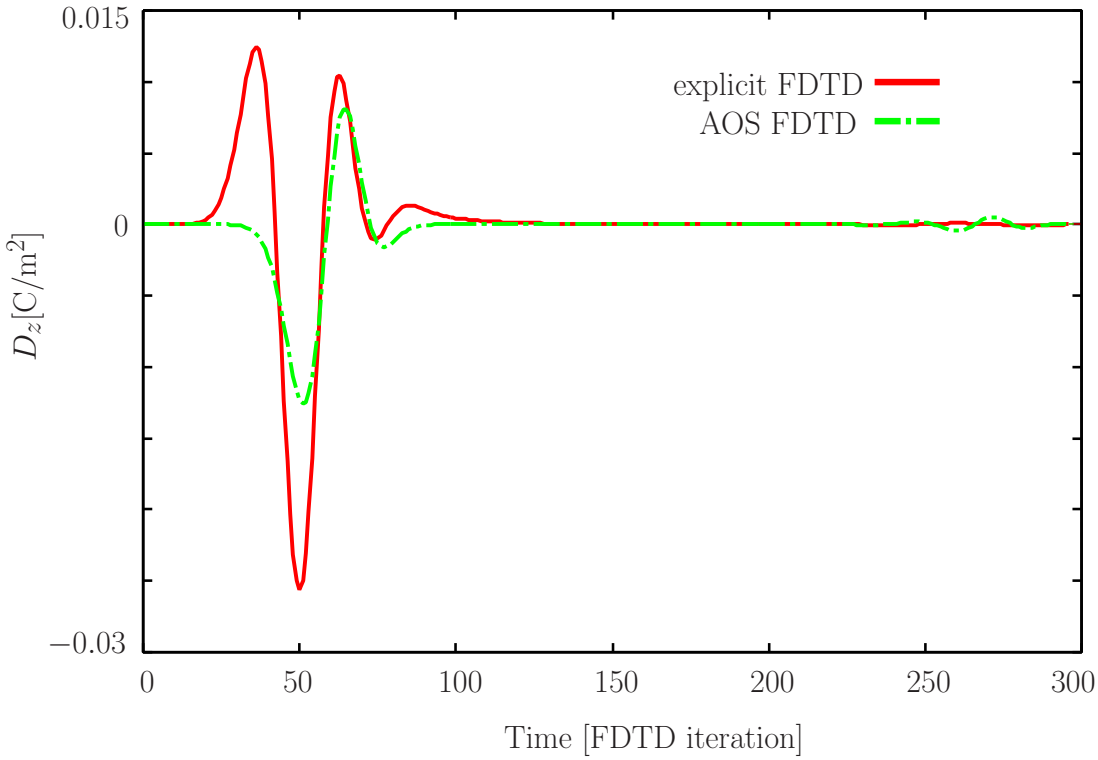

Figure 4.25: Observation of the D_z component at point $(74, 64, 64)$ in the 3D-FD-AOS-FDTD scheme when the excitation waveform used to excite the x direction part of the D_z component is (4.8) and the excitation waveform used to excite the y direction part of the D_z component is (4.9).

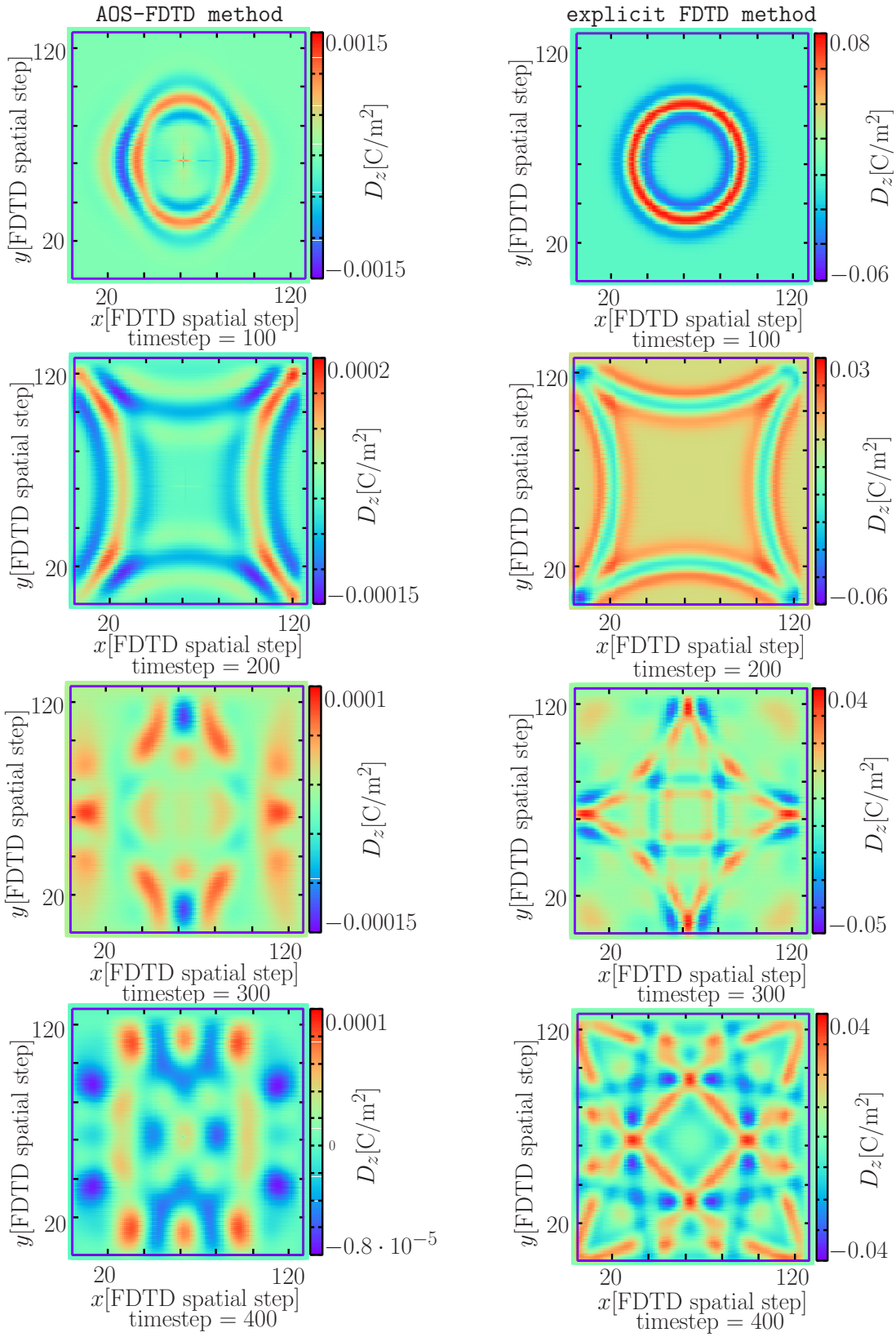

Figure 4.26: Observation of the D_z component in the plane $z = 64\Delta z$ in the 3D-FD-AOS-FDTD scheme when the excitation waveform used to excite the x direction part of the D_z component is (4.8) and the excitation waveform used to excite the y direction part of the D_z component is (4.9).

Chapter 5

Modified AOS FDTD method

5.1 Introduction

So far, Chapter 4 has presented the observation of different excitation waveforms in the 3D-FD-AOS-FDTD algorithm presented in Figure 2.2. In Chapter 5, we are going to introduce a modified 3D-FD-AOS-FDTD algorithm. The modified 3D-FD-AOS-FDTD scheme computes the calculations of the x direction part and the y direction part of the D_z component and calculates the average between the result of the calculation of both parts of the D_z component before making the calculations of the rest of the components and averaging them.

As it was claimed in Section 4.1, two source excitation updates happen at each time step. An electromagnetic wave is radiated in a single point of each direction part of the D_z component at each time step Δt. In the modified 3D-FD-AOS-FDTD algorithm, we can set the source excitation updates either right after calculating the x direction part and the y direction of the D_z component and before averaging both parts of the component or simply before calculating the x direction part and the y direction of the D_z component. On the one hand, we have named 'approach 1' to the scheme when the source excitation updates occur after calculating the x direction part and the y direction of the D_z component. The algorithm of 'approach 1' of the 3D-FD-AOS-FDTD is shown in Figure 5.1. On the other hand, we have named 'approach 2' when the source excitation updates are given just before calculating the x direction part and the y direction of the D_z component. The algorithm of 'approach 2' is shown in Figure 5.2.

Finally, we have also introduced one more approach, 'approach 3'. The algorithm of 'approach 3' of the 3D-FD-AOS-FDTD scheme is shown in Figure 5.3.

In 'approach 3', as well as in 'approach 2', the source excitation updates occur before calculating the x direction part and the y direction part of the D_z component. Furthermore, in 'approach 3', there is not average between the single points of the x direction part and the y direction part of the D_z component where the electromagnetic wave is radiated.

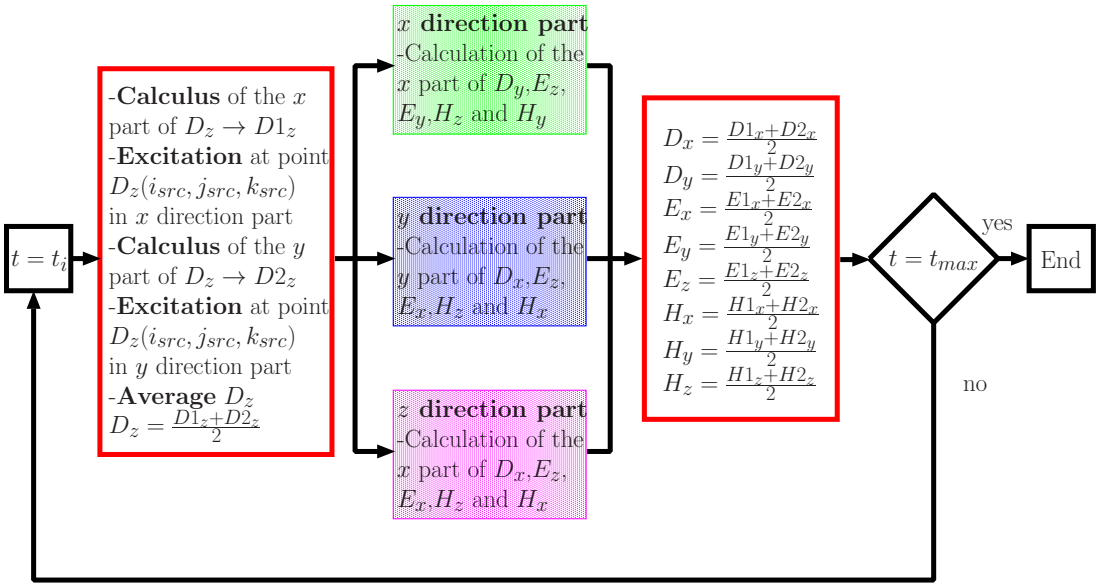

Figure 5.1: 'Approach 1' of the modified 3D-FD-AOS-FDTD algorithm.

To show the observation of the three approaches, we are going to implement all the schemes in the same scenario. The parameters of the scenario where the experiments have been performed are as follows:

- FDTD space: $128\Delta x \times 128\Delta y \times 128\Delta z$
- Number of time steps: 500
- $\Delta s = 10^{-3}$ m
- $\Delta t = 1.9245008 \cdot 10^{-12}$ seconds
- Location of the source: $(64\Delta x, 64\Delta y, 64\Delta z)$

Observation of the explicit FDTD scheme when the excitation waveform is an unmodulated Gaussian pulse will be shown as a reference.

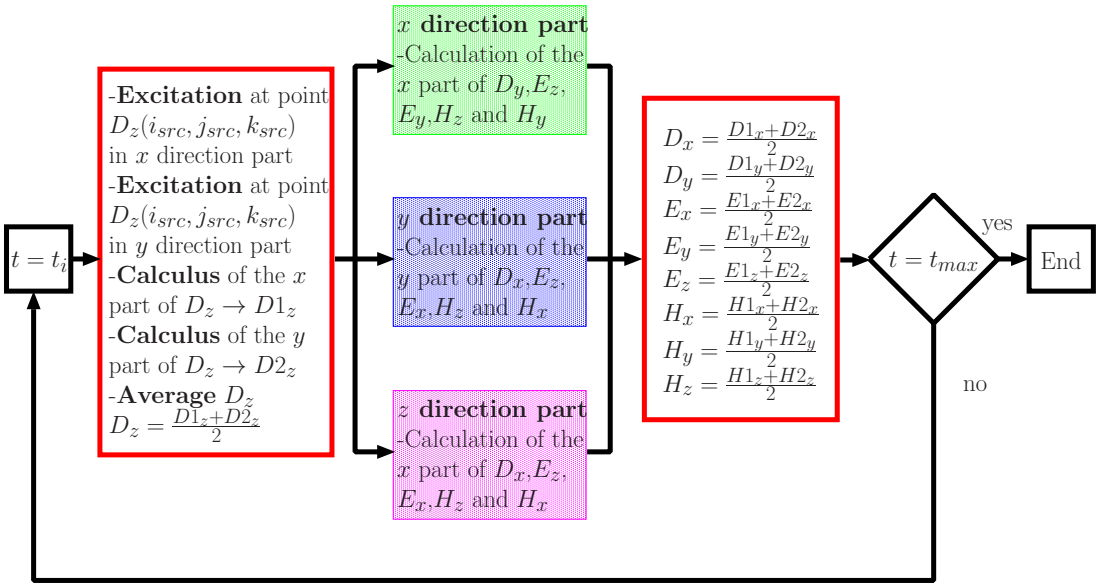

Figure 5.2: 'Approach 2' of the modified 3D-FD-AOS-FDTD algorithm.

5.2 'Approach 1' of the modified AOS-FDTD algorithm

As we have asserted, in 'approach 1' of the modified 3D-FD-AOS-FDTD scheme, the source excitation updates happen right after calculating the x direction part and the y direction part of the D_z component and before averaging both parts of the D_z component. Observation of the D_z component at point $(94, 64, 64)$ in 'approach 1' of the modified 3D-FD-AOS-FDTD scheme when the excitation waveform is an unmodulated Gaussian pulse diverges, it is shown in Figure 5.4. Observation of the same component at the same point in the explicit FDTD scheme when the excitation waveform is an unmodulated Gaussian pulse is shown as a reference. The amplitude of the observation of the modified 3D-FD-AOS-FDTD scheme has been multiplied by a factor of $-1 \cdot 10^{14}$.

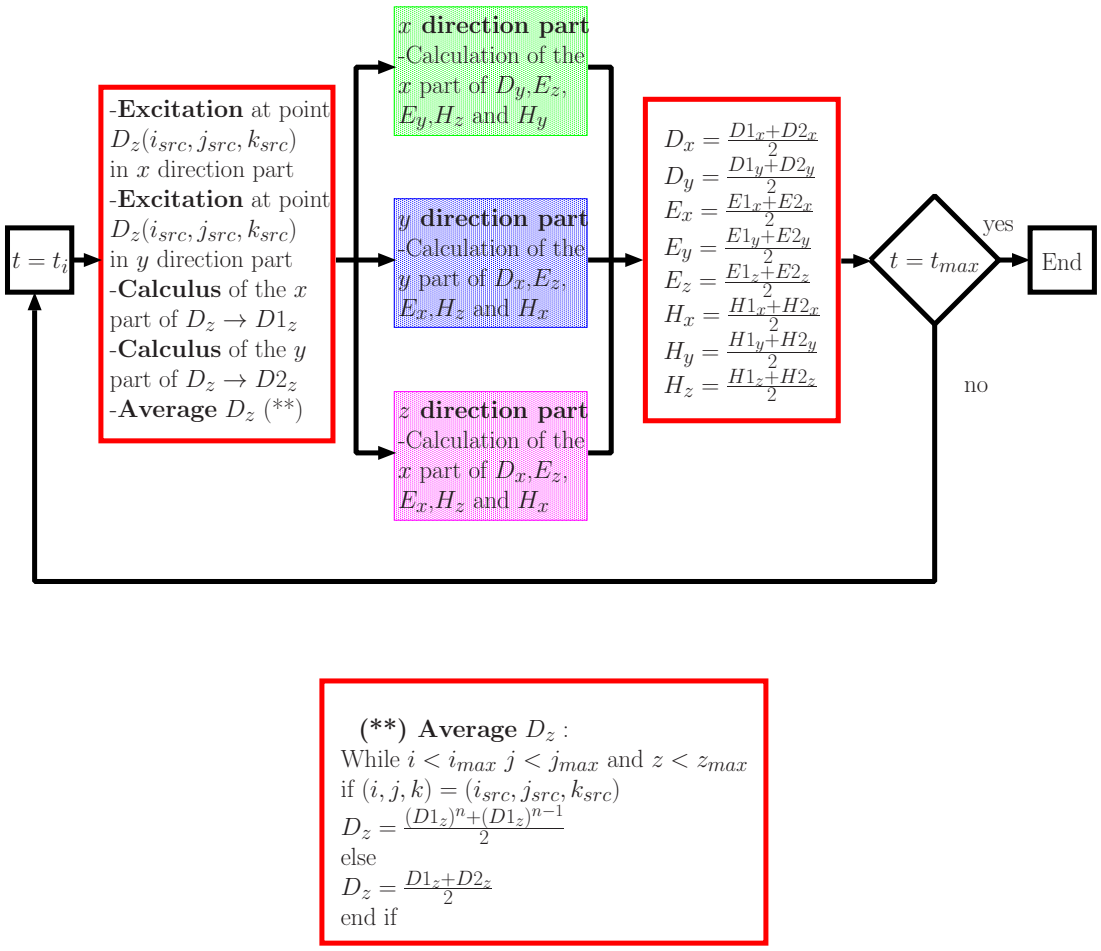

Figure 5.3: 'Approach 3' of the modified 3D-FD-AOS-FDTD algorithm.

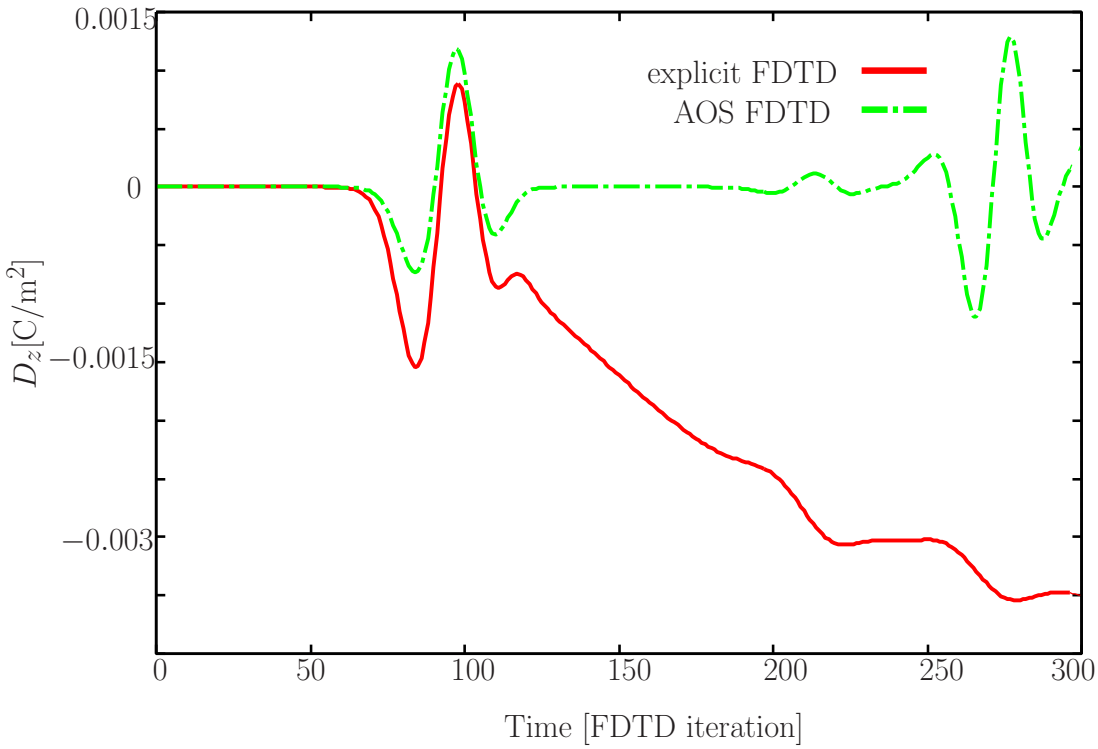

Figure 5.4: Observation of the field D_z at point $(94, 64, 64)$ in 'approach 1' of the modified 3D-FD-AOS-FDTD algorithm when the excitation waveform is a unmodulated Gaussian pulse.

In 'approach 1' of the modified 3D-FD-AOS-FDTD scheme when the excitation waveform is built considering past and future values of the value of an unmodulated Gaussian pulse at the current instant t, observation does not diverge. Figure 5.6 and Figure 5.7 shows observation at points $(94, 64, 64)$ and $(74, 64, 64)$ in 'approach 1' of the modified 3D-FD-AOS-FDTD scheme when the excitation waveform is the one shown in Figure 5.5. Observation of the same component at the same point in the explicit FDTD scheme when the excitation waveform is an unmodulated Gaussian pulse is shown as a reference. Note that the amplitude of the 3D-FD-AOS-FDTD scheme does not decrease with the propagation distance.

Figure 5.8 shows the observation of the D_z component in the plane $64\Delta z$ in 'approach 1' of the modified 3D-FD-AOS-FDTD scheme when the excitation waveform is built considering past and future values of the value of an unmodulated Gaussian pulse at the current instant t. Observation of the same component in the same plane in the explicit FDTD scheme when the excitation waveform is an unmodulated Gaussian pulse is shown as a reference. Because in 'approach 1' of the modified 3D-FD-AOS FDTD scheme the calculations of the x direction part and the y direction part of the D_z component and the average between them are carried out before calculating the parts of the rest of the components, the same value of the D_z component is used to calculate the x direction part and the y direction part of the electric E_z component. That makes that observation of the D_z component in the plane $64\Delta z$ in the modified 3D-FD-AOS-FDTD scheme, it is more similar to the observation of the D_z component in the plane $64\Delta z$ in the explicit FDTD scheme when the excitation waveform is a unmodulated Gaussian pulse. Furthermore, it also implies that the amplitude of the observation of the D_z component in 'approach 1' of the modified 3D-FD-AOS-FDTD scheme does not reduce with the propagation distance.

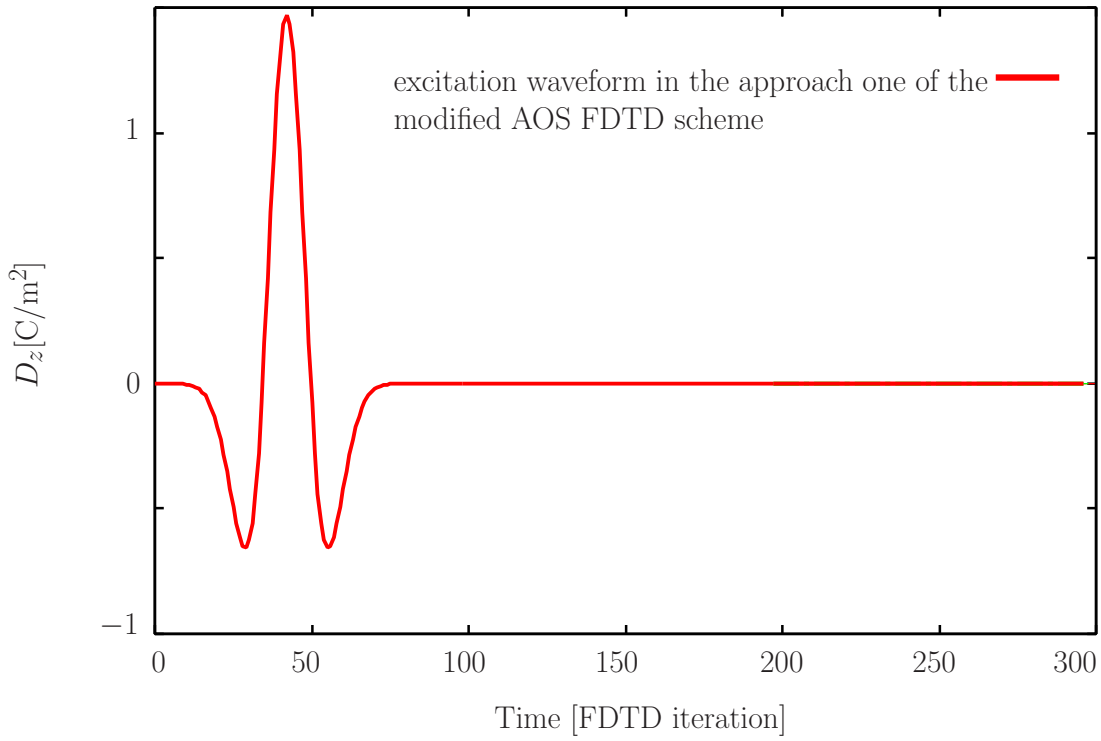

Figure 5.5: Excitation waveforms in 'approach 1' of the modified 3D-FD-AOS-FDTD scheme when the excitation waveform is built considering past and future values of the value of a Gaussian pulse at current instant t.

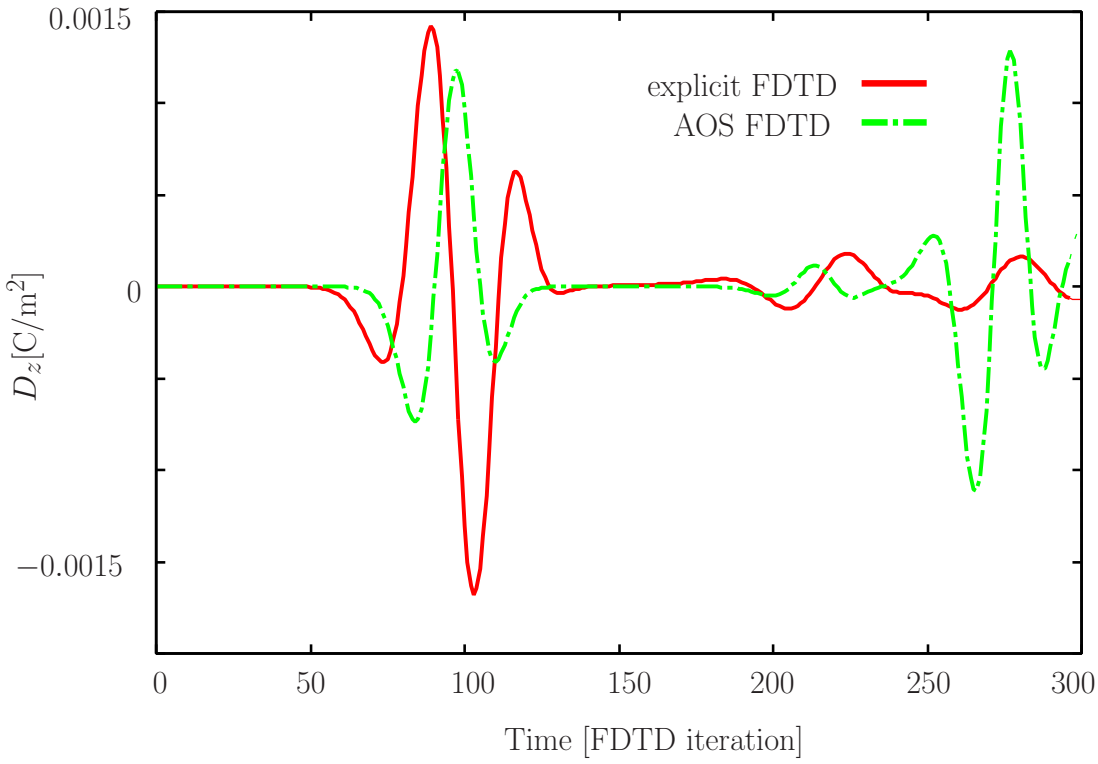

Figure 5.6: Observation of the D_z component in 'approach 1' of the modified 3D-FD-AOS-FDTD scheme at point $(94, 64, 64)$ when the excitation waveform is that shown in Figure 5.5.

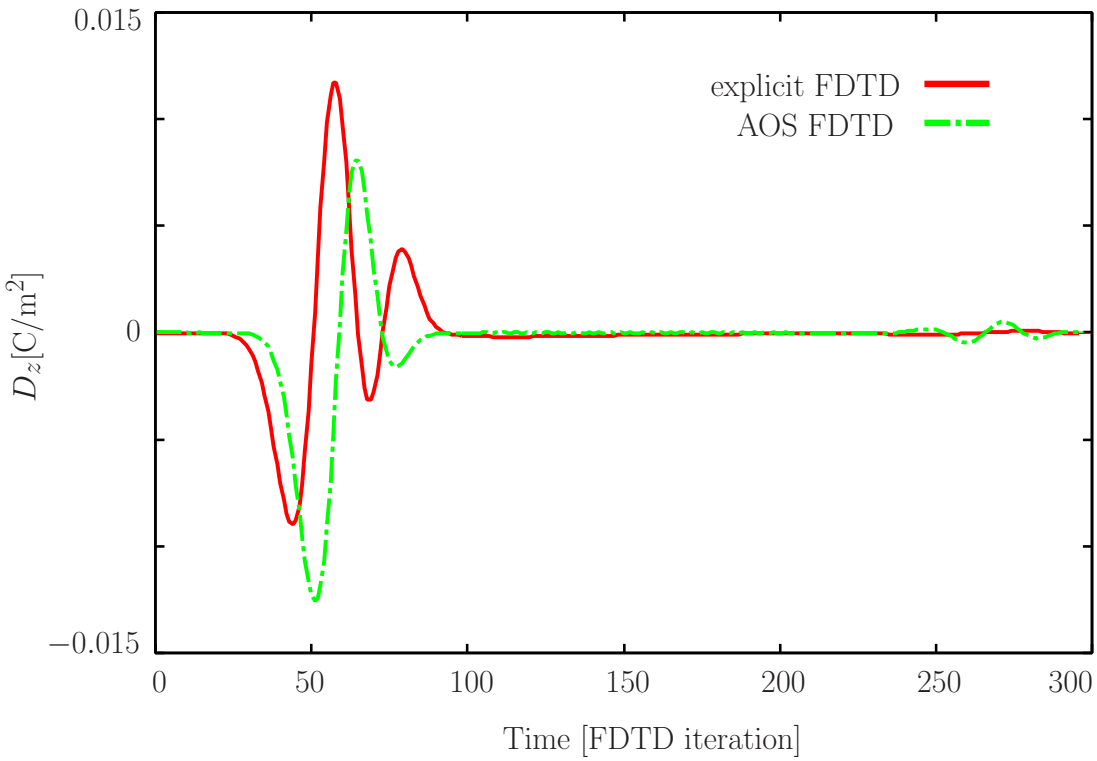

Figure 5.7: Observation of the D_z component in 'approach 1' of modified 3D-FD-AOS-FDTD scheme at point $(74, 64, 64)$ when the excitation waveform is the one shown in Figure 5.5.

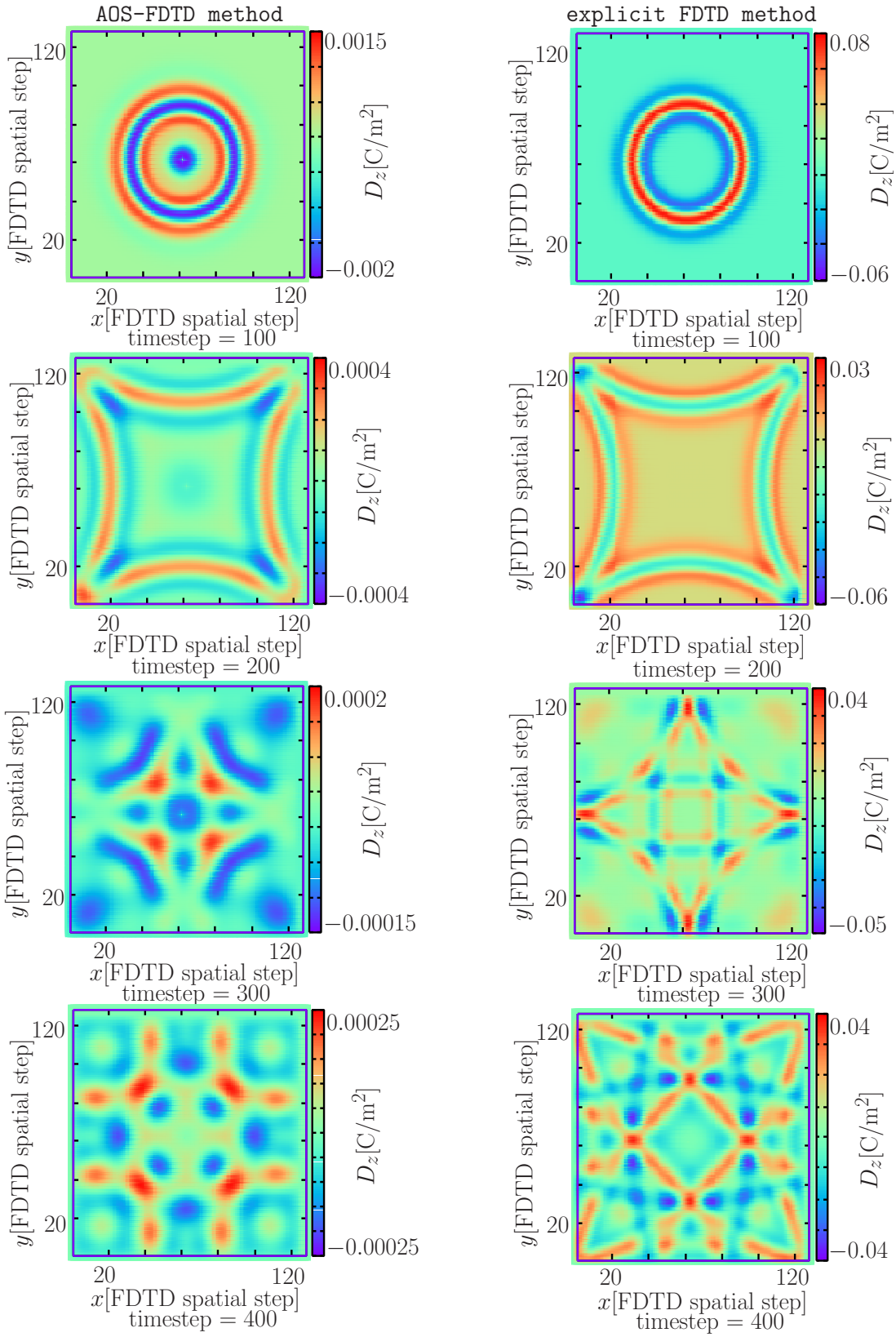

Figure 5.8: Observation of the D_z component in the plane $z = 64\Delta z$ in 'approach 1' of the modified 3D-FD-AOS-FDTD scheme when the excitation waveform is that shown in Figure 5.5.

5.3 'Approach 2' of the modified AOS-FDTD algorithm

In 'approach 2' of the modified 3D-FD-AOS-FDTD scheme, the source excitations updates occur before calculating the x direction part and the y direction part of the D_z component. In the modified 3D-FD-AOS-FDTD scheme, when the excitation waveform used in each direction part of the D_z component is an unmodulated Gaussian pulse and the unmodulated Gaussian pulse used in each direction part of the D_z component has the peak centre postion of the pulse at same time Δt, observation diverges.

When the excitation updates in both parts of the component D_z are unmodulated Gaussian pulses, the observation does not diverge if the peak centre position of each unmodulated Gaussian pulse of both updates are not at the same time Δt. For example, when the excitation waveform in the x direction part of the D_z component is $D_z(i_{src}, j_{src}, k_{src}) = J_z(t_n)$ and the excitation waveform in the y direction part of the D_z component is $D_z(i_{src}, j_{src}, k_{src}) = J_z(t_n + \Delta t)$, where $J_z(t_n)$ is a function of time, observation at points $(94, 64, 64)$ and $(74, 64, 64)$ does not diverge. Figure 5.9 shows the unmodulated Gaussian pulse of each part of the D_z component used in 'approach 2' of the modified AOS scheme. Figure 5.10 and Figure 5.11 show the observation of the D_z component at points $(94, 64, 64)$ and $(74, 64, 64)$ respectively. Observation of the same field at the same point in the explicit FDTD scheme when the excitation waveform is an unmodulated Gaussian pulse is shown as a reference. The amplitude of the observation of the modified 3D-FD-AOS-FDTD scheme has been multiplied by a factor of -2 in Figure 5.10 and in Figure 5.11. Note that the amplitude of the observation in 'approach 2' of the modified 3D-FD-AOS-FDTD scheme does not decrease with the propagation distance.

As in 'approach 2' of the modified 3D-FD-AOS-FDTD scheme the source excitations updates are given right before calculating the x direction part and the y direction part of the D_z component, the value of source excitation updated at current time step Δt is used to calculate the x direction part and the y direction part of the D_z component. That also gives stability to the whole computation and proves that the observation of an unmodulated Gaussian pulse in the 3D-FD-AOS-FDTD does not diverge.

Figure 5.12 shows the observation of the D_z component in the plane $z =$

$64\Delta z$ in 'approach 2' of the modified 3D-FD-AOS-FDTD scheme. Observation of the same component in the same plane in the explicit FDTD scheme when the exciattion waveform is an unmodulated Gaussian pulse is shown as a reference. Observation of the D_z component in the plane $z = 64\Delta z$ in 'approach 2' of the modified 3D-FD-AOS-FDTD scheme is quite different of the observation of the D_z component in the plane $z = 64\Delta z$ in the explicit FDTD scheme.

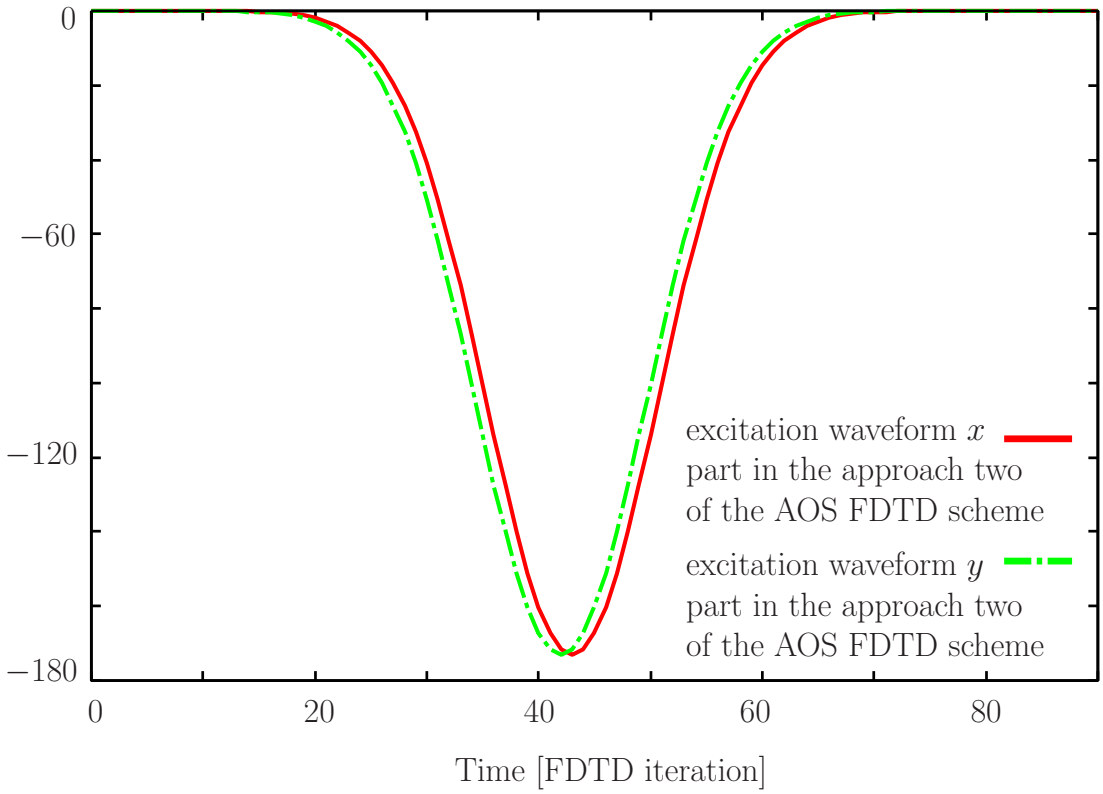

Figure 5.9: Excitation waveforms used in the x direction part and in the y direction part in 'approach 2' of the modified 3D-FD-AOS-FDTD.

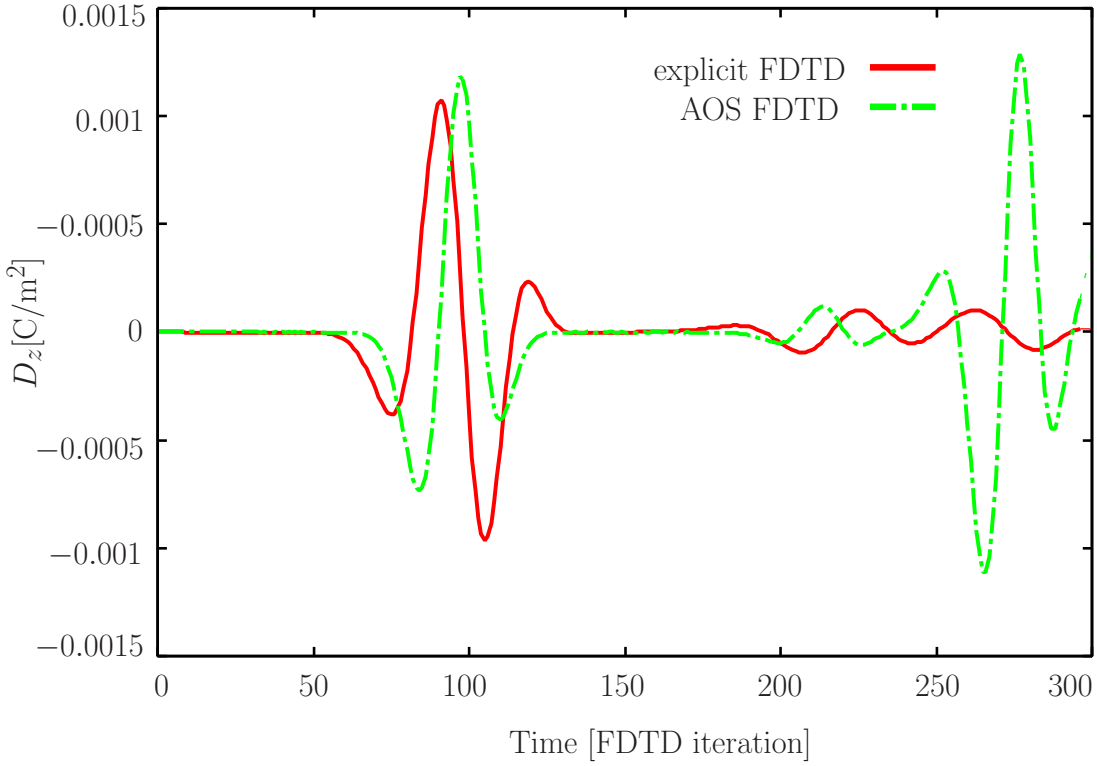

Figure 5.10: Observation of the D_z component at point $(94, 64, 64)$ in 'approach 2' of the modified 3D-FD-AOS-FDTD algorithm when the excitation waveforms used in each direction part of the D_z component are those shown in Figure 5.9.

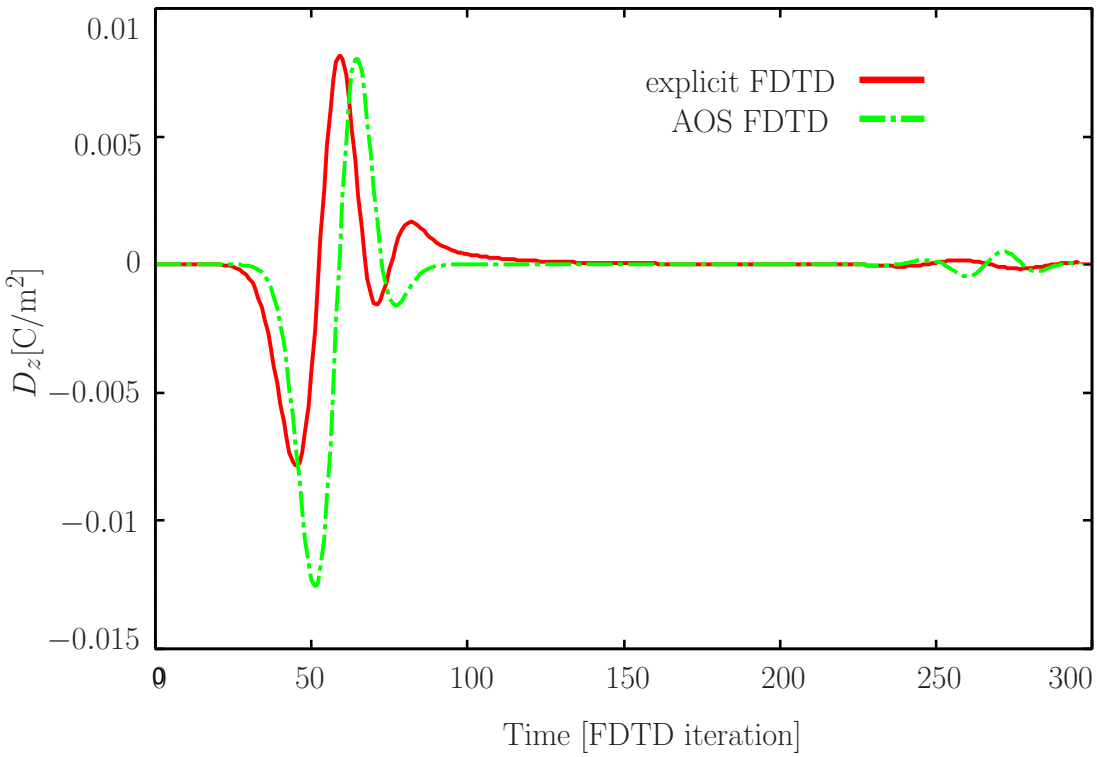

Figure 5.11: Observation of the D_z component at point $(74, 64, 64)$ in 'approach 2' of the modified 3D-FD-AOS-FDTD algorithm when the excitation waveforms used in each direction part of the D_z component are those shown in Figure 5.9.

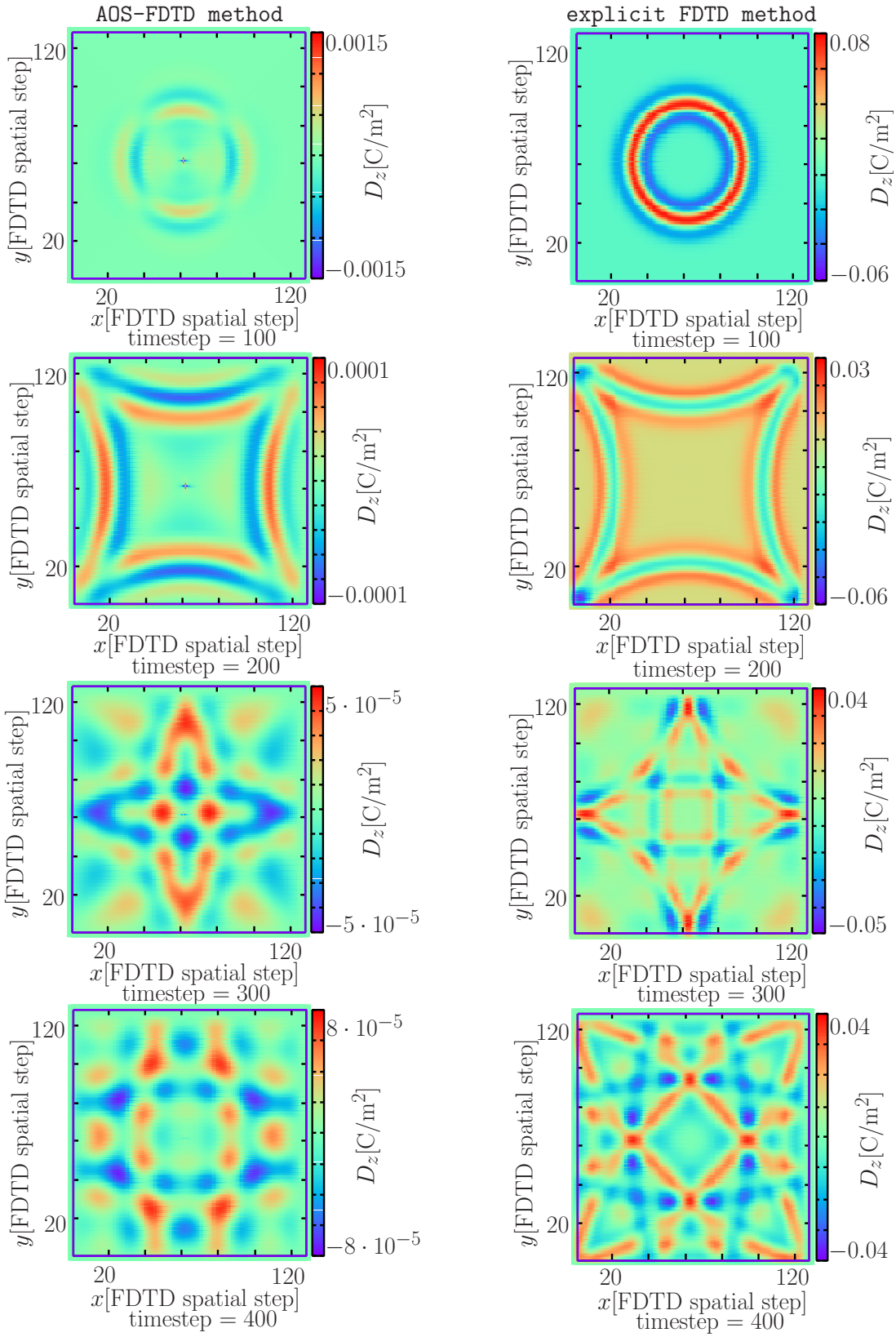

Figure 5.12: Observation of the D_z component in the plane $z = 64\Delta z$ in 'approach 2' of the modified 3D-FD-AOS-FDTD scheme when the excitation waveforms used in each direction part of the D_z component are those shown in Figure 5.9.

5.4 'Approach 3' of the modified 3D-FD-AOS-FDTD algorithm

In 'approach 3' of the modified 3D-FD-AOS-FDTD algorithm, equal than in 'approach 2', the source excitations updates occur before calculating the x direction part and the y direction part of the D_z component. Furthermore, in 'approach 3' there is not an average between the single points where the source excitation is updated in the x direction part of the D_z component and in the y direction part of the D_z component. So far, the average of both parts of a component was made by adding the value of the same single point of each part of the component and dividing by two. For instance, the average of every single point of both split parts of the D_z component was calculated by:

$$D_z^n(i,j,k) = (D_{z\,\text{x part}}^n(i,j,k) + D_{z\,\text{y part}}^n(i,j,k))/2 \tag{5.1}$$

for all the elements of the D_z component

In 'approach 3', there is not an average between the single points of both parts of the D_z component where the electromagnetic wave source is radiated. After calculating the x direction part and the y direction part of the D_z component in each time step, the point in the x direction part where the electromagnetic field is radiated keeps the same value. At the same time, the value of the point of the y direction part where the electromagnetic field is radiated, it is calculated averaging the value of the single point of the x direction part where the electromagnetic field was radiated at current time step t. The value of the single point of the x direction part where the electromagnetic field is radiated at the previous time step $t - \Delta t$, as follows:

$$D_z^n(i,j,k) = (D_{z\,\text{x part}}^n(i,j,k) + D_{z\,\text{x part}}^{n-1}(i,j,k))/2 \tag{5.2}$$

When in 'approach 3' of the 3D-FD-FDTD-AOS scheme the excitation waveforms of both excitation updates are the same unmodulated Gaussian pulse the observation does not diverge. Figure 5.13 and Figure 5.14 show the observation of the D_z component at points $(94, 64, 64)$ and $(74, 64, 64)$ respectively, when the excitation waveform is an unmodulated Gaussian pulse. Note that the amplitude reduces with the propagation distance in 'approach 3' of the modified 3D-FD-AOS-FDTD scheme when the excitation waveform is an unmodulated

Gausian pulse. The amplitude of the modified 3D-FD-AOS-FDTD scheme at point $(94, 64, 64)$ has been divided by a factor of -6 and at point $(74, 64, 64)$, it has been divided by a factor of -8.

Figure 5.15 shows the observation of the D_z component in the plane $z = 64\Delta z$ in 'approach 3' of the modified 3D-FD-AOS-FDTD scheme when the excitation waveform is an unmodulated Gausian pulse. Observation of the same component in the same plane in the explicit FDTD scheme when the exciattion waveform is an unmodulated Gaussian pulse is shown as a reference. Observation of the D_z component in the plane $z = 64\Delta z$ in 'approach 3' of the modified 3D-FD-AOS-FDTD scheme when the excitation waveform is an unmodulated Gausian pulse is quite different from the observation of the D_z component in the plane $z = 64\Delta z$ in the explicit FDTD scheme when the excitation waveforms used in each direction part of the D_z component is an unmodulated Gaussian pulse.

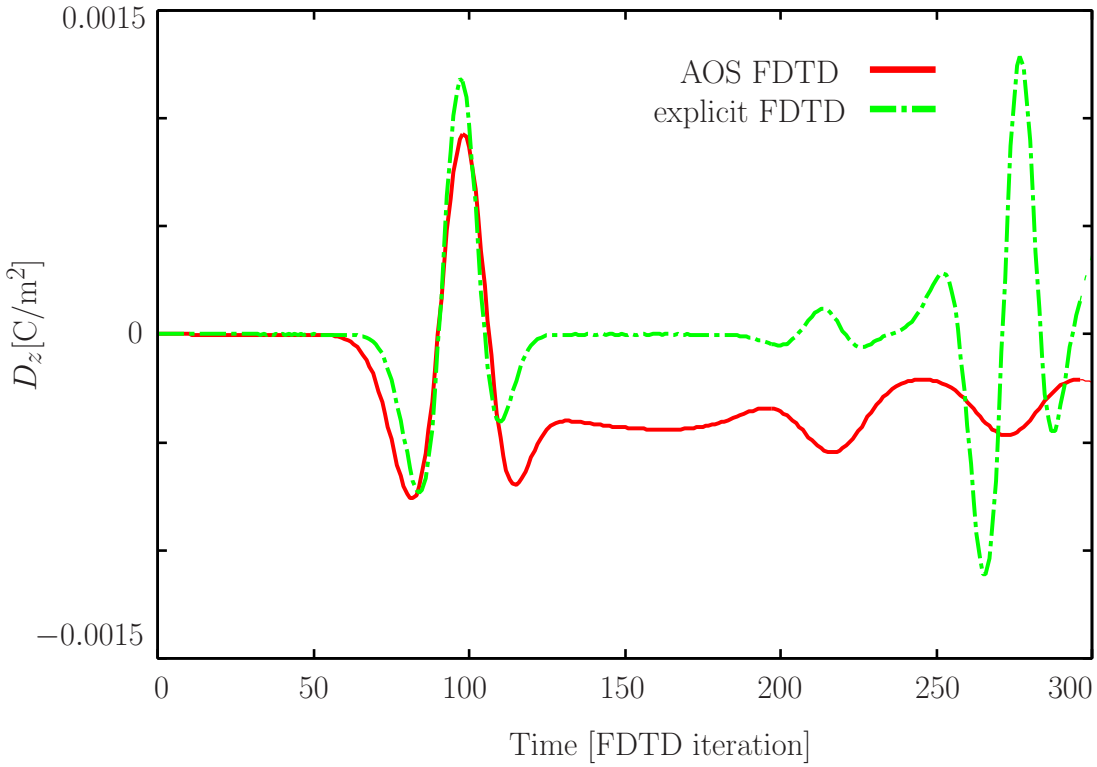

Figure 5.13: Observation of the D_z component at point $(94, 64, 64)$ in 'approach 3' of the modified 3D-FD-AOS-FDTD algorithm when the excitation waveform is an unmodulated Gaussian pulse.

In 'approach 3' of the modified 3D-FD-AOS-FDTD when the excitation waveform is built with past and future values of an unmodulated Gaussian pulse at

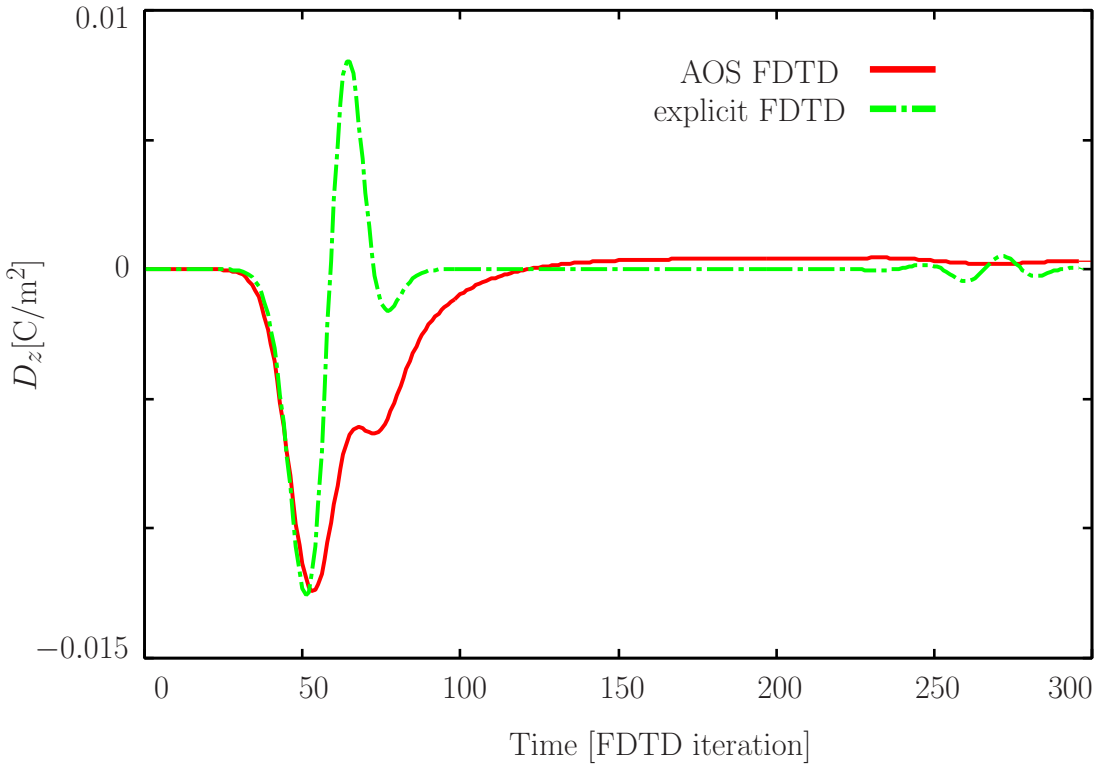

Figure 5.14: Observation of the D_z component at point $(74, 64, 64)$ in 'approach 3' of the modified 3D-FD-AOS-FDTD algorithm when the excitation waveform is an unmodulated Gaussian pulse.

current instant t, which shape is shown in Figure 5.5, observation is quite similar to that of the explicit FDTD scheme when the excitation waveform is an unmodulated Gaussian pulse. Figure 5.16 and Figure 5.17 show the observation of 'approach 3' of the modified 3D-FD-AOS-FDTD scheme at points $(74, 64, 64)$ and $(94, 64, 64)$, respectively. Note that the amplitude of 'approach 3' of the modified 3D-FD-FDTD scheme increase with the propagation distance when the excitation waveform is built with past and future values of an unmodulated Gaussian pulse. Amplitude of 'approach 3' of the modified 3D-FD-FDTD scheme at point $(94, 64, 64)$ has been multiplied by a factor of 10 and amplitude of 'approach 3' of the modified 3D-FD-FDTD scheme at point $(74, 64, 64)$ has been multiplied by a factor of 15.

Figure 5.18 shows the observation of the D_z component in the plane $z = 64\Delta z$ in 'approach 3' of the modified 3D-FD-AOS-FDTD scheme when the excitation waveform is built with past and future values of an unmodulated Gaussian pulse at current instant t. Observation of the same component in the same plane

in the explicit FDTD scheme when the exciattion waveform is an unmodulated Gaussian pulse is shown as a reference. Observation of the D_z component in the plane $z = 64\Delta z$ in 'approach 3' of the modified 3D-FD-AOS-FDTD scheme is quite similar to the observation of the D_z component in the plane $z = 64\Delta z$ in the explicit FDTD scheme when the excitation waveforms of both direction part updates are the same Gaussian pulse.

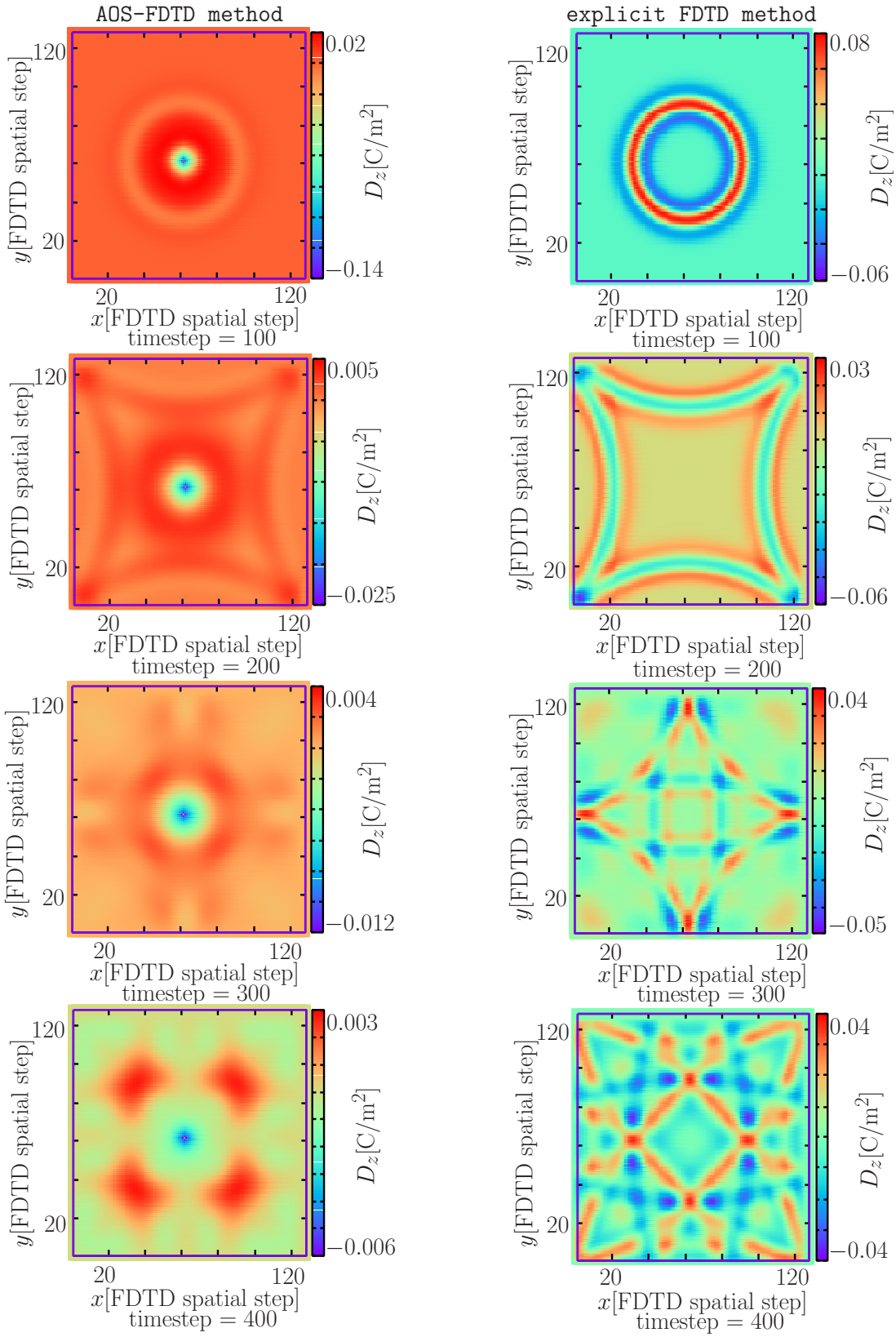

Figure 5.15: Observation of the field D_z in the plane $z = 64\Delta z$ in 'approach 3' of the modified 3D-FD-AOS-FDTD scheme when the excitation waveform is an unmodulated gausian pulse.

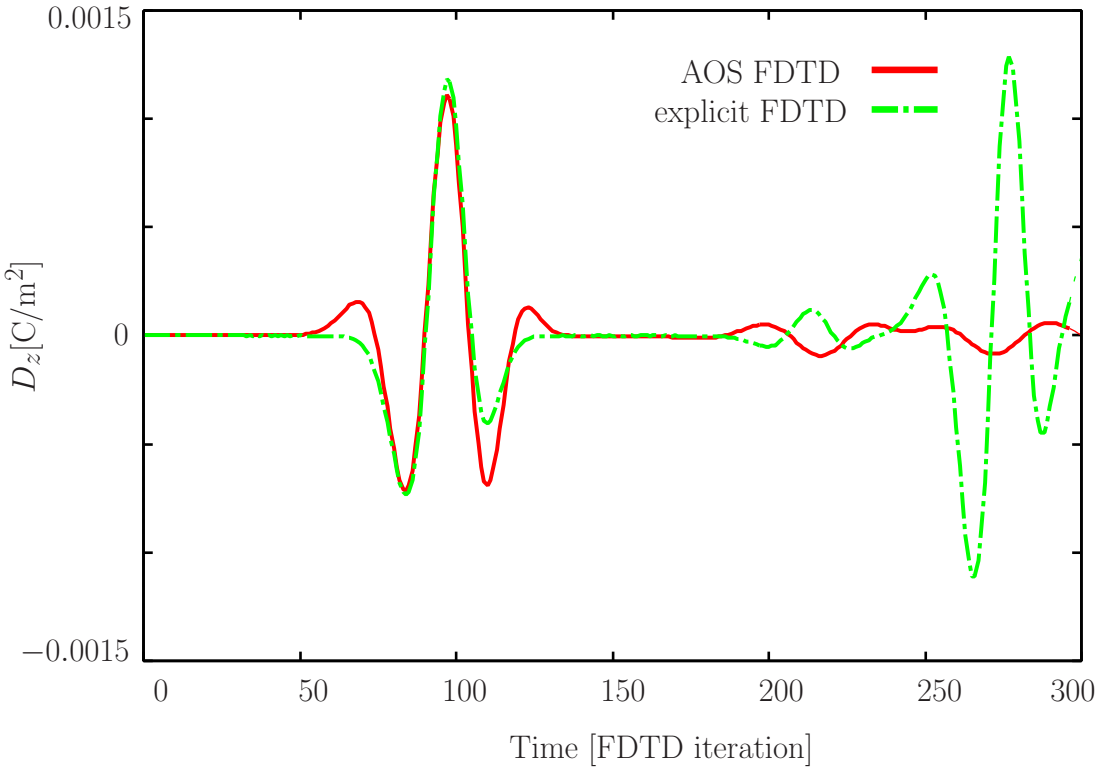

Figure 5.16: Observation of the D_z component at point $(94, 64, 64)$ in 'approach 3' of the modified 3D-FD-AOS-FDTD algorithm when excitation waveform is built with past and future values of an unmodulated Gaussian pulse at current instant t.

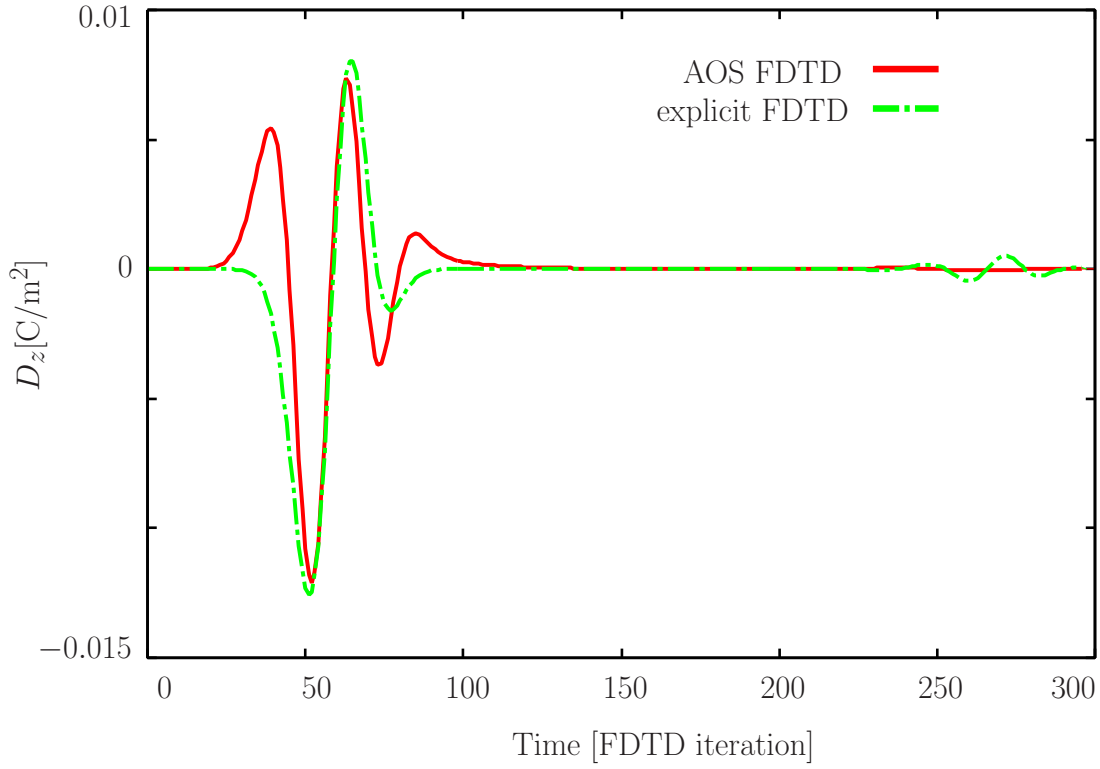

Figure 5.17: Observation of the D_z component at point $(74, 64, 64)$ in 'approach 3' of the modified 3D-FD-AOS-FDTD algorithm when excitation waveform is built with past and future values of an unmodulated Gaussian pulse at current instant t.

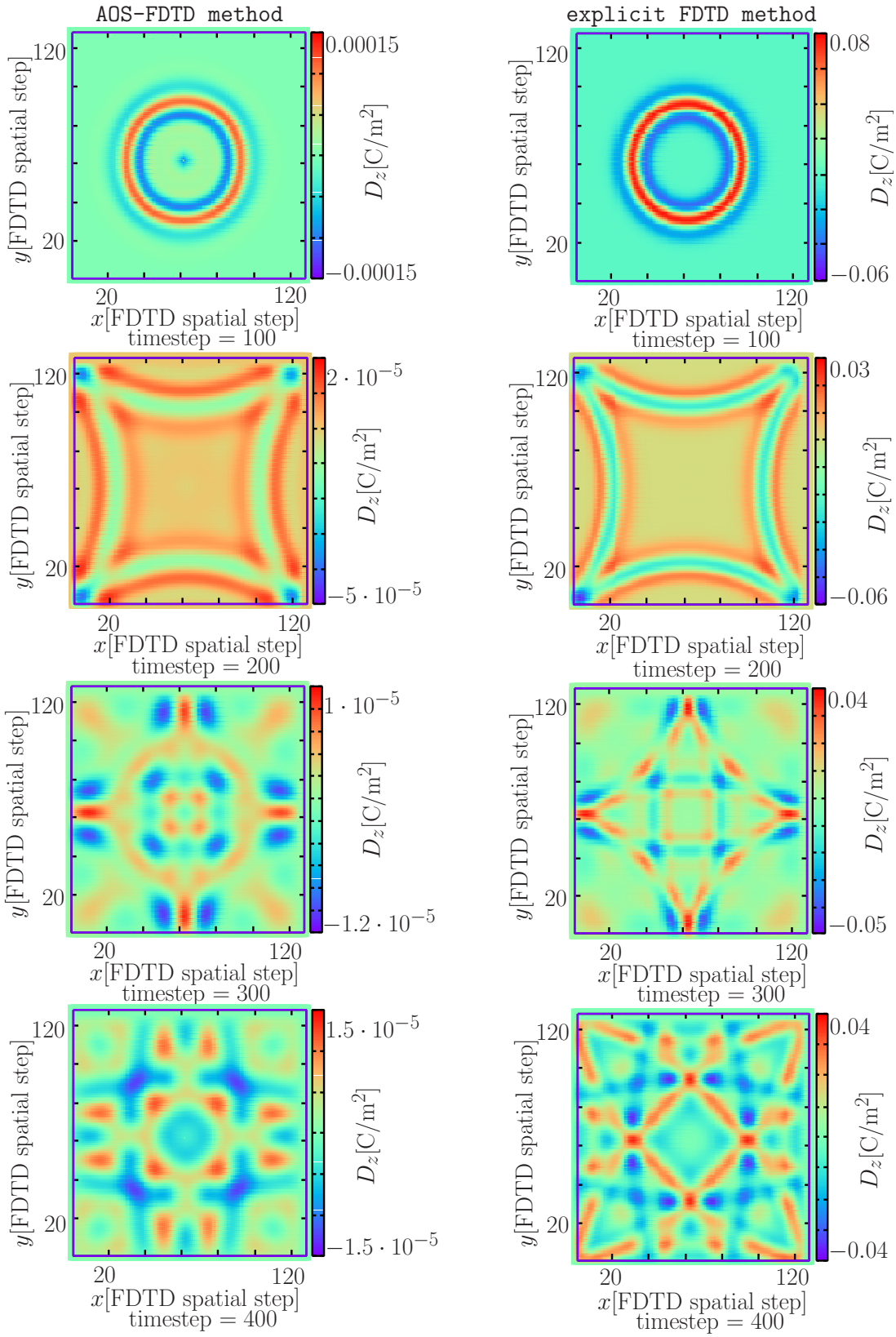

Figure 5.18: Observation of the field D_z in the plane $z = 64\Delta z$ in 'approach 3' of the modified 3D-FD-AOS-FDTD scheme when the the excitation waveforms is the one shown in Figure 5.5.

Chapter 6

Simulated results

6.1 Introduction

We are going to study the unconditional stability of the leapfrog 3D-FD-AOS-FDTD method beyond the Courant Friedrichs Lewy condition showing the performance of the scheme with different Courant-Friedrichs-Lewy numbers (CFLN). The CFLN is an upper limit on the time step of the Courant Friedrichs Lewy (CFL) stability condition. The CFLN is dened as the ratio between the time step of the three-dimensional FD-AOS-FDTD method and the maximum allowable time step of the conventional three-dimensional FDTD method. As we have mentioned in Section 1.6, the CFL condition shown in (1.41) set the maximum time step size in the explicit FDTD method, keeping it stable. Thus, CFLN= $\frac{\Delta t}{\Delta t_{CFL}}$ where Δt is the time step and Δt_{CFL} is the critical time step given by $\Delta t_{CFL} = (c\sqrt{\Delta x^{-2} + \Delta y^{-2} + \Delta z^{-2}})^{-1}$ where c is the speed of light.

The 3D-FD-AOS-FDTD algorithm used in the experiments in Chapter 6, is presented in Section 5.4 and named in this Thesis 'approach 3'of the modified 3D-FD-AOS-FDTD scheme. The algorithm of 'approach 3':

- computes the calculations of the x direction part and the y direction part of the component D_z and calculates the average between the result of the calculation of both parts of the component D_z before making the calculations of the rest of the components and averages them.

- there is not an average between the single points of the x direction part and the y direction part of the component D_z where the electromagnetic field is radiated.

Figure 5.5 shows the excitation waveform used in the experiments of this Chapter 6. The excitation waveform used is built with past and future values of an unmodulated Gaussian pulse in the current instant t.

The parameters of the scenario where the experiments have been performed are as follows:

- FDTD space: $128\Delta x \times 128\Delta y \times 128\Delta z$
- Number of time steps: 500
- $\Delta s = 10^{-3}$ m
- $\Delta t = 1.9245008 \cdot 10^{-12}$ seconds
- Location of the source: $(64\Delta x, 64\Delta y, 64\Delta z)$

Observation of the explicit FDTD scheme when the excitation waveform is an unmodulated Gaussian pulse will be shown as a reference.

6.2 CFL number = 2

Figure 6.1 and Figure 6.2 show the observations at points $(94, 64, 64)$ and $(74, 64, 64)$ respectively, in 'approach 3' of the modified 3D-FD-AOS-FDTD scheme with a CFL number equals to two when the excitation waveform is that shown in Figure 5.5. The observation signal of the explicit 3D-FD-FDTD method when the excitation waveform is an unmodulated Gaussian pulse, is shown as a reference.

When CFLN equals to two the observed waveform of the 3D-FD-AOS-FDTD method is quite similar to the reference. Note that the amplitude is reduced with the propagation distance in the 3D-FD-AOS-FDTD scheme. Observation in the 3D-FD-AOS-FDTD scheme at points $(94, 64, 64)$ and $(74, 64, 64)$ has been multiplied by a factor of 10 and 5 respectively.

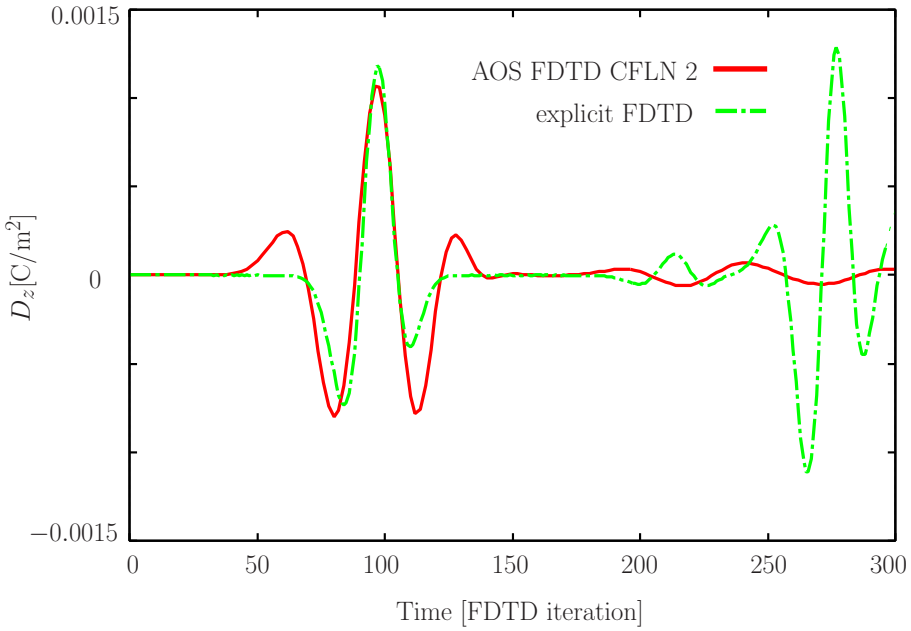

Figure 6.1: Observation at point $(94, 64, 64)$ when CFLN is equals to two in 'approach 3' of the modified 3D-FD-AOS-FDTD scheme with a CFL number equals to two when the excitation waveform is that shown in Figure 5.5.

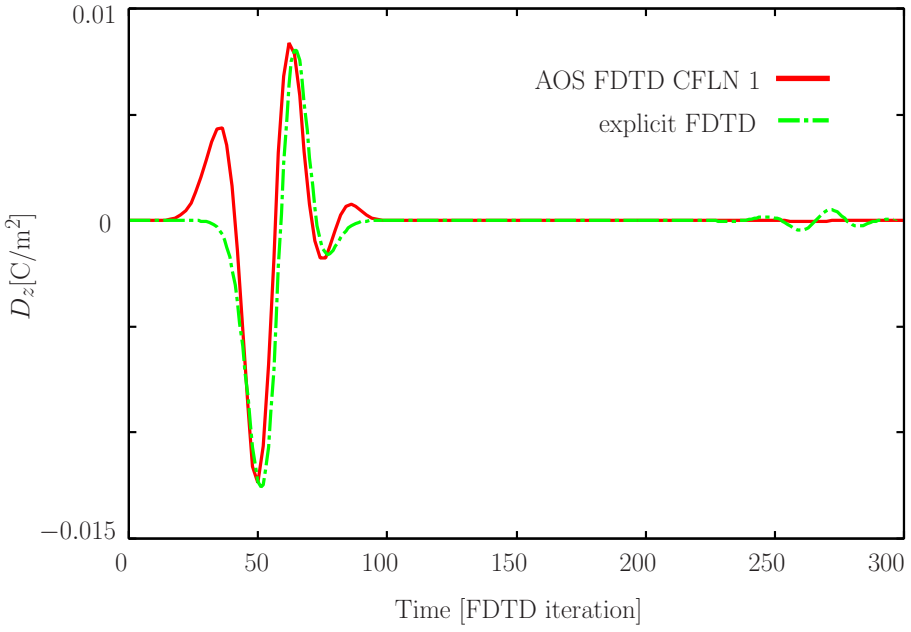

Figure 6.2: Observation at point $(74, 64, 64)$ when CFLN is equals to two in 'approach 3' of the modified 3D-FD-AOS-FDTD scheme with a CFL number equals to two when the excitation waveform is that shown in Figure 5.5.

6.3 CFL number = 3

Figure 6.3 and Figure 6.4 show the observations at points $(94, 64, 64)$ and $(74, 64, 64)$ respectively, in 'approach 3' of the modified 3D-FD-AOS-FDTD scheme with a CFL number equals to three when the excitation waveform is that shown in Figure 5.5. The observation signal of the explicit 3D-FD-FDTD method when the excitation waveform is an unmodulated Gaussian pulse, is shown as a reference.

When CFLN equals s to three the observed waveform of the 3D-FD-AOS-FDTD method is quite similar to the reference. Note that the amplitude is reduced with the propagation distance in the 3D-FD-AOS-FDTD scheme. Observation in the 3D-FD-AOS-FDTD schemes at points $(94, 64, 64)$ and $(74, 64, 64)$ has been multiplied by a factor of 10 and 2 respectively.

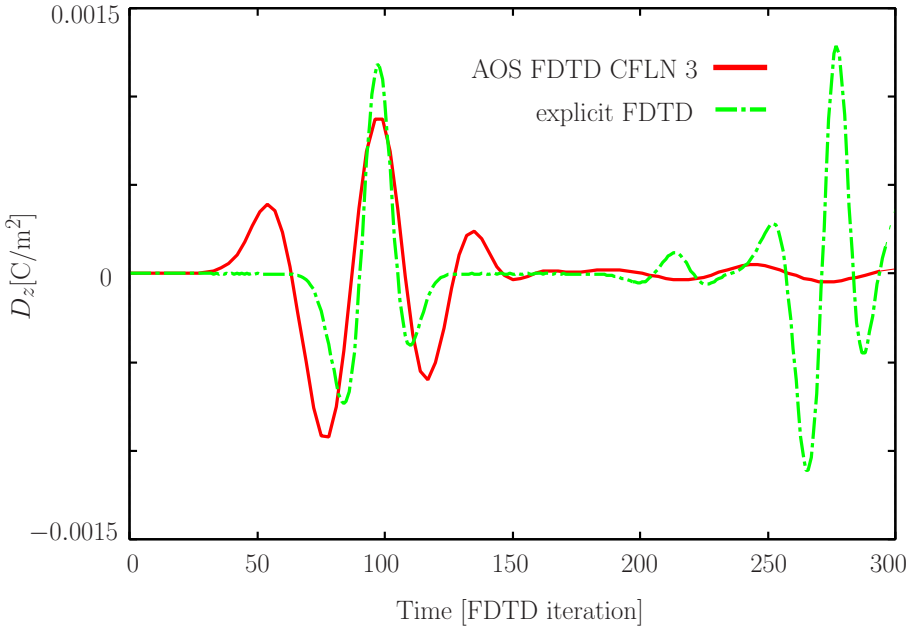

Figure 6.3: Observation at point $(94, 64, 64)$ when CFLN is equals s to three in 'approach 3' of the modified 3D-FD-AOS-FDTD scheme with a CFL number equals to three when the excitation waveform is that shown in Figure 5.5.

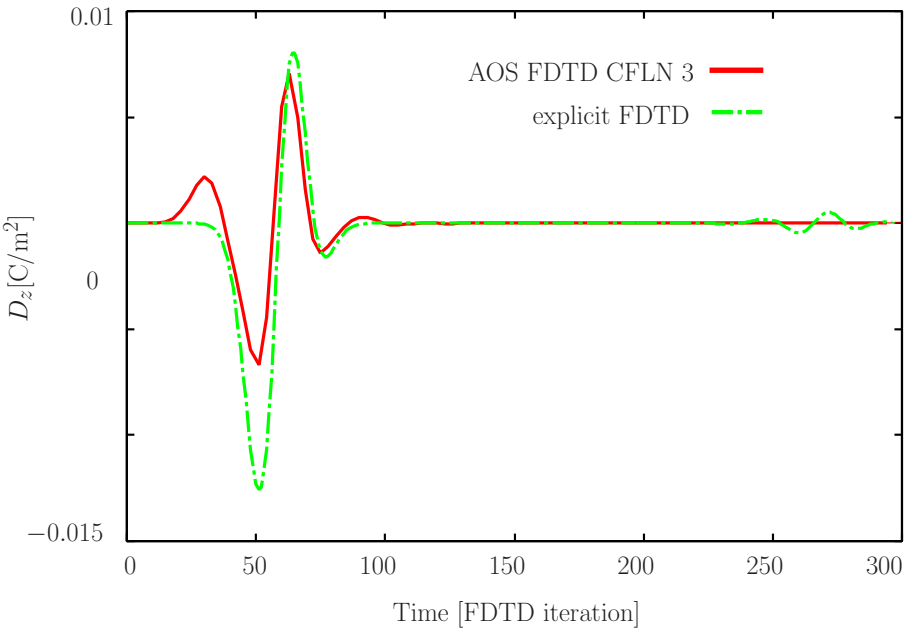

Figure 6.4: Observation at point $(74, 64, 64)$ when CFLN is equals to two in 'approach 3' of the modified 3D-FD-AOS-FDTD scheme with a CFL number equals to three when the excitation waveform is that shown in Figure 5.5.

6.4 CFL number = 4

Figure 6.5 and Figure 6.6 show the observations at points $(94, 64, 64)$ and $(74, 64, 64)$ respectively, in 'approach 3' of the modified 3D-FD-AOS-FDTD scheme with a CFL number equals to four when the excitation waveform is that shown in Figure 5.5. The observation signal of the explicit 3D-FD-FDTD method when the excitation waveform is an unmodulated Gaussian pulse, is shown as a reference.

When CFLN equals to four the observed waveform of the 3D-FD-AOS-FDTD method starts to be slightly different to the reference. Note that the amplitude is reduced with the propagation distance in the 3D-FD-AOS-FDTD scheme. Observation in the 3D-FD-AOS-FDTD schemes at points $(94, 64, 64)$ and $(74, 64, 64)$ has been multiplied by a factor of 10 and 2 respectively.

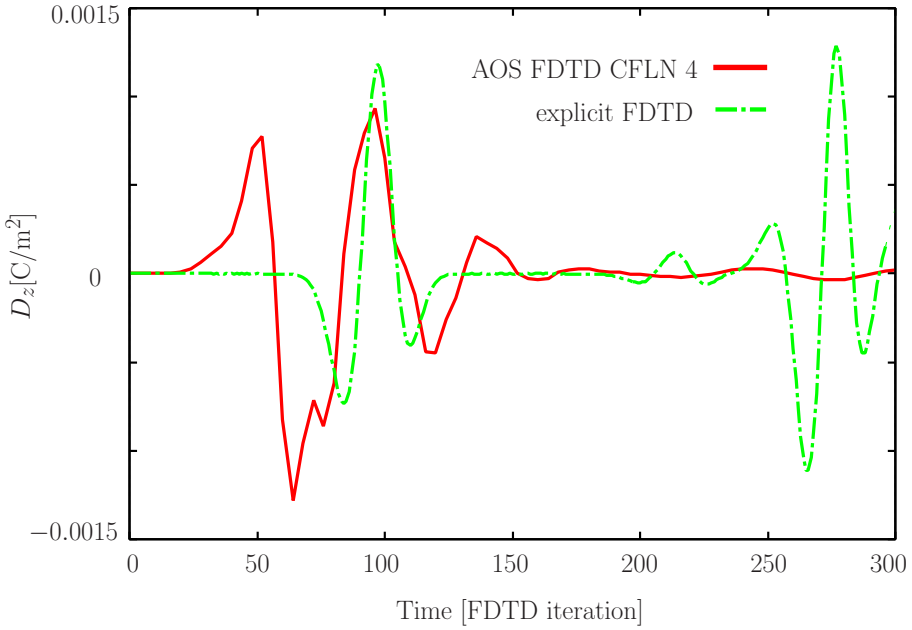

Figure 6.5: Observation at point $(94, 64, 64)$ when CFLN is equals to two in 'approach 3' of the modified 3D-FD-AOS-FDTD scheme with a CFL number equals to four when the excitation waveform is that shown in Figure 5.5.

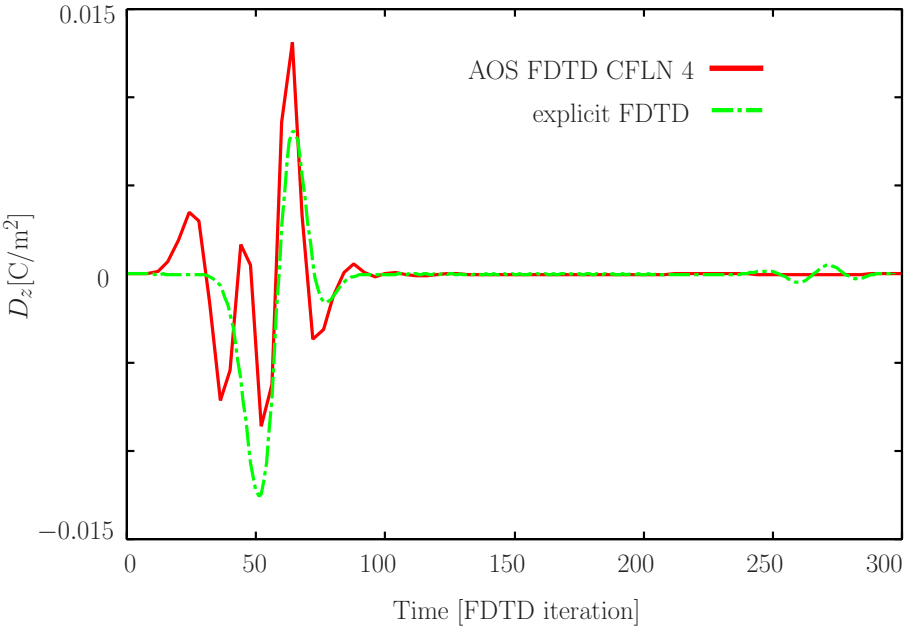

Figure 6.6: Observation at point $(74, 64, 64)$ when CFLN is equals to two in 'approach 3' of the modified 3D-FD-AOS-FDTD scheme with a CFL number equals to four when the excitation waveform is that shown in Figure 5.5.

Chapter 7

Conclusions and Future Work

The implementation of implicit FDTD methods makes it possible to deal with low frequency EM problems. In recent years it has been demonstrated that the implicit FDTD methods improve the FDTD computational efficiency and reduce the CPU calculation time, while they remain accurate. Unlike other numerical techniques such as LOD and ADI, independence between the fractional steps in the AOS method make it a perfect candidate to be parallelized. Thus, it makes it worth to study the implementation of the AOS-FDTD scheme.

As many practical applications involve materials of interest, we have developed and tested a three-dimensional frequency-dependent AOS-FDTD algorithm. In the 3D-FD-AOS-FDTD method, each field value has three components and each component is split into two direction parts. We have implemented a 3D-FD-AOS-FDTD scheme where firstly the calculations of both direction parts of each component are calculated independently and after both direction parts of each component are averaged, finding that the scheme is unstable when the excitation waveform is an unmodulated Gaussian pulse. Then, we have modified the AOS algorithm by computing the calculations of both directions parts of the component D_z and by averaging the results from both parts before computing the parts of the rest of the components and averaging them. Here, the same value of the D_z component flux density field update is passed to the calculation of both parts of the E_z electric field for the computation of the E_z electric field update, leading to a more similar observation in the plane Δz between the 3D-FD-AOS-FDTD scheme and the explicit 3D-FD-FDTD scheme.

As the excitation method chosen in the development of a FDTD scheme has a significant impact on the results of the simulation, we have changed the modified

3D-FD-AOS-FDTD algorithm to carry out the excitation before computing the D_z component flux density eld update. It seems to give stability to the whole computation. Observation does not diverges when the excitation waveforms used in each direction part of the component D_Z are an unmodulated Gaussian pulse with the peak centre position of both unmodulated Gaussian at different time step t.

After that, we have changed the average between the single points of both parts of the D_z component, where the source excitation is located. Hence, the 3D-FD-AOS-FDTD scheme shows a similar observation to the explicit FDTD scheme, when the excitation waveform in the 3D-FD-AOS-FDTD scheme is built with past and future values of the current value of a unmodulated Gaussian pulse and the excitation waveform in the explicit 3D-FD-FDTD scheme is an unmodulated Gaussian pulse.

Finally, we have studied the unconditional stability of the leapfrog 3D-FD-AOS-FDTD method beyond the Courant Friedrichs Lewy condition by showing the performance of the scheme with different Courant-Friedrichs-Lewy numbers. The scheme keeps accurate and stable when the CFLN number is smaller than four.

The main line of research that we should carry out now, from now on would deal with a further investigation on different models of excitement, as this seems to be the problem, given that observation of the AOS-FDTD scheme does not fully coincide with the observation of the explicit FDTD scheme. On the other hand, we should parallelize the 3D-FD-AOS-FDTD scheme to study the potential advantage of the independence between of the diferent fractional steps on the computation.

Bibliography

[1] K. S. Yee. Numerical Solution of Initial Boundary Value Problems Involving Maxwell's Equations in Isotropic Media. *IEEE Antennas and Propagation Magazine*, Vol.14(No.3):302–307, May 1966.

[2] K. O. Friedrichs R. Courant and H. Lewy. ber Die Partiellen Differenzengleichungen der Mathematischen Physik. *Mathematische Annalen*, Vol.100(No.1):32–74, 1928.

[3] A. Taflove and S.C. Hagness. *Computational Electrodynamics : The Finite-Difference Time-Domain Method.* Artech House, third edition edition, 2005.

[4] F. Costen. *High Speed Computational Modeling in the Applicaton of UWB Signals.* PhD thesis, Kyoto University, 2005.

[5] J-P. Brenger F. Costen and A. K. Brown. Comparison of FDTD Hard Source With FDTD Soft Source and Accuracy Assessment in Debye Media. *IEEE Transactions on Antennas and Propagation*, Vol.57(No. 7):20142022, July 2009.

[6] D. M. Sullivan. *Electromagnetic Simulation Using the FDTD Method.* Wiley-IEEE Press, second edition edition, 2013.

[7] R. Chen Y. Yang and E. K. Yung. The Unconditionally stable Crank Nicolson FDTD Method for Three-Dimensional Maxwell's Equations. *Microwave and Optical Technology Letters.*, Vol.48(No.8):16191622, May 2006.

[8] F. Costen H. K. Rouf and S. Gonzlez Garcia. 3D Crank-Nicolson Finite Difference Time Domain Method for Dispersive Media. *IEEE Antennas and Propagation Magazine*, Vol.45(No.19):961–962, September 2009.

[9] T. Namiki. A New FDTD Algorithm Based on Alternating-Direction Implicit Method. *IEEE Transactions on Microwave Theory and Techniques*, Vol.47(No.10):2003–2007, October 1999.

[10] T. Namiki. 3-D ADIFDTD MethodUnconditionally Stable Time-Domain Algorithm for Solving FullVector Maxwells Equations. *IEEE Transactions on Microwave Theory and Techniques*, Vol.48(No.10):1743–1748, October 2000.

[11] T. Su Y. Liu W. Yu, R. Mittra and X. Yang. *Parallel Finite-Difference Time-Domain Method*. Artech House, first edition edition, 2006.

[12] J. Yamauchi M. Muraki and H. Nakano. Effīcient Implicit FDTD Algorithm Based on Locally One-Dimensional Scheme. *Electronics Letters*, Vol.41(No.19):10461047, September 2005.

[13] L. Tan. Unconditionally Stable LODFDTD Method for 3-D Maxwells Equations. *IEEE Microwave and Wireless Components Letters*, (Vol.17, February 2007.

[14] T. Hemmi. *Locally One Dimensional Dinite Difference Time Domain Method with Frequency Dependent Media for Three Dimensional Biomedical Applications*. PhD thesis, University of Manchester, 2013.

[15] J. Weickert. *Anisotropic Difusion in Image Processing.* Tuebner, third edition edition, 1998.

[16] B. M. Romeny J. Weickert and M. A. Viergever. *Effīcient and Reliable Schemes for Nonlinear Diffusion Filtering.* IEEE Transactions on Image Processing, third edition edition, 1998.

[17] D. Ringo. Lapack: Linear algebra package @ONLINE November, 2013.

[18] K. Kunz R. Standler R. Luebbers, F. Hunsberger and M. Schneider. A Frequency-Dependent Finite-Difference Time-Domain Formulation for Dispersive Materials. *IEEE Transactions on Electromagnetic Compatibility,*, Vol.32(No.3):222–227, 1990.

[19] A. Karlsson G. Kristensson and S. Rikte. Electromagnetic Wave Propagation in Dispersive and Complex Material with Time Domain Techniques. *Academic Press Loondon*, Vol.17(No.12):277–294, 2001.

[20] K. Shlager and J. Schneider. A Selective Survey of the Finite-Fifference Time-Domain Literature. *IEEE Antennas and Propagation Magazine*, Vol.37(No.4):39–57, 1995.

[21] J. Booske M. Lazebnik, M. Okoniewski and S. C. Hagness. Highly Accurate Debye Models for Normal and Malignant Breast Tissue Dielectric Properties. *IEEE Microwave and Wireless Components Letters,*, Vol.17(No.12):822–824, 2007.

[22] F. Costen and A. Thiry. Alternative Formulation of Three Dimensional Frequency Dependent ADI-FDTD Method. *IEICE Electronics Express*, Vol.1(No.17):528–533, 1987.